INFORMATION TO USERS

This manuscript has been reproduced from the microfilm master. UMI films the text directly from the original or copy submitted. Thus, some thesis and dissertation copies are in typewriter face, while others may be from any type of computer printer.

The quality of this reproduction is dependent upon the quality of the copy submitted. Broken or indistinct print, colored or poor quality illustrations and photographs, print bleedthrough, substandard margins, and improper alignment can adversely affect reproduction.

In the unlikely event that the author did not send UMI a complete manuscript and there are missing pages, these will be noted. Also, if unauthorized copyright material had to be removed, a note will indicate the deletion.

Oversize materials (e.g., maps, drawings, charts) are reproduced by sectioning the original, beginning at the upper left-hand corner and continuing from left to right in equal sections with small overlaps. Each original is also photographed in one exposure and is included in reduced form at the back of the book.

Photographs included in the original manuscript have been reproduced xerographically in this copy. Higher quality 6" x 9" black and white photographic prints are available for any photographs or illustrations appearing in this copy for an additional charge. Contact UMI directly to order.

UMI

A Bell & Howell Information Company
300 North Zeeb Road, Ann Arbor MI 48106-1346 USA
313/761-4700 800/521-0600

Université d'Ottawa · University of Ottawa

Exploiting Solitons in All-Optical Networks

By

Ahmad K. Atieh, B. Sc., M. Sc.

A thesis submitted to the

School of Graduate Studies and Research

in partial fulfillment of the requirements for the degree of

Doctor of Philosophy

in Electrical Engineering

Ottawa-Carleton Institute for Electrical and Computer Engineering

School of Information Technology and Engineering (Electrical & Computer Engineering)

Faculty of Engineering

University of Ottawa

June, 1997

Abstract

Two key components, the pulse generator and optical signal demultiplexer, needed for the implementation of all-optical soliton-based local area and wide area networks are investigated. The technology of generating a bright soliton pulse train from a sinusoidal pulse train produced as the beat signal of two distributed feedback laser diodes passed through a so-called comblike fiber structure is developed. A design methodology for this structure is discussed, and using this approach a soliton pulse source is constructed generating 1553 nm pulses at a repetition rate of 50 GHz, with pulses of full width at half maximum of 2.0 ps. The fiber structure used to generate the bright soliton pulse train employs the lowest average power for the beat signal ever reported in the literature, and the shortest length of fiber. The same structure (with a different design) is also used to produce a 47.6 GHz dark soliton pulse train with a full width at half maximum of 3.8 ps. This is the first reported use of this structure to generate dark solitons. It is shown that the comblike dispersion profile fiber structures may also be exploited for soliton pulse compression producing widths as short as 200 fs.

Two approaches to implementation of optical signal demultiplexing are discussed. These are the nonlinear optical loop mirror (NOLM) and the separation of multilevel time division multiplexed signal pulses in the frequency domain by exploiting the relationship between the pulse's energy (i.e. pulse amplitude and width) and the Raman self-frequency shift. A modification of the NOLM scheme is investigated where feedback that adjusts the power of the control signal (by controlling the gain of an erbium-doped fiber amplifier

introduced into the control signal input path) is employed to make the structure insensitive to the state of polarization of the signal and control pulses.

In order to better understand the physical phenomena exploited in optical fiber soliton transmission and the above schemes, two experiments are conducted to measure the fiber nonlinear ratio (n_2/A_{eff}) and the Raman time constant (T_R) in single-mode fibers at 1550 nm. The fiber nonlinear ratio was measured for standard telecommunication fiber, dispersion shifted fiber, and dispersion compensating fiber. A value of 3.0 fs for the Raman time constant was measured and is recommended for soliton pulse propagation modeling in single-mode optical fibers.

Acknowledgments

The work presented in this thesis was carried out at the Institute for National Measurement Standards at the National Research Council of Canada (NRC).

I am grateful to my supervisors, Drs. Jacek Chrostowski and Peter Galko, for their continuous support, scientific advice, and encouragement. I would like to thank the members of my examining committee, Drs. Pierre Berini, Robert Harrison, Barry Syrett, and Réal Vallée, for taking the time to read the thesis and their helpful comments.

I wish to express my gratitude to Dr. Piotr Myslinski for his continual encouragement, valuable suggestions and assistance during the work on the thesis. I also wish to thank Dr. Miroslaw Florjanczyk from Optiwave Corporation for his initial work on the computer software used for solving the nonlinear Schrödinger equation, Ross Misner and Alfred Dufour from NRC for their help in building the optical autocorrelator and preparing the laser diodes for the bright and dark solitons experiments, and Frances Misner for proofreading the thesis. I wish to thank my colleagues at the NRC and University of Ottawa: Drs. Simon Boothroyd, Jason Hong, and Hamid Hatami-Hanza.

I am grateful to the Jordan University of Science and Technology and the Canadian International Development Agency for providing me with a scholarship to complete my studies at University of Ottawa.

Most importantly, special thanks for my parents, brothers, and sisters in Jordan for their continuous encouragement and support. Above all, sincere gratitude to my wife Ala Assaf and my sons Khaled and Muath for their support, encouragement, and patience during my studies.

Contents

List of Figures

List of Tables

Abbreviations

AND	AND Logic Gate.
ARPA	Advanced Research Project Agency.
ASE	Amplified Spontaneous Emission.
ASK	Amplitude Shift Keying.
ATM	Asynchronous Transfer Mode.
Att	Attenuator.
BPF	Bandpass Filter.
ccw	counter clockwise.
CDPF	Comblike Dispersion Profile Fiber.
cw	clockwise.
CW	Continuous Wave.
DCF	Dispersion Compensating Fiber.
DDF	Dispersion Decreasing Fiber.
DFB	Distributed Feed Back.
DIF	Dispersion Increasing Fiber.
DSF	Dispersion Shifted Fiber.
EA	Electro-Absorption.
EDFA	Erbium Doped Fiber Amplifier.
F-8L	Figure-8 Fiber Laser.
FA	High Power Fiber Amplifier.
FC	Fiber Coupler.

FSK	Frequency Shift Keying.
FWHM	Full Width at Half Maximum.
FWM	Four-Wave Mixing.
GVD	Group Velocity Dispersion.
ISO	Isolator.
KdV	Korteweg and de Vries.
LAN	Local Area Network.
$LiIO_3$	Lithium Iodate.
Nd:YAG	Neodymium:Yttrium Aluminum Garnet.
Nd^{+3}	Neodymium ions.
NOLM	Nonlinear Optical Loop Mirror.
NRC	National Research Council.
NRZ	Non Return to Zero.
NSE	Nonlinear Schrödinger Equation.
OAC	Optical Autocorrelator.
OC	Optical Carrier.
OS	Oscillator.
OSA	Optical Spectrum Analyzer.
PANDA	Polarization maintaining AND Absorption reducing fiber.
PC	Polarization Controller.
PMD	Polarization Mode Dispersion.
PSK	Phase Shift Keying.
QS/ML	Quality factor Switched/Model Locked .

RF	Radio Frequency.
RZ	Return to Zero.
SBS	Stimulated Brillouin Scattering.
SDH	Synchronous Digital Hierarchy.
sech	hyperbolic secant.
SHG	Second Harmonic Generation.
SMF	Single Mode Fiber.
SOP	State Of Polarization.
SPM	Self-Phase Modulation.
SRS	Stimulated Raman Scattering.
STF	Standard Telecommunication Fiber.
tanh	hyperbolic tangent.
TD	Time Delay.
TDM	Time Division Multiplexing.
TL	Transform Limited.
WAN	Wide Area Network.
WDM	Wavelength Division Multiplexing.
XPM	Cross-Phase Modulations.

List of Symbols

λ	Optical wavelength.
L	Fiber length.
c	Speed of light in vacuum.
D	Fiber dispersion.
B	Data bit rate.
η	Chromatic dispersion index.
$\delta\omega$	Chirp.
$\phi(t)$	Electrical field phase.
n_L	Linear refractive index.
n_2	Nonlinear refractive index.
I	Light intensity.
n	Light refractive index.
P	Signal average power.
A_{eff}	Fiber effective core area.
γ	Fiber nonlinear strength.
L_{NL}	Nonlinear scaling length.
P_0	Pulse peak power.
ν	Signal optical frequency.
$\hat{K}$	Propagation constant.
T_R	Raman time constant.

v_g	Group velocity.
β_1	Inverse of group velocity.
β_2	Group velocity dispersion.
β_m	The m-th order dispersion.
$\chi^{(3)}$	Third order susceptibility.
E	Electrical field.
ϕ_{NL}	Nonlinear phase shift.
λ_D	Zero dispersion wavelength.
$A(Z,T)$	Slowly varying amplitude of the optical signal electrical field.
α	Fiber attenuation (dB/km).
Z, z	Position parameter.
T, t	Time parameter.
L_D	Dispersion scaling length.
T_0	Pulse half width at $1/e$ intensity point.
N	Soliton order.
z_0	Soliton period.
$u(t)$	Normalized electrical field.
Γ	Normalized fiber loss.
Δ_{MS}	Mean square chirp.
Δt	Pulse temporal width at FWHM.
$\Delta \nu$	Pulse spectral width at FWHM.
τ_a	Pulse autocorrelation width at FWHM.

τ_p	Pulse width at FWHM.
n_2/A_{eff}	Fiber nonlinear ration.
α'	Fiber attenuation (m^{-1}).
T_d	Time delay.
$f(t)$	Nonlinear response function.
$\chi_R^{(3)}$	Raman resonant complex part of the third order susceptibility.
$\chi_{NR}^{(3)}$	Electron non-resonant real part of the third order susceptibility.
$\Delta\omega$	Angular frequency deviation from the optical central frequency.
g_R	Raman gain coefficient.
Im( )	Imaginary part of the argument.
$g(\tau)$	Constant depends on the pulse width.
τ_{FWHM}	Pulse temporal width at FWHM.
Δf	Frequency shift from the signal central frequency.
k	Coupling ratio for a fiber coupler.
$v(t,z)$	Normalized slowly varying field of the control signal.
T_0	Signal pulse half width at $1/e$ intensity point.
T_1	Control pulse half width at $1/e$ intensity point.
$\overline{B}$	Modal birefringence.
n_s, n_f	Effective mode indices.
L_B	Beat length.
u_s, v_s	Signal and control electrical field on the slow polarization axis.
u_f, v_f	Signal and control electrical field on the fast polarization axis.

d_{12}	Walk-off parameter.
N	Number of soliton eigenvalues.
η_n	The n-th eigenvalue.

Chapter 1

Introduction

1.1 Motivation

Optical fiber has become the transmission medium of choice for handling the very high data-rate signals that are envisaged to be increasingly necessary in the near future. This is because of its huge bandwidth and low attenuation. Indeed, optical fiber is already found in most areas of telecommunications including undersea cable systems, long-haul networks known as wide-area networks (WAN), subscriber loop systems serving residential and commercial customers, cable television distribution networks, and local-area networks (LAN). The networks of the future must serve the customer with a wide range of broadband services ranging from interactive real-time multimedia services to sporadic bandwidth-intensive "bursty" traffic. Current network technologies using synchronous digital hierarchy (SDH) for transmission and asynchronous transfer mode (ATM) for switching cannot meet the future demands because of the imposed bottleneck of electronics. One solution is to use all-optical networks.

All-optical networks can be implemented using either the wavelength-division multiplexing (WDM) approach, where signals at different optical carriers (i.e., different wavelengths) representing different channels are multiplexed together on a single fiber, or using the time-division multiplexing (TDM) technique, where the channels that transmit data using ultra-short pulses are interleaved to form a single data stream at a single wavelength as shown in Fig. 1.1. WDM technologies have reached an advanced stage of development and most components are commercially available. In contrast, TDM is

currently under development and key components are confined to the research laboratories.

TDM is of interest because it overcomes some of the serious limitations that arise in WDM [1], such as spectral nonuniformity due to the concatenation of amplifiers, crosstalk arising from non-ideal filters and imperfect switches, limits imposed by the optical fiber nonlinearities, the need for complex control schemes for wavelength stabilization, as well as expensive multiwavelength laser sources and stable filters. Moreover, TDM has features that make it very attractive for future networks, such as simple access to high aggregate data rates, compatibility with existing technologies such as SDH, simplified amplifier and dispersion management, and the possible ability to overcome the effects of fiber nonlinearities by using optical solitons for data transmission. For these reasons TDM is investigated in this thesis.

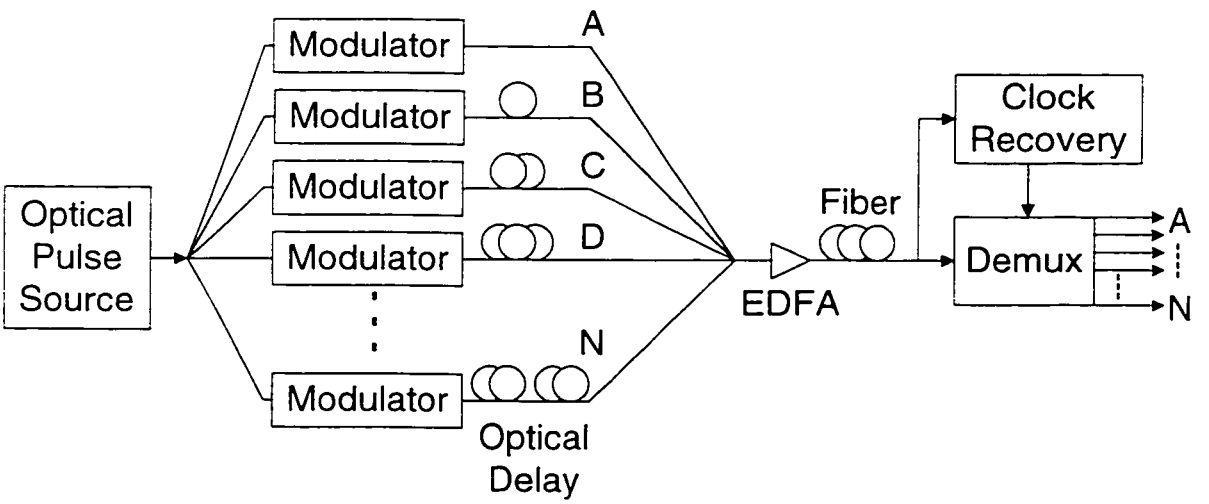

Fig. 1.1 Optical time-division multiplexing block diagram.

The vision of an optical communications network that inspires this thesis is illustrated in Fig. 1.2, where many supercomputers that run at ultra-high speeds of over 50 GHz are connected in a backbone ring topology. Each of these computers serves heterogeneous users that may run at the ring speed, or less. The network can offer bandwidth-on-demand or guaranteed bandwidth for each user. This configuration is also applicable to high-speed video servers or terabyte media banks. This network architecture is under investigation at the National Research Council Canada (NRC). Although the network is designed to operate at 50 GHz, it is possible in principle to scale it to higher speeds, such as 100 GHz or 200 GHz. Fifty GHz was chosen because it is close to the available modulator's operating speed, which is limited by the electronics, and it is equivalent to 20 channels of WDM networks that employ the OC-48 standard that runs at 2.5 Gbit/s. The suggested network is applicable for LANs as well as WANs.

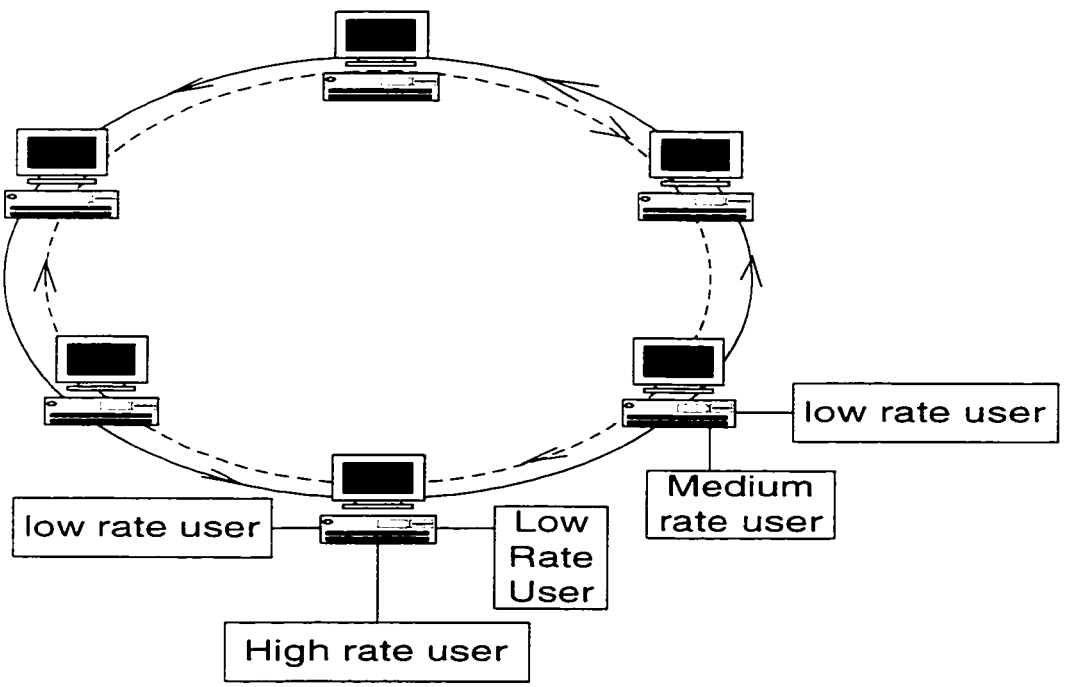

Fig. 1.2 All-optical 50 GHz ring network architecture.

The key technologies required to implement such a network are optical sources, multiplexing/demultiplexing techniques, clock recovery circuits, optical switches, pulse compressors, and optical transmission-management approaches. To design the optical fiber transmission links, it is necessary to determine the physical parameters of the fiber, such as dispersion, attenuation, and nonlinear parameters. Dispersion and attenuation are well-known phenomena and have long been accurately measured. On the other hand, fiber nonlinear parameters, which are crucial in ultra-high-rate data communication systems have been investigated only recently.

In this thesis, some technologies that can be employed in such an all-optical network (consisting of optical sources, optical demultiplexing schemes, and pulse compressors) are developed, and the experimental results of the fiber nonlinear parameter measurements for different types of optical fibers are presented. The optical sources investigated for this network are soliton sources. Soliton pulses represent an elegant means of overcoming the harmful effects of the optical fibers, such as dispersion and nonlinearities which will be discussed later. There are two types of optical solitons, known as "bright" and "dark" both of which are generated here.

1.2 Optical Fiber Phenomena

To implement ultra-high-speed local area or wide area all-optical networks, it is necessary to understand the basic element of these networks, which is the optical fiber. In low-speed data transmission, fiber is a relatively simple medium; but at high speeds and over long distances, optical fibers manifest several effects which are deleterious to their use. These effects are primarily those of fiber attenuation, dispersion, and phenomena associated with the nonlinear characteristics of the fiber.

The limitation that fiber attenuation places on point-to-point optical transmission is a result of the limited output power of available optical sources, as well as the limitations on achievable receiver sensitivity. To attain the longest transmission links, sources emitting light at approximately the wavelength where fiber attenuation is minimal (λ=1.55 μm) must be used. The recent development of optical amplifiers, however, greatly reduces the limitations imposed by fiber attenuation.

Higher-speed-fiber optical transmission schemes have used single-mode optical fibers exclusively to transport data pulses. These fibers experience two forms of dispersion that place limitations on the transmitted-data rate and transmission distance. These are chromatic dispersion and polarization-mode dispersion. The former is the result of both the frequency (or wavelength) dependency of the fiber material's refractive index, which corresponds to a wavelength dependency in the group velocity of the propagated signals, and to the effect of the fiber's geometry. This causes the different spectral components present in a random train of pulses to arrive at different times at the receiver, effectively broadening the pulses. The difference in the propagation times of the different components increases with fiber length, and ultimately would produce so much intersymbol interference at the receiver that the data would effectively be lost. An estimate of the maximum length that would allow transmission in the presence of this effect is given by Chesnoy et al. [2] as:

$$L = \frac{\eta \pi c}{\lambda^2 B^2 D}, \tag{1.2.1}$$

where λ is the wavelength of the optical source, B is the bit rate, D is the fiber dispersion (differential time delay per unit length per unit wavelength), c is the velocity of light, and

η is the "chromatic dispersion index" which is a parameter that depends on the modulation scheme used and the "chirp" of the optical source. The chirp of an optical source refers to the change of the source's frequency as a result of the modulation process. It is defined as the negative derivative with respect to time of the electrical field phase $\phi(t)$ of the optical output:

$$\delta\omega = -\frac{\partial\phi}{\partial t}. \tag{1.2.2}$$

To increase the distance over which the optical signals can be successfully propagated, both the fiber dispersion and attenuation must be reduced. This can be accomplished by employing fibers that are specially designed and manufactured to produce zero dispersion at the same wavelength as the minimum fiber attenuation. Such fibers are called "dispersion-shifted fibers" (DSF) and are now commercially available.

The latter form of dispersion mentioned above, "polarization-mode dispersion", arises from the different propagation speeds of the different polarization components of the transmitted signals. This is a result of "modal birefringence", brought about by a departure of the fiber core geometry from that of a perfectly cylindrical form, and some material anisotropy, which forces light to propagate in different polarization modes at different speeds.

Fiber nonlinearity refers to the dependence of the refractive index of the fiber material on the intensity of the light signal. Overall, the refractive index of a polarization mode can be expressed as:

$$n = n_1(\omega) + n_2 I, \tag{1.2.3}$$

where $n_L(\omega)$ is the base frequency-dependent refractive index, and n_2 is the nonlinearity coefficient of the refractive index manifesting the variation of the refractive index as a linear function of intensity, I, of the optical field ($I = P/A_{eff}$, where P is the power of the optical signal and A_{eff} is the effective-mode field-area of the fiber). The consequences of nonlinearity for the propagation of pulse trains are the phenomena of self-phase modulation (SPM), cross-phase modulation (XPM), stimulated Brillouin scattering (SBS), stimulated Raman scattering (SRS), four-wave mixing (FWM), Raman self-frequency shift, and self-steepening. These phenomena can be both detrimental and fortuitous to optical communication systems.

SPM is the phenomenon where the phase of the signal is modulated as the amplitude of the optical signal varies. It is a significant effect, i.e., the phase fluctuations so produced are significant when the fiber length and intensity are sufficiently long. The length of the fiber necessary for the effect to be significant is the nonlinear scaling length given by:

$$L_{NL} = \frac{1}{\gamma P_0}. \tag{1.2.4}$$

where P_0 is the peak power of the incident light signal, and γ is a parameter reflecting the extent of the nonlinearity:

$$\gamma = \frac{2\pi}{\lambda}\frac{n_2}{A_{eff}}. \tag{1.2.5}$$

SPM ordinarily has the effect of broadening the optical pulse's spectrum, but is also responsible for the existence of a soliton pulse which will not change its width in the presence of chromatic dispersion at wavelengths greater than those for which the

dispersion is zero (this refers to pulse propagation in the "anomalous dispersion regime"). Such pulses will be discussed in detail in subsequent chapters.

XPM refers to the effect created when two signals of different optical frequencies (ν_1 and ν_2), propagate simultaneously in an optical fiber, and the phase shift that each signal acquires depends not only on its own intensity, but also on the other signal's intensity. The nonlinear interaction may also produce optical signals at new frequencies ($\nu_3=2\nu_1-\nu_2$ and $\nu_4=2\nu_2-\nu_1$) if phase-matching and frequency-matching conditions are satisfied by all the signals present in the fiber. These conditions are:

$$\vec{K}_3 + \vec{K}_4 - \vec{K}_1 - \vec{K}_2 = 0, \tag{1.2.6}$$

where $\vec{K}_i = n_i \omega_i / c$, n_i is the refractive index of the fiber material at the angular frequency ω_i; and

$$\nu_3 + \nu_4 = \nu_1 + \nu_2. \tag{1.2.7}$$

The phenomenon of XPM can be exploited to produce all-optical demultiplexing of an optical pulse train, which will be demonstrated later.

The vibration induced in the glass lattice of the optical fiber by the optical signals may produce other nonlinear processes. These processes are the SRS and SBS processes. Yet another effect of the nonlinearity of the fiber is that caused by the nonlinearity-induced dependence of the group velocity on the intensity. This effect is known as "self-steepening" and produces an asymmetry in the SPM-broadened pulse spectrum. It is only significant for ultra-short pulses of subpicosecond widths.

As stated above, the nonlinear effects are mostly deleterious to the propagation of pulses. They can, however, help in another basic problem for ultra-high-rate optical

communication systems, which is that electronic signal processing cannot perform many of the commonly-needed tasks, such as multiplexing and demultiplexing of signals at the desired pulse rates. This leads to a search for optical means of performing these functions, thereby producing all-optical communication systems.

In ordinary high-rate optical transmission systems, optical data pulses (rectangular or Gaussian) are generated at a wavelength approximately matching the zero dispersion wavelength of the fiber. The fibers used are standard telecommunication fiber (STF) or DSF. In these systems, fiber nonlinearities and dispersion set a limit on the maximum propagation distance data-rate product. This approach of transmission may be termed "linear transmission". An alternative method has been investigated in recent years, where the nonlinearity of the fiber may be exploited to compensate for dispersion in the fiber. This balancing of the effects only occurs when the pulses employed have a certain set of shapes and intensities, producing pulses which are termed "solitons". The basic form of these, the "fundamental bright solitons", continually balance dispersion and nonlinear effects as they propagate. They have an electrical field which has a hyperbolic secant profile. Together with the use of optical fiber amplifiers, very long-distance transmission of optical pulses using solitons is possible [3,4].

Various schemes to generate bright solitons have been reported in the literature. These methods differ in their complexity, reliability, flexibility to generate solitons at different rates, and cost. One of the most promising is a scheme in which a beat signal from the combination of two separate single-frequency distributed feedback lasers (DFB) is launched into a fiber structure which serves to shape the input pulses (represented by the cycles of the beat signal) into pulses with the soliton profile. The fiber structure used

consists of a concatenation of alternatively-segmented DSF and STF. The segments of STF are much shorter than those of DSF, so the dispersion profile of the fiber structure has an appearance similar to the teeth of a comb, hence the name "comblike dispersion profile fiber" (CDPF) is coined for the structure. This structure has been explored in the literature by different research groups [5,6] and shows great promise as a practical means of generating soliton pulse trains, as it is relatively inexpensive and easy to implement. The methodology of the design and optimization of the structure are not well discussed in the literature. In considering the design approach, it will be demonstrated (through the design and construction of a 50 GHz soliton pulse source) that significant improvements over previously- reported designs are possible.

Hasegawa and Tappert [7] have proposed an alternative class of pulses that propagate without distortion. These are termed "dark solitons", as the pulse might be considered to exist not in the presence of light, but rather, in its absence. Their shape follows a hyperbolic tangent profile. Dark solitons are of interest since they show greater stability than bright solitons with respect to perturbations such as amplifier noise, fiber attenuation, and intra-pulse SRS. Little attention has hitherto been paid to techniques for the generation and manipulation of these pulses. The use of CDPF structures previously used to generate a bright soliton pulse train will be used to generate dark soliton pulse trains. This technique is demonstrated by the design and construction of a 47.6 GHz dark soliton pulse source.

As mentioned, there is a need for an all-optical communication system when ultra-high bit rates are employed. One of the basic functions that are required in this regard is that of demultiplexing. A structure known as a "nonlinear optical loop mirror" (NOLM)

shows promise as a practical means of achieving the desired functionality. This structure depends on the XPM effect between a low-intensity, high-repetition rate signal (the data signal) and a high-intensity, low-repetition rate control signal. In practice, the scheme has difficulties with respect to polarization fluctuations of the signals involved. The structure can be made polarization insensitive (as will be investigated) by controlling the gain of an erbium-doped fiber amplifier (EDFA) with a feedback signal generated from the output signals of the structure.

An alternative approach of demultiplexing that will also be explored is one which exploits another aspect of the nonlinear optical behavior known as "Raman self-frequency shift" effect, where the frequency of an optical signal shifts as it propagates in the optical fiber (the amount of the shift being dependent on the signal width). If we use multi-amplitude fundamental soliton pulses to represent each signal, then the frequency shift of the various amplitude signals will differ, thereby allowing the stream to be separated on the basis of frequency. The Raman self-frequency shift effect is clearly pronounced when the pulse width is in the subpicosecond regime. To achieve that, it is necessary to employ pulse compressors. This can be done with relatively simple fiber structures that have a comblike dispersion profile. This is demonstrated by the construction of a fiber structure which compresses the solitons to a duration as small as 200 fs.

1.3 Achievements

The following is a list of the contributions and achievements in this thesis:

1. A 50 GHz bright soliton pulse train is generated using less average power than previously reported for the beat signal launched into a comblike dispersion profile fiber structure;

2. A 47.6 GHz dark soliton pulse train is generated by using a comblike dispersion profile fiber structure for the first time;
3. A novel all-optical polarization-insensitive demultiplexer using a nonlinear optical loop mirror is investigated;
4. Signal demultiplexing of a multilevel communication system using the Raman self-frequency shift effect for a burst of 40 Gbit/s pulses is demonstrated;
5. Pulse compressors using comblike dispersion profile fiber structures capable of compressing soliton pulses down to 200 fs are designed and constructed;
6. The fiber nonlinear ratio (n_2/A_{eff}) is measured for standard telecommunication fiber, dispersion shifted fiber, and dispersion compensating fiber (DCF);
7. The Raman time constant (T_R) that appears in the generalized nonlinear Schrödinger equation (NSE) is measured in single mode fibers at 1550 nm.

1.4 Thesis Outline

In Chapter 2, the nature and character of bright solitons is discussed and the means for their generation is reviewed. The design consideration for the comblike structure is discussed, and the results of the design and construction of a 50 GHz source using two distributed-feedback laser diodes operating at 1550 nm are presented. In Chapter 3, the theory of dark solitons, and the possibility of using a comblike structure to form them, is considered. As well as, a system to generate a 47.6 GHz dark soliton pulse train is designed, constructed, and characterized. All-optical signal demultiplexing using the NOLM is reviewed in Chapter 4, and a novel scheme to achieve polarization-independent demultiplexing using the NOLM is proposed. Signal demultiplexing of a multilevel amplitude shift keying time-division multiplexed soliton signal is also

demonstrated, and a technology for pulse compression necessary for multilevel signal demultiplexing is constructed. Optical fiber characterization is presented in Chapter 5, where the fiber nonlinear parameters are measured. These parameters are the nonlinear ratio (n_2/A_{eff}) and the fiber T_R. Conclusions and suggestions for future work are discussed in Chapter 6.

Chapter 2

Generation of Multigigahertz Bright Soliton Pulse Train

2.1 Introduction

In general, solitons may be defined as the stationary solutions of the NSE that governs light pulse propagation in single mode fibers. These solutions have special shapes depending on whether the fiber dispersion is positive or negative. When the fiber dispersion is negative at the light wavelength (group velocity dispersion β_2 is positive), the fiber exhibits normal dispersion. The opposite occurs in the so-called "anomalous dispersion regime" in which β_2 is negative. Bright solitons are the solutions in the anomalous dispersion regime and the pulse electrical field has a hyperbolic secant shape. The particle-like behavior of a soliton pulse enables it to propagate indefinitely in a lossless fiber without the pulse changing shape. In reality, as a soliton pulse propagates in a real fiber, its amplitude decays due to ever-present fiber attenuation; however, with adiabatic amplification (keeping the pulse energy constant at the output of each amplifier) to compensate for fiber attenuation, these pulses can be made to propagate over thousands of kilometers in a lossy dispersive fiber without changing their shape [8-10]. This makes these pulses promising candidates for use in ultra-high-speed wide area and local area networks.

In this chapter, the theory behind solitons and the techniques that have been previously employed to generate them are reviewed in detail. These techniques are considered in the context of their application as pulse sources in a communication system.

Design issues associated with existing systems and the creation of more efficient structures than hitherto reported in the literature are considered. The most promising of these techniques is one based on propagating beat signals in CDPF structures. A 50 GHz fundamental bright soliton pulse source which is superior to similar structures previously reported in the literature will be constructed in this manner.

2.2 Theory

Fiber dispersion plays a critical role in optical communications. When short data pulses propagate through a fiber link, the different spectral components into which the pulse can be decomposed travel at different speeds given by $c/n(\omega)$ (where $n(\omega)$ is the refractive index at the given angular frequency ω of the component) resulting in pulse broadening. Mathematically, the effects of the fiber dispersion may be separated into different terms by expanding the mode propagation constant $\beta(\omega)$ about the center frequency ω_0 in a Taylor series:

$$\beta(\omega) = n(\omega)\frac{\omega}{c} = \beta_0 + \beta_1(\omega - \omega_0) + \frac{1}{2}\beta_2(\omega - \omega_0)^2 + \frac{1}{6}\beta_3(\omega - \omega_0)^3 + \cdots, \qquad (2.2.1)$$

where

$$\beta_m = \left[\frac{d^m\beta(\omega)}{d\omega^m}\right]_{\omega=\omega_0}, \qquad (m = 0,1,2,\ldots). \qquad (2.2.2)$$

The coefficient β_1 is the inverse of the group velocity; β_2 is generally termed the group velocity dispersion (GVD) coefficient; and more generally, β_m is termed the mth order dispersion coefficient.

In addition to dispersion, fiber exhibits nonlinear effects due to the third order susceptibility, $\chi^{(3)}$, which is responsible for the nonlinear refraction phenomenon. This is referred to as the intensity dependence of the refractive index which is given by:

$$n = n_L(\omega) + n_2|E|^2. \tag{2.2.3}$$

where $n_L(\omega)$ is the linear part of the refractive index at angular frequency ω; $|E|^2$ is the optical intensity in the fiber; and $n_2 = \frac{3}{8n_L}\mathrm{Re}\{\chi_{xxxx}^{(3)}\}$ is the nonlinear refractive index for a linearly-polarized electrical field. The most interesting nonlinear effect that results from the intensity dependence of the refractive index is self-phase modulation. It is responsible for pulse spectral broadening, inducing a nonlinear phase shift in the propagated field given by:

$$\phi_{NL} = \frac{2\pi n_2}{\lambda} L|E|^2. \tag{2.2.4}$$

When light pulses propagate in a fiber with dispersion and nonlinear effects, their behavior depends on the sign of the dispersion, $D = -(2\pi c/\lambda^2)\beta_2$. In the normal dispersion regime where $D<0$ (i.e., when $\lambda<\lambda_D$, where λ_D is the zero dispersion wavelength), the higher frequency components (blue shifted) travel slower than the lower frequency components (red shifted). The opposite occurs in the anomalous dispersion regime where $D>0$ (i.e., when $\lambda>\lambda_D$). In this regime, both the dispersion and nonlinear effects can be made to cancel each other making possible the existence of soliton pulses.

Optical pulses propagating in a single mode fiber link (with widths in the picosecond range) are governed by the simplified NSE given by [11]:

$$\frac{\partial A(Z,T)}{\partial Z} + \beta_1 \frac{\partial A(Z,T)}{\partial T} + i\frac{1}{2}\beta_2 \frac{\partial^2 A(Z,T)}{\partial T^2} - i\gamma|A(Z,T)|^2 A(Z,T) + \frac{1}{2}\alpha A(Z,T) = 0, \quad (2.2.5)$$

where $A(Z,T)$ is the slowly varying amplitude of the propagated field measured in units of $W^{1/2}$ at position Z and time T in the fiber; α is the fiber loss; and $\gamma = \frac{2\pi}{\lambda}\frac{n_2}{A_{eff}}$ is a measure of the strength of the nonlinearity of the fiber, in which n_2 is the nonlinear refractive index, A_{eff} is the effective core-area of the fiber, and λ is the light wavelength.

The propagated pulses may encounter chromatic dispersion, nonlinear effects or both. To distinguish between cases where one or the other effect is more pronounced, it is useful to introduce two length scales, known as the "dispersion length L_D" and the "nonlinear length L_{NL}". They are defined by:

$$L_D = \frac{T_0^2}{|\beta_2|}, \text{ and} \quad (2.2.6)$$

$$L_{NL} = \frac{1}{\gamma P_0}, \quad (2.2.7)$$

where P_0 is the pulse peak power at the fiber input, and T_0 is the pulse's width (defined to be the half width at the $1/e$ intensity point). Depending on the fiber length, L, we may have one of the following cases: i) if $L \ll L_D$ and $L \ll L_{NL}$, it can be shown that neither dispersion nor nonlinear effects plays a significant role during the optical pulse propagation in the fiber, i.e., a pulse maintains its shape during propagation; ii) if $L \geq L_D$ and $L \ll L_{NL}$, it can be shown that the nonlinear effects are negligible compared to the dispersive effects; iii) if $L \ll L_D$ but $L \geq L_{NL}$, it can be shown that the nonlinear effects dominates the GVD, which leads to spectral broadening of the pulses and pulse shaping is

possible; iv) if L is longer than, or comparable to, both L_D and L_{NL}, both effects are significant in the fiber, and it is possible to generate optical soliton pulses when the propagation is in the anomalous dispersion regime. We are primarily interested in the last situation.

Optical solitons are special types of pulses that can propagate undistorted over indefinite distances in a lossless fiber if they have the correct shape, width, and power. If an optical pulse has a hyperbolic secant shape and satisfies $N^2 = L_D / L_{NL} = 1$, it will be called a "fundamental soliton". When N^2 is greater than 1, the soliton pulses are termed "higher-order solitons". Higher-order solitons have a periodic evolution pattern, where the original shape recovers every length, $z_0 = (\pi / 2) L_D$. Through the period, different shapes of the propagated pulse have evolved as shown in Fig. 2.1 for the third order soliton pulse, (N=3); the original pulse shape is reconstructed at the end of the propagation period, z_0.

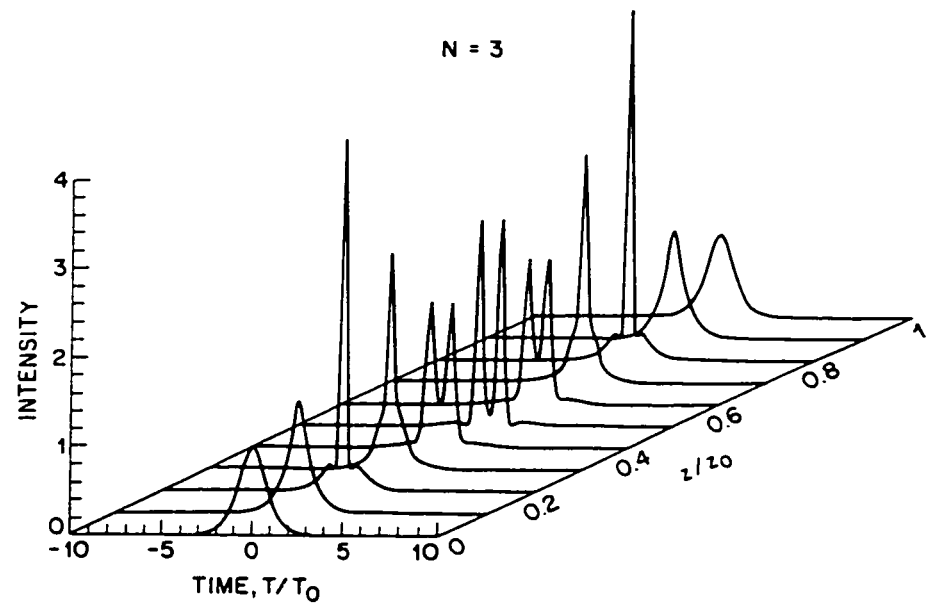

Fig. 2.1 Pulse evolution for high order solitons (N=3) (after Ref. 11).

2.3 Literature Review

The concept of "solitary waves" was reported in 1838 by John Scott Russell [12]. He noticed that a wave of water (which was formed when a boat suddenly stopped in a canal in Scotland) continued its course along the canal without change of form or diminution of speed. In 1895, D. J. Korteweg and G. deVries [13] mathematically described waves in shallow water using a nonlinear partial differential equation which carries their initials (KdV). The particle-like behavior of the solitary wave was first described by Zabusky and Kruskal in 1964 [13]. It was they who coined the word "soliton" to describe the solution for the KdV equation, which they determined numerically. These waves do not break up and disperse when they collide. Zakharov and Shabat [15] showed in 1971 that solitons could be generated in a nonlinear dispersive medium. They solved the NSE that describes both the nonlinear and dispersive effects using the inverse scattering transform method. In 1973, Hasegawa and Tappert [16] pointed out that solitary waves can be readily generated in optical fibers. Seven years later, in 1980, Mollenauer et al. [17] demonstrated soliton propagation in optical fibers. The delay in conducting such an experiment was as a result of the inadequacy of the technology to fabricate single mode fibers with sufficiently low loss.

This achievement opened the way for the extensive study of soliton generation both theoretically and experimentally. Different schemes to produce solitons have been investigated in the past ten years. In 1984, Mollenauer and Stolen [18] built a soliton laser source using a length of single-mode polarization-preserving fiber in the feedback loop of a mode-locked color-center laser ($\lambda \sim 1.4$–$1.6\ \mu m$). A theoretical study of this "soliton laser" was conducted by Haus et al. [19]. Fiber Raman lasers were used to generate

solitons by Islam et al. [20] in 1986. By synchronously pumping a loop of polarization-preserving dispersion-shifted fiber with 10 ps pulses from a mode-locked color-center laser, they demonstrated the first fiber Raman laser with a 240 fs pulse width. Different modifications for this scheme were proposed by Kafka et al. [21] and Gouveia-Neto et al. [22].

The effect of Raman self-scattering (self-frequency shift) has also been exploited to produce solitons. In 1987, Zysset et al. [23] succeeded in the generation of first-order solitons of 77-250 fs duration at 1.37-1.49 μm. These solitons are generated in a single mode fiber by coupling pulses of 1 ps duration and 0.66 GW/cm^2 peak intensity from a dye laser synchronously pumped by an Nd:YAG laser. The repetition rates of the solitons generated by the foregoing methods are equal to the pulse repetition rates of the mode-locked pump lasers, which are in the order of 100 MHz. These rates are not sufficient for high-speed optical communication systems which are intended for applications at multigigahertz rates. Therefore, alternate means for soliton generation at high-repetition rates must be found. A significant boon to the research for generating optical solitons took place when EDFAs were developed.

Hasegawa [24] suggested a method for generating high repetition rates in 1984. His proposal was based on using a continuous wave (CW) radiation modulation instability in optical fibers. He showed theoretically that a sinusoidal modulated optical wave can be developed into a soliton-like pulse train as it propagates along a fiber in the anomalous dispersion regime. This approach for generating solitons was first realized by Tai et al. in 1986 [25]. The modulated signal they used was generated by mixing the optical output signals of two lasers to control the repetition rate of the generated pulse

train. The first laser they used is a pump (carrier) Nd:YAG at 1319 nm, and the other one is an external-grating cavity single-mode InGaAsP diode, whose wavelength is tuned to be in the vicinity of the YAG laser by adjusting the grating angle. Unfortunately, this method gave a non-stable pulse sequence: the large pedestal between the pulses caused a nonlinear interaction among the pulses as they propagated in the fiber.

A stable train of nearly independent solitons was investigated numerically by Dianov et al. in 1989 [26]. Slowly varying the GVD along the fiber length or the use of adiabatic amplification of a periodically modulated CW signal in a fiber were suggested. An experimental realization of this method was accomplished in 1992 [27] using a special design of a dispersion decreasing fiber (DDF). A CW QS/ML Nd:YAG laser and a Fabry-Perot interferometer were installed in the oscillator cavity of the laser to produce dual frequency pulses. The dual frequency signal was generated in a different way by Chernikov et al. in 1992 [28]. The beat signal was generated using two DFB lasers. The resulting signal was fed into the DDF described in [27]. In the same year, Chernikov et al. [29] proposed the use of tailored fibers instead of the DDF. This configuration uses a DSF piece spliced to a DDF piece. A slight modification was made in [30] to this configuration by using another DSF piece next to the DDF piece. All of these modifications were done to enhance the quality of the generated pulse train and to control the resulting pulse widths.

In 1993, Shipulin et al. [31] proposed a new method for transforming the CW beat signal into solitons by using a dispersion increasing fiber (DIF) piece followed by a DDF piece. This scheme is more suited to generating repetition rates of a few tens of gigahertz, as it requires shorter fiber lengths (~5 km) than DDF pieces which require lengths of

more than 10 km for rates below 50 GHz. All of these methods, however, require special fibers, which makes the realization more costly and less reliable. To overcome this difficulty, Chernikov et al. [32,5] proposed and demonstrated a more practical technique for transforming the beat signal into soliton pulse train using CDPF structures.

Around the same time, two other schemes were proposed for high-repetition-rate soliton generation. The first used a mode-locked semiconductor laser with either an external cavity [33] or monolithic integrated optics [34]. This method is sensitive to ambient temperature and vibration because of the use of an optical resonator which limits the output repetition rates. The second method used gain switching of DFB lasers with an ultra-narrow-band optical filter [35,36]. The spectral quality of the generated pulses is poor due to the large frequency chirping produced in the process. External cavity mode-locking was also used by Geisler [37]. Recently, new approaches have been proposed to generate soliton pulse trains. Electroabsorption (EA) modulators were suggested in 1993 by Suzuki et al. [38,39].

Here, a comprehensive study for generating a train of ultra-high-speed bright soliton pulses at 1553 nm using the CDPF structure is presented. The fiber structure employed for pulses generation uses the lowest average power for the input signal ever reported. The generated solitons have a width of 2.2 ps ["full width at half maximum" (FWHM)], at a repetition rate of 50 GHz [40].

2.4 Modeling and Numerical Calculation

As mentioned, perhaps the simplest technique used to date for generating ultra-high repetition rate trains of optical solitons is that proposed by Chernikov et al. [5]. This method is based on propagating a beat signal in a series of alternating commercially-available segments of DSF and STF. The beat signal launched into the CDPF structure was generated by a dual frequency erbium fiber laser. In this work, the beat signal is generated by beating the outputs of two CW single frequency DFB laser diodes. When the beat signal propagates in the DSF segments, the pulses encounter the SPM nonlinear effect only, because the dispersion is close to zero, which broadens the pulses spectrum. After words, the signal propagates in the STF segments, which has a dispersion effect only because their lengths are too small to trigger the nonlinear effects. As a result, the signal is temporally broadened. By adjusting the lengths of each fiber, it is possible to balance the two effects and generate bright soliton pulses.

The electrical field of the light signal launched into the first segment thus has the form of:

$$u(t) = a \sin(\pi t / T), \tag{2.4.1}$$

where $1/T$ represents the generated soliton repetition rate, and a is the pulse peak field. The fiber segments are constructed from a length of DSF spliced to a length of STF. The selection of the number of segments and their lengths is based on the numerical computation of the signal shapes along the structure. The computation is based on solving the NSE governing the propagation of pulses in these fibers given by (2.2.5). It is useful to employ a frame of reference moving with the pulse group velocity v_g (known as the

retarded frame). This can be achieved by the transformation $T = t\text{-}Z/v_g = t\text{-}\beta_1 Z$. To simplify the computation, the pulse envelope $A(Z,T)$ and both the time T and space Z coordinates are normalized according to :

$$U(Z,T) = \frac{A(Z,T)}{\sqrt{P_0}}. \tag{2.4.2}$$

$$u(Z,T) = N^2 U(Z,T), \tag{2.4.3}$$

where P_0 is the pulse peak power, N is the soliton order given by:

$$N^2 = \frac{L_D}{L_{NL}} = \frac{\gamma P_0 T_0^2}{|\beta_2|}. \tag{2.4.4}$$

$$t = \frac{T}{T_0}. \tag{2.4.5}$$

$$z = \frac{Z}{L_D}. \tag{2.4.6}$$

Employing these transformations, a normalized NSE is obtained given by:

$$i\frac{\partial u}{\partial z} + \frac{1}{2}\frac{\partial^2 u}{\partial t^2} + |u|^2 u + i\Gamma u = 0, \tag{2.4.7}$$

where $u(z,t)$ is the normalized field at the normalized position z and normalized time t, and $\Gamma = \alpha' T_0^2 / |\beta_2|$ is the normalized fiber loss, in which α' is the fiber attenuation in m^{-1} given by:

$$\alpha' = \alpha(\text{dB/km}) \log_e(10) / 10^4. \tag{2.4.8}$$

The normalized equation does not have the group velocity term presented in equation (2.2.5) as a result of employing the retarded frame of reference.

The normalized NSE is solved based on the standard split-step Fourier method that is well explained in [11, Section 2.4.1]. This method obtains an approximate solution

by assuming that the dispersion and nonlinear effects act independently over a small step distance h. This method is accurate to the second order of h. To verify the numerical computations, the fiber structure reported in [5] was computed; then computations were made using parameters of the fibers available for the experimental realization [41]. The parameters of the fibers were either provided by the supplier, or separately measured. In this situation, a beat signal at an optical wavelength of 1553 nm, with an average power of 125 mW, was launched into the CDPF structure. Two types of DSF were used because the required lengths were not available in one type. The dispersions in the DSF fibers used were 0.29 ps/(km nm) and 0.44 ps/(km nm), and 17 ps/(km nm) in the STF. The nonlinear ratio (n_2/A_{eff}) of the DSF and STF are independently measured as 5.63×10^{-10} W^{-1}, and 3.27×10^{-10} W^{-1}, respectively [42]. Splice loss of 0.13 dB between the fiber pieces was measured in the experimental system and incorporated into the calculation.

The CDPF structures were designed by studying the pulse shape and phase at the output of each segment until the desired pulse shape and spectrum were obtained. The most important design parameter is the length of the DSF and STF pieces which determine the quality of the generated solitons. The first DSF piece should be sufficiently long to introduce enough new frequency components to give the desired pulse compression. The lengths of the STF pieces are designed to produce zero chirp at their output, where the chirp $\delta\omega$ is the time derivative of the electrical field phase given by:

$$\delta\omega = -\frac{\partial\phi}{\partial t}. \tag{2.4.9}$$

This condition preserves the balance between the nonlinearity that is produced in the DSF segment and the dispersion that is produced in the STF segment. The optimal length of

each STF piece was set to minimize the integral of the squared chirp over the pulse FWHM, i.e., to minimize

$$\Delta_{MS} = \int_{FWHM} |\delta\omega(z,t)|^2 dt . \qquad (2.4.10)$$

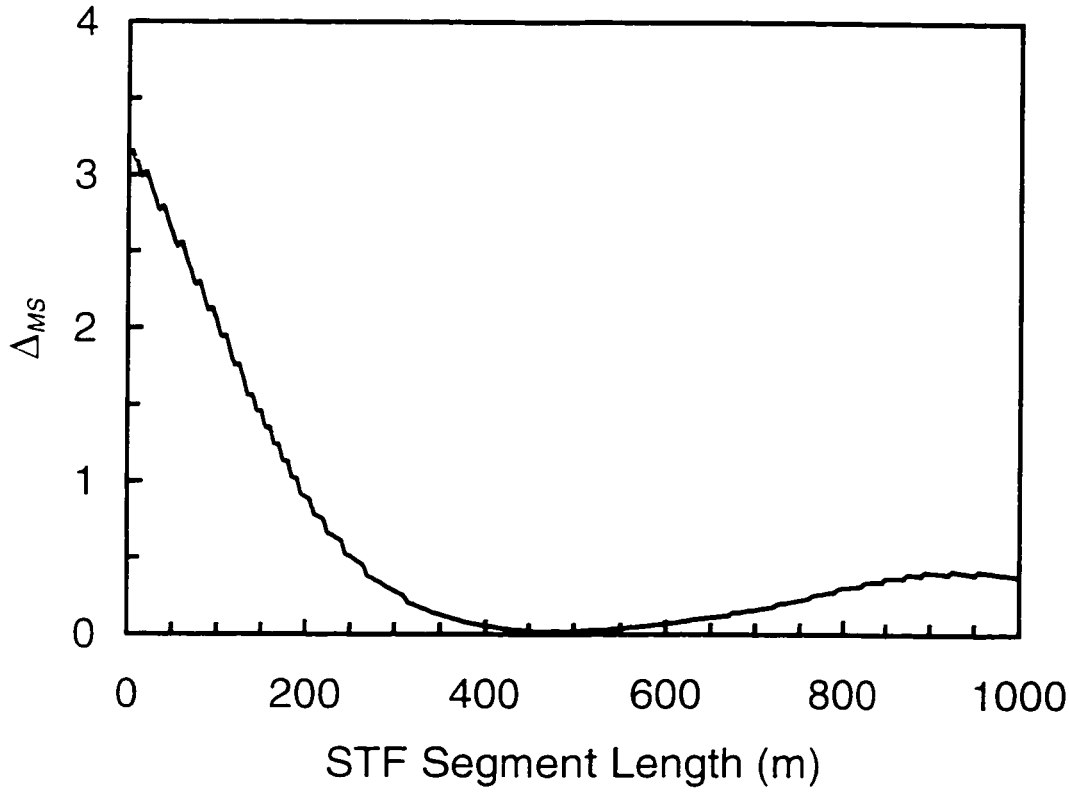

Fig. 2.2 Calculated mean square chirp of the generated pulses at different positions for the first STF segment in the comblike dispersion profile fiber (CDPF) structure.

The optimal length of the first DSF piece produces a phase of approximately 0.33π (recommended in [5] as a rule of thumb). Fig. 2.2 shows the calculated mean square chirp (Δ_{MS}) at different positions for the first STF segment. The lengths of the first DSF and STF pieces are 3000 m and 500 m, respectively. The above procedure was used

for subsequent pieces, resulting in gradually decreasing lengths, with the final segments measuring 300 m of DSF and 13.5 m of STF, respectively. The total length of the CDPF structure is approximately 6.64 km. Fig. 2.3 shows the CDPF structure used in the experiments to generate a bright soliton pulse train. It consists of 14 pieces of DSF and STF.

Table 2.1 shows the length and dispersion of the designed comblike dispersion profile fiber structure. The fiber structure is optimal in the sense that each segment in the structure was designed to achieve minimum chirp at its output. This condition ensures that the pulses at the segment's output balances the effects of nonlinearity produced in the dispersion shifted fiber and the dispersion produced in the standard telecommunication fiber piece.

Fiber piece number	Length (m)	Dispersion (ps/km/nm)
1	3000	0.29
2	500	17
3	1000	0.44
4	120	17
5	600	0.29
6	53	17
7	375	0.44
8	34	17
9	300	0.44
10	24	17
11	300	0.29
12	16	17
13	300	0.29
14	13.5	17

Table 2.1 Designed length and dispersion for the CDPF structure used for bright soliton generation

The numerical calculation showed a train of bright soliton pulses at a 50 GHz repetition rate, as illustrated in Fig. 2.4. The resulting FWHM pulse width is τ_p= 2.0 ps. The phase across these pulses is constant, which implies transform-limited pulses ($\Delta t \Delta \nu$ = 0.3148, where Δt and $\Delta \nu$ are the pulse temporal and spectral FWHM widths, respectively). The pulse is called transform limited if it is not chirped, i.e., the pulse spectrum is equivalent to the Fourier transform of its field. The phase difference between the neighboring pulses is π. The π phase jumps that appear between the pulses correspond to the electrical field vector that reaches zero amplitude at these points and subsequently changes direction.

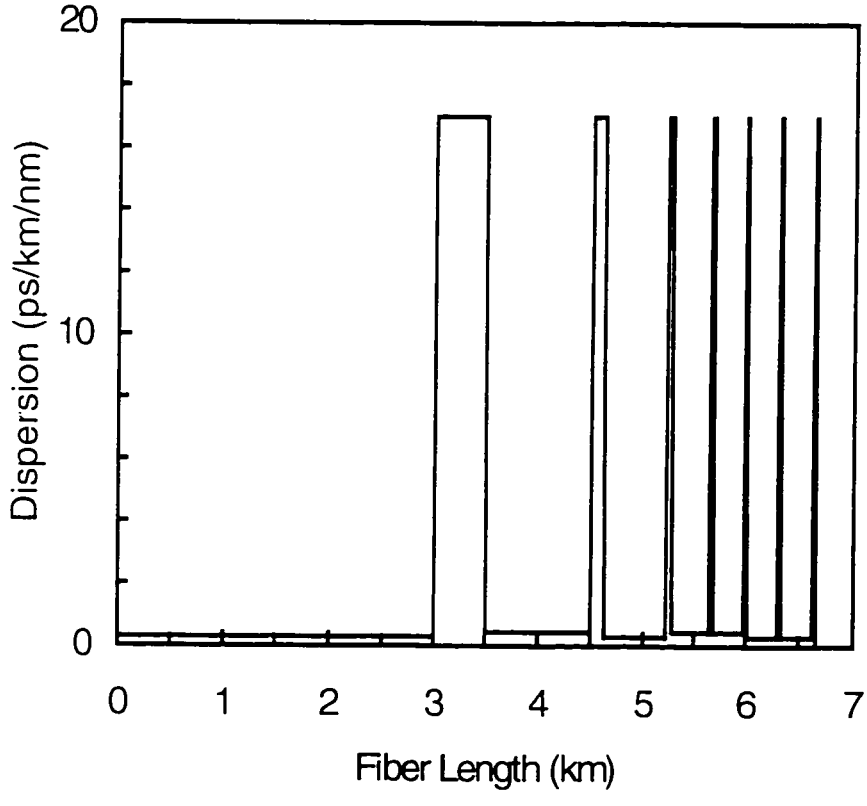

Fig. 2.3 CDPF structure used for generating bright soliton pulse train.

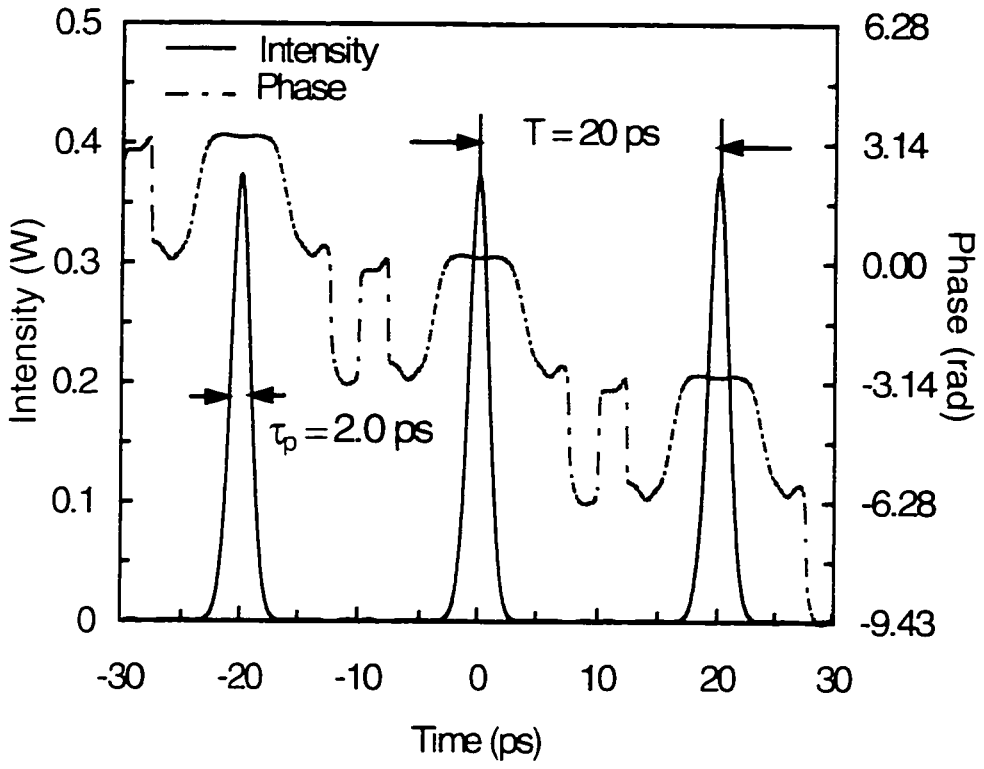

Fig. 2.4 Intensity of bright soliton pulse train and relative phase results from numerical calculation. Note the flat phase across the pulses which implies transform-limited pulses.

Fig. 2.5 shows the autocorrelation of the intensity of the resulting bright soliton pulses on a logarithmic scale. This figure illustrates the tails of the generated pulses which is not clear on a linear scale. The level of the signal in the tail is more than 22 dB lower than the pulse's peak. This ratio is one of the quality measures of an optical soliton source. The FWHM of the pulses autocorrelation is τ_a = 3.1 ps, which satisfies τ_p/τ_a = 0.6482 for hyperbolic secant pulses [43]. The spectrum of these pulses is shown in Fig. 2.6. The envelope of this spectrum corresponds to a $sech^2$ spectral shape.

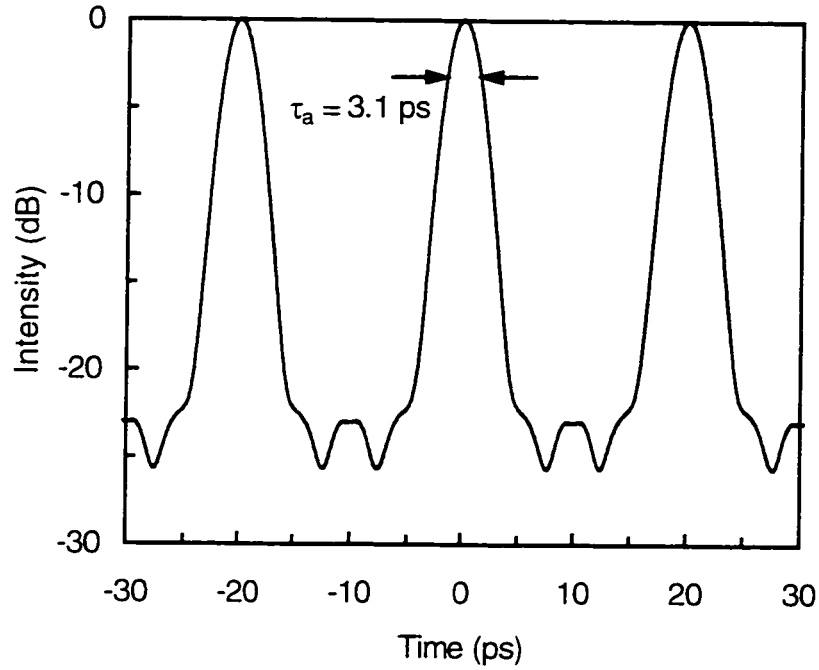

Fig. 2.5 The computed intensity autocorrelation for the soliton pulse train output from the CDPF structure (logarithmic scale).

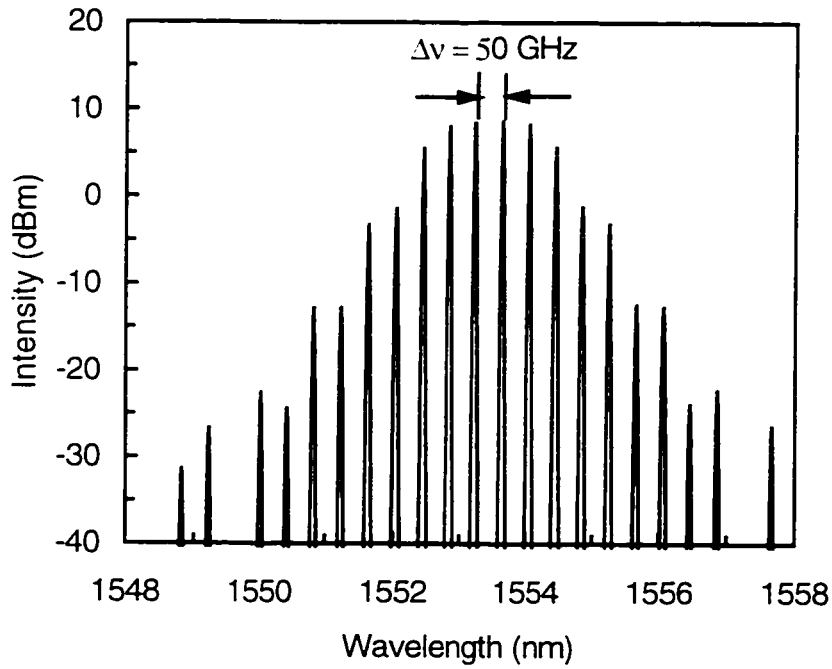

Fig. 2.6 Numerical calculation of the intensity spectrum result for a bright soliton pulse train.

2.5 Experimental Results

Fig. 2.7 shows the block diagram of the experimental setup used to generate a bright soliton pulse train. The signal launched into the first fiber segment is generated by beating two CW single-frequency signals from DFB laser diodes around 1553 nm. This signal is amplified to the desired power level using an EDFA and erbium/ytterbium-doped fiber amplifier. The beat signal repetition rate is controlled by tuning the temperature of the DFB laser diodes, which changes their operating wavelength. A bandpass filter is used between the amplifiers to reduce the effect of spontaneous emission noise which affects the timing jitter of the generated pulses.

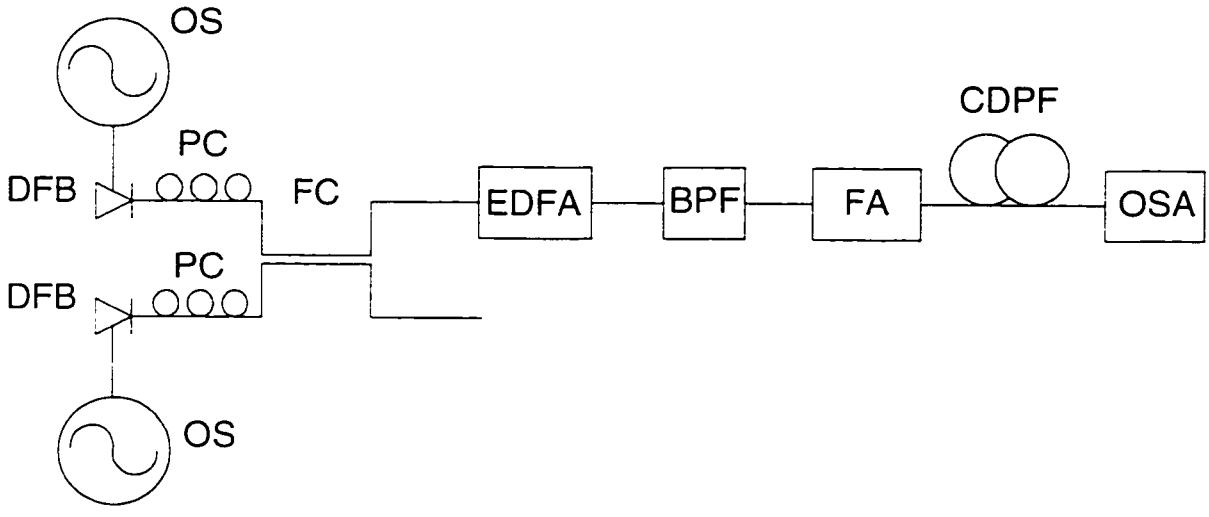

Fig. 2.7 Experimental setup used for generating a bright soliton pulse train. BPF: bandpass filter; OS: 40 kHz oscillator; OSA: optical spectral analyzer; EDFA: erbium-doped fiber amplifier; FA: high power fiber amplifier; DFB: distributed feedback laser diode; FC: 50/50% fused silica fiber coupler; CDPF: comblike dispersion profile fiber structure; PC: polarization controller.

When launching the high-intensity beat signal into the fiber, part of the launched power is reflected back due to the SBS nonlinear effect. This phenomenon prevents the generation of a soliton pulse train. Therefore, SBS was suppressed by externally modulating the DFB laser diodes with a 40 kHz sinusoidal signal. This frequency was optimized experimentally for the comblike structures, and it gives negligible SBS backward-reflected power. The modulation increases the laser line width to about 420 MHz, which is enough to avoid power loss due to the SBS for input signals with average powers of up to 22 dBm. For more details on SBS measurements and suppression in the comblike fiber structure, refer to Appendix A.

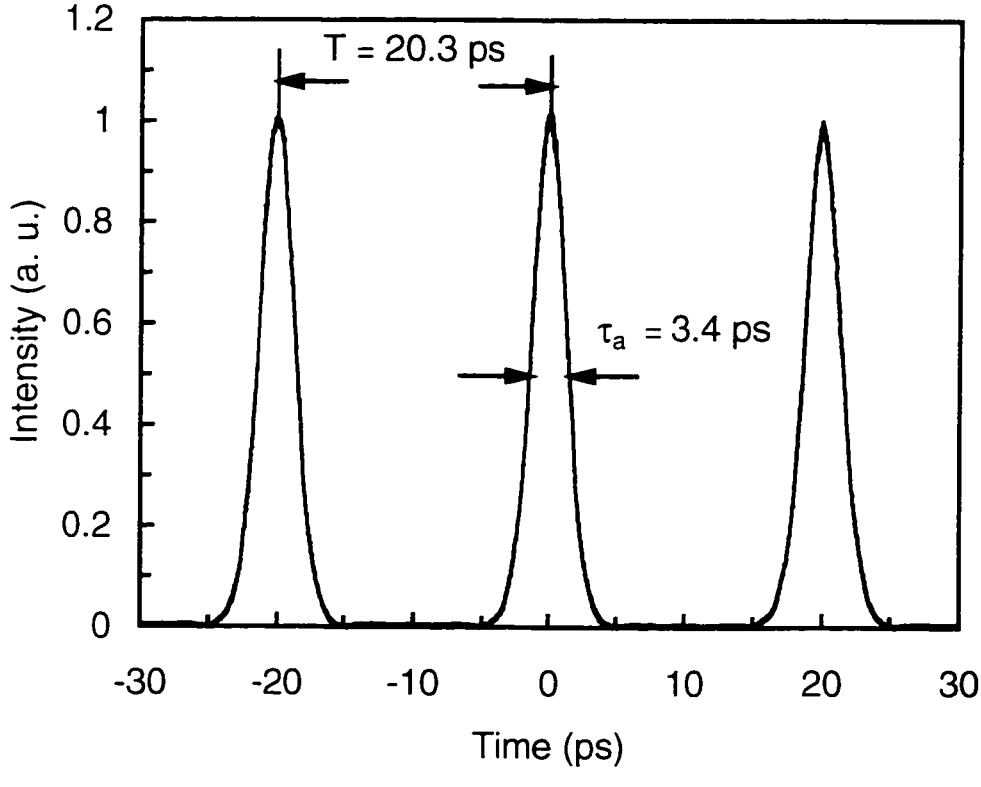

Fig. 2.8 Intensity autocorrelation of the measured bright soliton pulse train.

An optical autocorrelator was built to measure the bright soliton pulse train. The pulse's autocorrelation is measured using the second harmonic generation (SHG) of an overlapping replica of the pulse [44]. The autocorrelator employs a $LiIO_3$ crystal as the SHG to obtain higher measurement sensitivity. The intensity autocorrelation of the generated bright soliton pulse train is shown in Fig. 2.8 on a linear scale, and in Fig. 2.9 using a logarithmic scale. The autocorrelation of the measured soliton pulses have a FWHM τ_a = 3.4 ps, which is equivalent to a FWHM pulse duration of τ_p = 2.2 ps. The measured spectrum of these pulses is shown in Fig. 2.10. There is very close agreement between the experimental results and those predicted by the numerical computation. This is particularly remarkable, as the model has no single adjustable parameter. The generated bright soliton pulses have very good quality, in that they are pedestal, and background, free. The pulse pedestal results when some energy is shed outside the wings of an ideal temporal profile of a soliton pulse. A comparison between the experimental results and those published in the literature [5,6] is summarized in Table 2.2. This shows a successful generation of bright soliton pulses using only 125 mW, the lowest average input signal power ever used in CDPF structures.

CDPF	Soliton train repetition rate (GHz)	Input signal average power (mW)	Length (km)	Number of fiber pieces	Output pulse FWHM (ps)
Swanson et al. [5]	40	250	4.65	9	2.91
Chernikov et al. [6]	59.1	190	7.5	20	2.2
This work	49.3	125	6.6	14	2.2

Table 2.2 Comparison between reported CDPF structures.

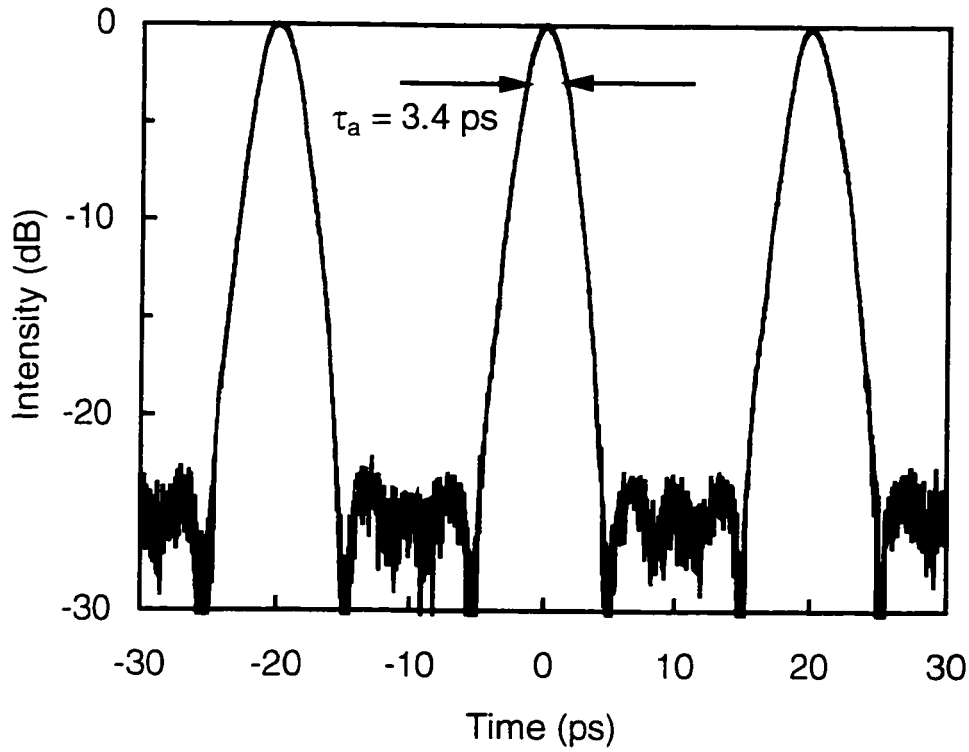

Fig. 2.9 Intensity autocorrelation measured for bright soliton pulse train on a logarithmic scale.

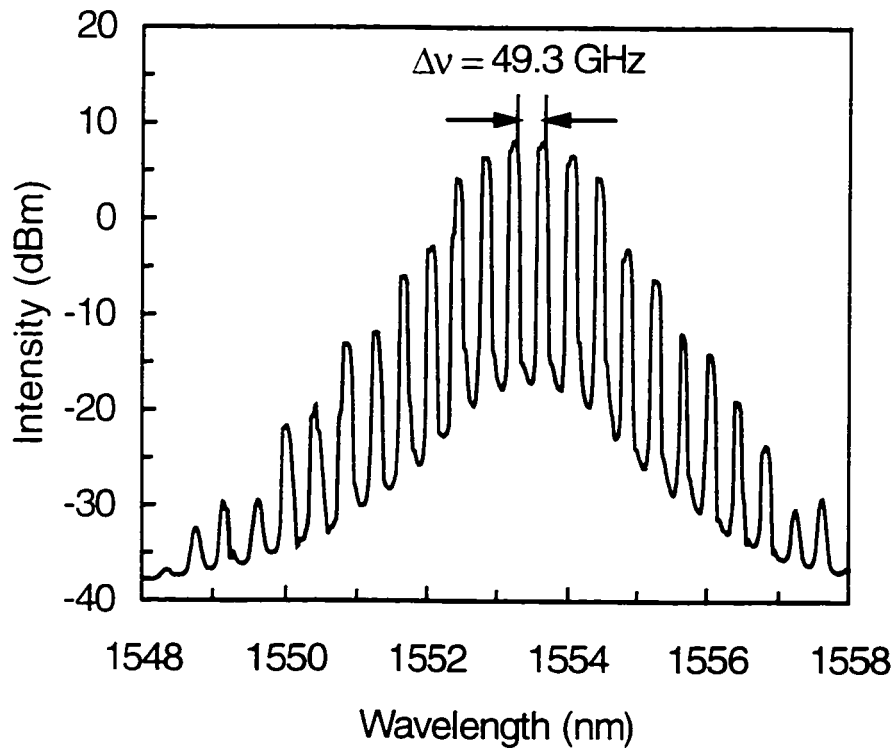

Fig. 2.10 Intensity spectrum measured for bright soliton pulse train.

Chapter 3

Generation of Multigigahertz Dark Soliton Pulse Train

3.1 Introduction

As discussed in the preceding chapter, the stationary solutions of the NSE governing the propagation of light waves in an optical fiber are the so-called "bright solitons" when propagation takes place in the anomalous dispersion regime. When propagation takes place in the normal dispersion regime, Hasegawa and Tappert [7] showed that the stationary solution to the NSE is quite different with the electric field following a hyperbolic tangent profile as depicted in Fig. 3.1. The optical intensity is thus constant, except where the pulse is localized. Thus, one can describe the signal pulse as manifesting its presence in the absence of light, a viewpoint which made Hasegawa and Tappert term this solution as "*dark solitons*". Dark solitons are sometimes called "black solitons" because they have zero intensity at the pulse center. When the intensity at the pulse center is nonzero, the pulse is called "gray soliton". The black solitons have a constant phase with a discontinuity of π at the pulse center, while gray solitons have a non constant, but gradual, phase.

It has been shown [45,46] that dark soliton pulses are less sensitive than bright solitons to the effects of perturbations such as amplifier noise, fiber losses, and intra-pulse stimulated Raman scattering. It was found that dark soliton pulses, propagating in a lossy fiber, spread in time at approximately half the rate of bright solitons. Dark solitons are also less sensitive to background noise; the background noise affects primarily the

background of the dark pulses, resulting in lower pulse-shape distortion. Although optical amplifiers can be used to compensate for the fiber loss to achieve ultra-long distances, they generate amplified spontaneous emission (ASE) noise, which produces random frequency shift in the propagated pulses. The effect of random frequency shift on dark solitons results in a timing jitter $\sqrt{2}$ times lower than that for bright solitons [47]. One pays, however, for these advantages when generating dark soliton pulses. The required average power for dark solitons is five times larger than that for bright solitons in a standard 1:5 duty cycle.

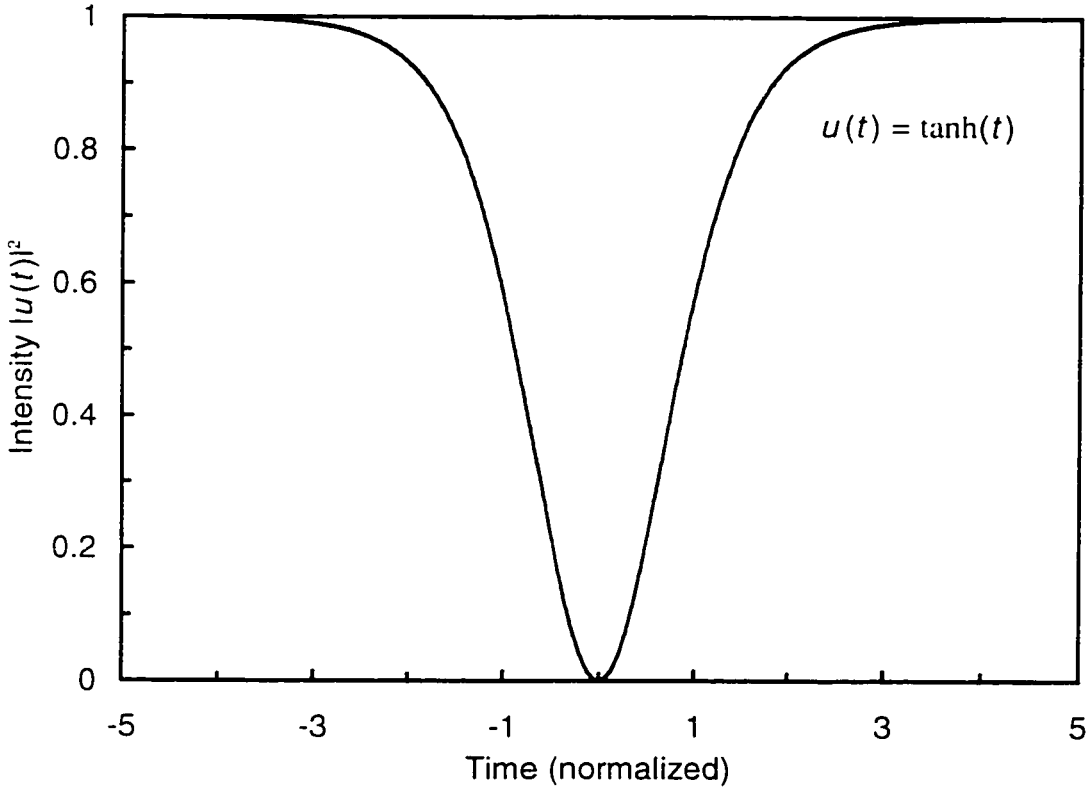

Fig. 3.1 Intensity profile of a dark soliton pulse.

In this chapter, the techniques that can be employed to produce trains of dark solitons will be considered. It will be shown that the same sort of CDPF structure used to generate bright solitons can be used to produce dark solitons. Section 3.2 reviews the methods previously reported in the literature to generate dark solitons; Section 3.3 discusses the possibility of using the CDPF structure for this purpose, and its design; Section 3.4 reports on the implementation of this approach to produce an (approximately) 50 GHz dark soliton pulse train at 1553 nm.

3.2 Literature Review

The first experimental realization of dark solitons was conducted by Emplit et al. in 1987 [48]. They used the spectral filtering technique of a mode-locked dye laser at a wavelength of 600 nm to generate dark soliton pulses that propagated in 52 m of single mode fiber (SMF). Another experiment was carried out by Krökel et al. [49] using a light-controlled fiber modulator to generate dark solitons. The generated pulses were propagated in 10 m of SMF. Weiner et al. [50] generated dark solitons using a Fourier pulse synthesis technique. A simpler way to produce a dark soliton pulse was proposed by Rothenberg [51]. It was based on the collision of two bright pulses in a fiber. Unfortunately, this approach leads to undesirable rapid-intensity modulation on a finite-width background. Several other methods have also been proposed: Zhao et al. [52] suggested the use of a wave-guide electro-optic modulator; Haelterman et al. [53] suggested the use of spectral filtering of a high-repetition-rate mode-locked laser source; and Williams et al. [54] experimentally demonstrated the generation of a quasi-continuous train of dark solitons based on the collision of two pulses in a fiber. In another

experiment, dark soliton pulses were generated at 850 nm using a shaping process based on the space-to-time transformation properties of a spectrograph-like arrangement [55].

Most of the above schemes for generating dark soliton pulses are not practical for telecommunications, as they require the use of wavelengths other than in the third optical window (1.3-1.6 mm). In addition, the input pulse peak power is in the range of several tens of watts.

Dark soliton pulse trains were also generated using DDF [56]. A 100 GHz pulse train was generated on a continuous background at 1548 nm. In a different approach, a pseudorandom dark soliton data train of 10 Gbps was generated using an AND gate and a T-flip flop circuit [57]. The generated train was detected using a one-bit-shifting technique with a Mach-Zehnder interferometer. The generated dark soliton pulse was propagated over 1 km in a single mode fiber.

Rothenberg et al. [58,59] used the same principle of pulse collision described in [51] to generate a train of dark solitons at 605 nm on a slowly decreasing intensity of the pulse background. Dianov et al. [26] suggested a scheme to generate a dark soliton train on a continuous background, based on the propagation of a beat signal of two CW DFB laser diodes in a DDF.

3.3 Using CDPF Structures to Generate Dark Solitons

In the scheme proposed here, a CDPF structure is used to generate a train of multigigahertz dark soliton pulses. The fiber structure is constructed from concatenated pieces of DSF and DCF. The fiber pieces have negative dispersion which is essential to generate dark soliton pulses. The negative dispersion implies that light propagation occurs in the normal dispersion regime, where the higher-frequency components (blue-shifted) of an optical pulse travel slower than the lower-frequency components (red-shifted) while propagating in the fiber. As a result, the pulse encounters spectral compression. The SPM nonlinear effect usually produces new frequency components which are red-shifted near the leading edge and blue-shifted near the trailing edge of the propagated light pulses. Group velocity dispersion, however, causes temporal pulse broadening. The overall effect on the propagating pulse in the fiber would be temporal broadening.

Fig. 3.2 shows the CDPF structure designed to generate dark soliton pulses. It is constructed from four pieces of fiber alternating between DSF and DCF, with dispersion of -0.63 and -87 ps/(km nm), respectively. The fiber nonlinear ratio (n_2/A_{eff}) of the DSF and DCF pieces is measured independently as 5.82×10^{-10} W^{-1} and 15.01×10^{-10} W^{-1}, respectively [42]. The fiber attenuation is 0.25 dB/km for the DSF, and 0.5 dB/km for the DCF pieces. Numerical calculations of the propagating signals were made by solving the normalized NSE in the normal dispersion regime given by:

$$i\frac{\partial u}{\partial z}-\frac{1}{2}\frac{\partial^2 u}{\partial t^2}+|u|^2u+i\Gamma u=0, \tag{3.3.1}$$

where $\Gamma = \alpha' T_0^2 / |\beta_2|$ is the normalized fiber loss, in which α' is the fiber attenuation in m^{-1} given by:

$$\alpha' = \alpha(\mathrm{dB/km}) \log_e(10) / 10^4, \tag{3.3.2}$$

where T_0 is the half width at the $1/e$ intensity point, and β_2 is the group velocity dispersion. The input signal launched into the fiber structure, and used in the calculations, has a sinusoidal envelope given by:

$$u(t) = a\sin(\pi t/T), \tag{3.3.3}$$

where $1/T$ represents the generated soliton repetition rate, and a is the pulse peak field.

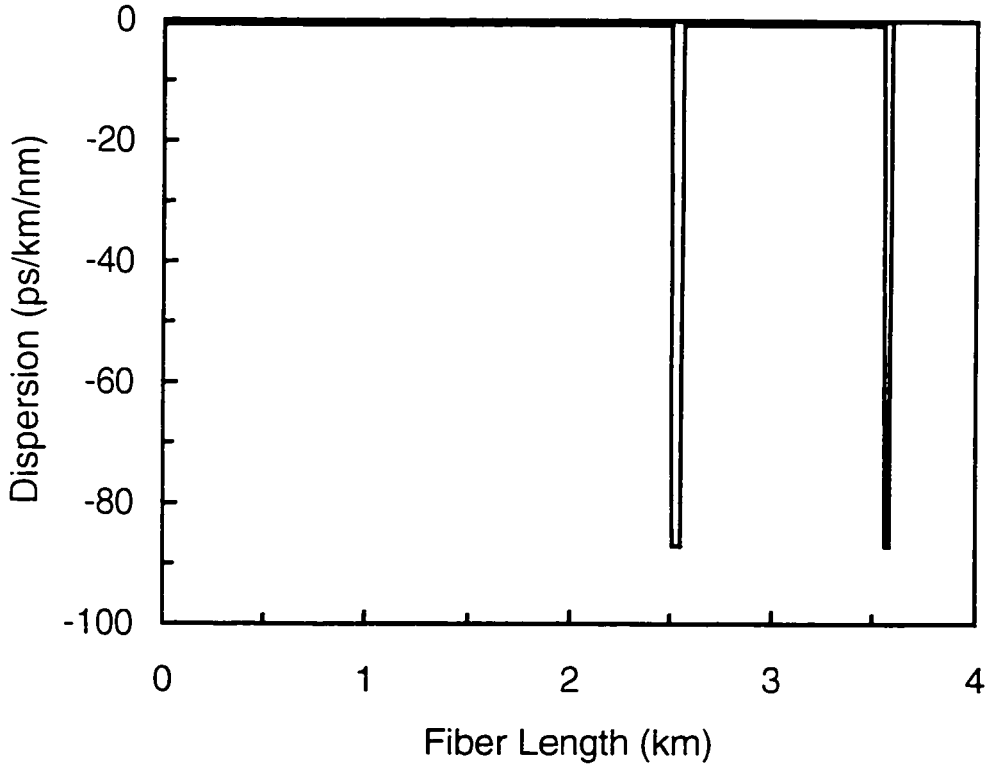

Fig. 3.2 CDPF structure used for generation of a dark soliton pulse train.

The average power of the sinusoidal beat signal launched into the first DSF piece is 125 mW. A splice loss of 0.4 dB between the fiber pieces was measured in the experimental system and used in the computations. When the sinusoidal beat signal propagates through the first DSF piece, the pulses broaden temporally and spectrally. This is due to the propagation of light in the normal dispersion regime of a fiber with nonlinear effects. This behavior is opposite to what happens to the bright soliton pulses, where temporal compression and spectral broadening take place. In the DCF pieces, more broadening occurs, as the dispersion is more effective than the nonlinearity of the fiber. In the second DSF piece, the effects of large amount of SPM-induced frequency chirp on the pulses, along with weak dispersion lead to significant pulse reshaping. The pulses become nearly rectangular, which represents the dark solitons' background. By adjusting the lengths of the fiber pieces, a train of dark soliton pulses can be generated. The total length of the CDPF structure used in the experiment is approximately 3.6 km.

Fig. 3.3(a) shows the results of the calculation for a dark soliton pulse train and its relative phases. A π phase jump appears at the center of these pulses. The intensity autocorrelation of the calculated train of dark soliton pulses is shown in Fig 3.3(b). The peaks shown in the figure represent the autocorrelation of the background of the dark soliton pulses. Note that the relation $\tau_p = 0.6482\tau_a$ typically used for bright solitons is not valid for dark solitons because of the different shapes of the electrical field profile of the two kinds of pulses. The intensity spectrum of the calculated train of dark soliton pulses is shown in Fig. 3.4.

(a)

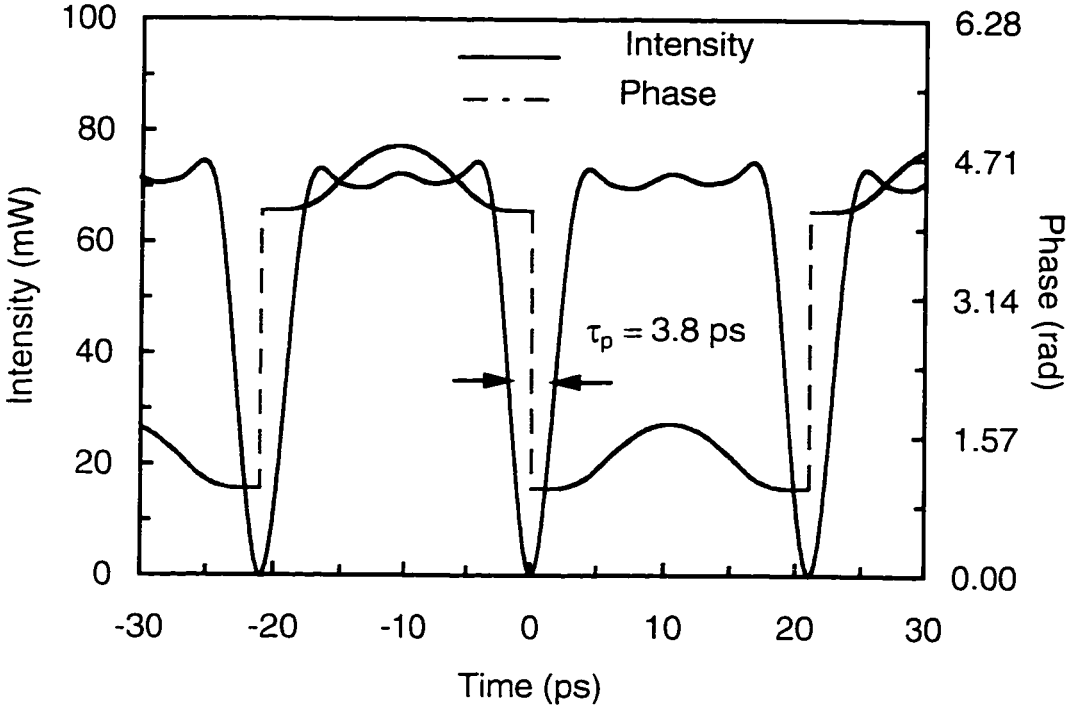

(b)

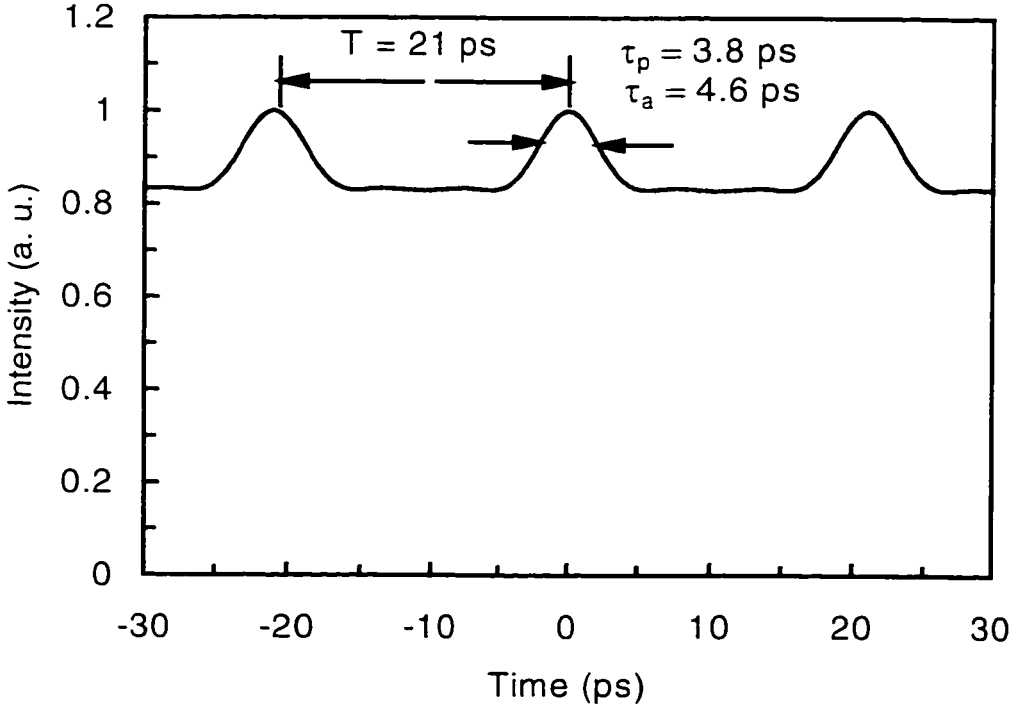

Fig. 3.3 Results of numerical calculation for dark soliton pulses. (a) Intensity and relative phase; note a π phase jump at the pulse center. (b) Intensity autocorrelation.

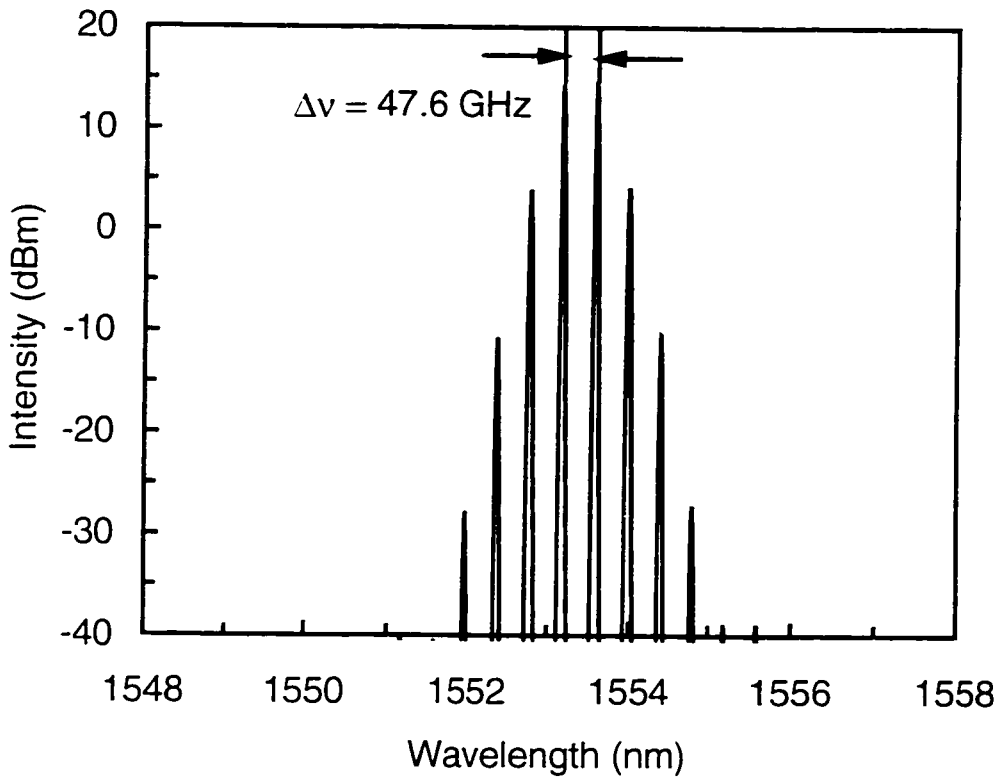

Fig. 3.4 Numerical calculation of the intensity spectrum for a dark soliton pulse train.

3.4 Experimental Results

Fig. 3.5 shows the experimental setup used to generate a train of dark soliton pulses using a CDPF structure which is similar to that used for the generation of bright soliton pulses. The CDPF structure resulting from the numerical calculation (shown in Fig. 3.2) is used to reshape the sinusoidal signal generated by beating two continuous single frequency signals from DFB laser diodes around 1553 nm. The wavelength separation of the two DFB lasers is related to the pulses repetition rate and can be controlled by tuning the temperature of the diodes. The repetition rate of the dark soliton train thus generated was 47.6 GHz. The generated signal was amplified to an average power of 125 mW using an EDFA followed by an erbium/ytterbium-doped fiber

amplifier. To reduce the effect of ASE produced by the first amplifier, a band-pass filter was used. The presence of ASE usually produces timing jitter at the receiver end, which is well-defined by the Gordan-Haus effect [60]. The high intensity signal applied to the CDPF structure exceeds the threshold for SBS. This nonlinear effect usually produces a backward-reflected power which prevents the generation of dark soliton pulse train. Stimulated Brillouin scattering was suppressed by externally modulating the DFB laser diodes with a 40 kHz sinusoidal signal. This frequency was optimized experimentally for the comblike structures, and it gives negligible SBS backward-reflected power. The modulation increases the laser linewidth to about 420 MHz. As a result, the SBS power threshold is increased to a level where input signals with average powers of approximately 22 dBm encounter negligible SBS effect. For more details on SBS, refer to Appendix A. The dark soliton pulses generated were measured with a second harmonic optical autocorrelator.

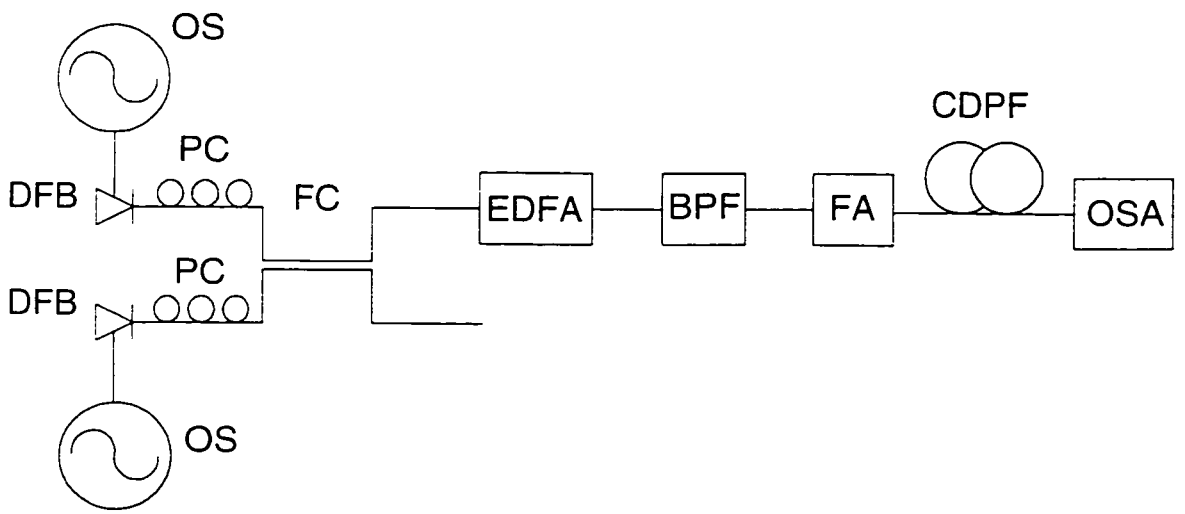

Fig. 3.5 Experimental setup used for generating dark soliton pulse train. BPF: bandpass filter; OS: 40 kHz oscillator; OSA: optical spectral analyzer; EDFA: erbium-doped fiber amplifier; DFB: distributed feedback laser diode; FC: 50/50% fused silica fiber coupler; CDPF: comblike dispersion profile fiber structure; PC: polarization controller; FA: high-power fiber amplifier.

Fig. 3.6 shows the measured intensity autocorrelation of the dark soliton pulse train. The measured FWHM of these pulses is τ_a=4.6 ps. The intensity autocorrelation measurement alone could be interpreted to be that of the intensity autocorrelation of any non-dark soliton pulses; however, due to: (i) the excellent agreement between the model and the experimental results for bright solitons presented in Chapter 2; (ii) the use of the same model for dark and bright solitons; (iii) the excellent agreement between the measured and calculated intensity autocorrelation of the dark soliton pulse trains shown in Fig. 3.6 and Fig. 3.3.b, respectively; and, (iv) the good match between the measured intensity spectrum shown in Fig. 3.7 for a dark soliton pulse train and the calculation in Fig. 3.4, the above results clearly indicate a train of dark solitons with a FWHM pulse width τ_p=3.8 ps.

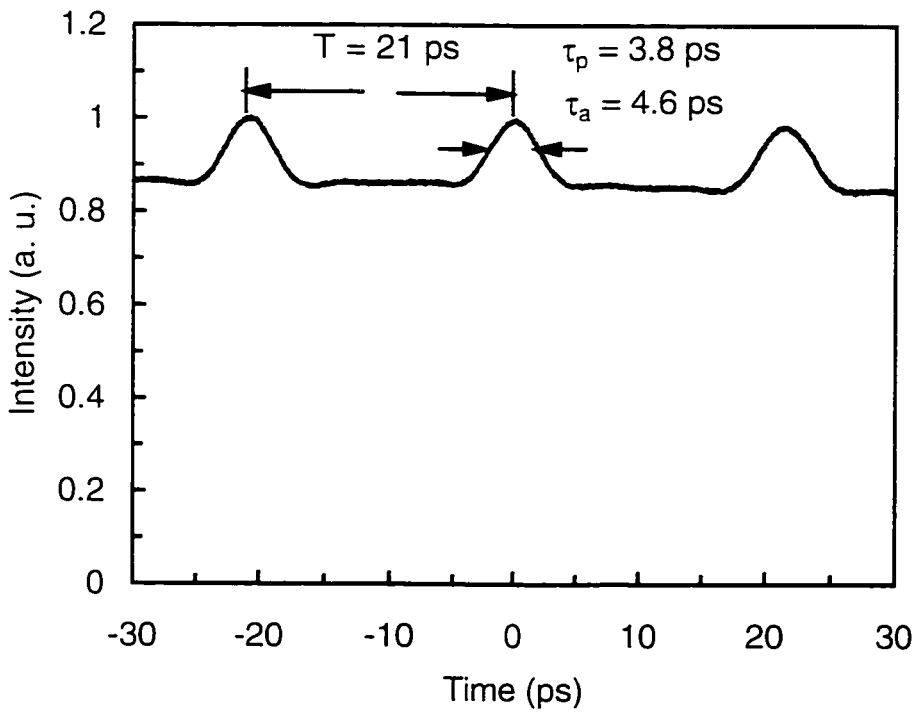

Fig. 3.6 Measured intensity autocorrelation for a dark soliton pulse train.

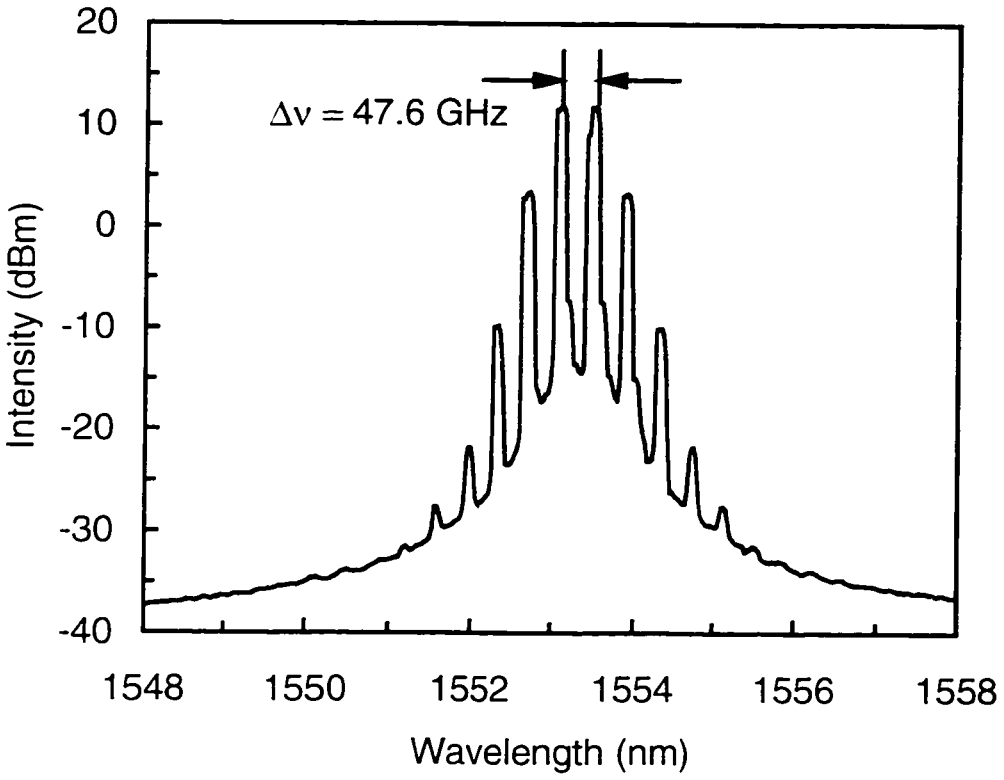

Fig. 3.7 Measured intensity spectrum for a dark soliton pulse train.

Chapter 4

All-Optical Soliton Demultiplexers

4.1 Introduction

As mentioned earlier, even the most advanced forms of electronics are currently unable to manipulate the signals that would be part of an ultra-high-speed system; hence, the need to seek optical means for basic operations required to interface low-rate signals to such a transmission system. These functions are those of multiplexer and demultiplexer. Of these, the demultiplexer is the more difficult problem. This chapter considers, in detail, one promising approach to constructing demultiplexer based on the NOLM.

The basic scheme of the NOLM is shown in Fig. 4.1. It consists of a fiber loop connected to two ports of a fiber coupler. On one side of the coupler is an input port from which an input signal can be split into two components at the opposite side ports, and an output port to which signal input from the opposite side ports can be collected in combined form. In the fiber loop there is a second device, a wavelength division multiplexer, that permits the introduction of a second control signal into the loop. The principle of operation of the loop is that the input signal is propagating in both directions, but the propagation characteristics are varied by the introduction of the control signal and the nonlinear nature of the loop to control the phase change of the signals that propagate in the different directions. This causes constructive interference for some input pulses and destructive interference for other pulses, thereby producing a "switching action". To achieve this effect, the control signal would have to be a high-intensity, low repetition

rate pulse stream. It may have the same wavelength but different states of polarization (SOP), different wavelengths but the same SOP, or different wavelengths and SOP. The state of polarization can be defined as the polarization type that the electrical field vector can take. This includes linear, elliptical, and circular polarization. The drift of the SOP of the signal and control pulses affects the demultiplexed signal. A modification to the NOLM is proposed here to overcome the effects of polarization drift of the input signals at the fiber loop on signal demultiplexing [61].

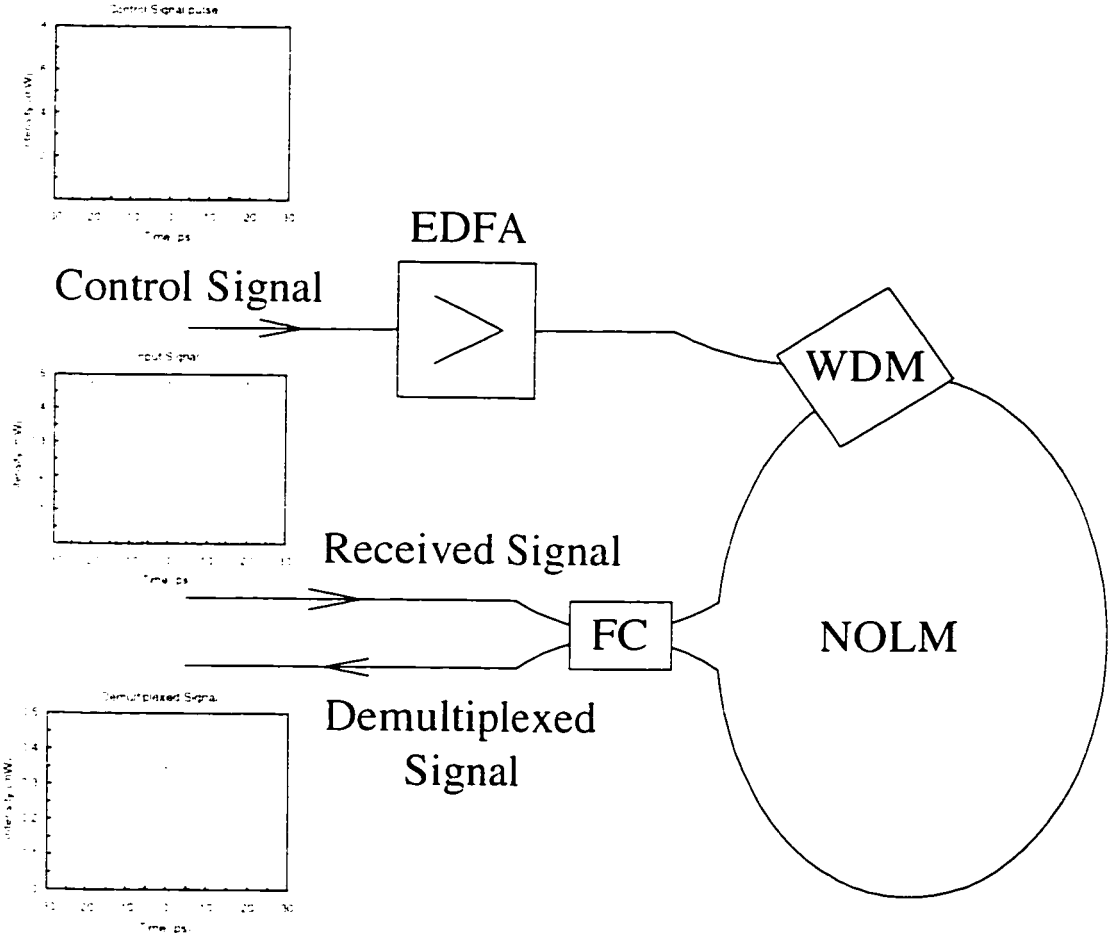

Fig. 4.1 All-optical signal demultiplexer using nonlinear optical loop mirror (NOLM). EDFA: erbium-doped fiber amplifier; WDM: wavelength division multiplexer; FC: fused silica fiber coupler.

In addition to the NOLM approach to TDM demultiplexing, it is possible to demultiplex multilevel soliton pulse trains by exploiting the Raman self-frequency shift (where signals suffer frequency shifts as they propagate in a fiber which varies with their width) [62]. Hatami-Hanza et al. [63] proposed a system in which the high-rate soliton pulse train was formed by multiplexing several different low-rate signals; each low-rate signal uses different pulse energy (i.e. amplitude and width), then recovering these low-rate signals in the form of a WDM signal from the combined signal through the Raman self-frequency shift effect. This system is discussed in the last section of this chapter where an experimental realization of such a demultiplexer is presented.

Section 4.2 of this chapter is devoted to the design of a NOLM demultiplexer. Subsection 4.2.1 presents a literature review of the techniques that use NOLM for signal demultiplexing. In Subsection 4.2.2, the theory of nonlinear loop mirror is discussed. The scheme for achieving polarization-insensitive all-optical demultiplexing is considered in Subsection 4.2.3. Section 4.3 presents an experimental implementation of signal demultiplexing in the frequency domain. Subsection 4.3.1 explains the theory of multilevel soliton communication systems. Subsection 4.3.2 presents soliton pulse compression as a technology necessary for multilevel soliton communication systems. In Subsection 4.3.3, the experimental demonstration of signal demultiplexing of a multilevel time-division multiplexed signal is presented.

4.2 Signal Demultiplexing In The Time Domain

4.2.1 Literature Review

The NOLM was first proposed by Doran et al. in 1988 [64] and then was experimentally demonstrated by them in 1989 [65]. The device was constructed from an optical directional coupler with its output terminals spliced together through a fiber cable which forms the loop shown in Fig. 4.2. This device is simple, stable in the sense that it is insensitive to thermal and external acoustic vibration, and it does not require interferometric adjustment, unlike other demonstrated schemes (Mach-Zehnder configuration, nonlinear polarization rotation, nonlinear coupling devices, and bi-modal fibers). Moreover, these other methods require large input-power levels to achieve the switching action (100-1000 W).

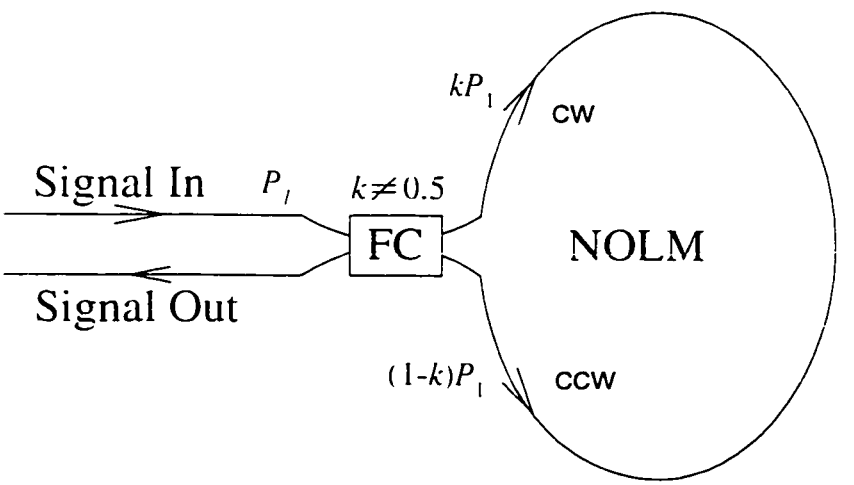

Fig. 4.2 Nonlinear optical loop mirror (NOLM) block diagram. FC: fiber coupler with k coupling ratio; cw: clockwise; ccw: counter clockwise. P_1 is the input signal power.

In the NOLM, the input signal to the coupler is split into two counter-propagating signals. They travel the same distance around the loop before returning to the coupler. Due to fiber nonlinearities that result from the intensity-dependent refractive index, each signal will acquire a phase shift ϕ produced by the SPM effect given by:

$$\phi = \frac{2\pi n_2 P_{in}}{\lambda A_{eff}} L, \tag{4.2.1}$$

where λ is the optical wavelength, A_{eff} is the effective mode area of the fiber, n_2 is the nonlinear refractive index, L is the loop length, and P_{in} is the input-pulse's peak power. If the coupling coefficient k is 0.5, the device acts as a mirror; i.e., an input pulse to the loop is reflected back to the same terminal because there is no differential phase shift between the two counter-propagating pulses. To break the symmetry in the loop, a coupler with $k \neq 0.5$ is used; or, as proposed by Fermann et al. in 1989 [66], an asymmetric element with loss or gain may be placed in the loop. In the latter case, a coupler with $k=0.5$ is used, which enhances the switching quality compared to the case with $k \neq 0.5$, because unequal signals inefficiently exploit the fiber nonlinearities. The new loop configuration is called a "nonlinear amplifier loop mirror". In his experiment, Fermann et al. [66] used a Nd^{+3} doped fiber amplifier with a gain of 6 dB to get a power level for the signal sufficient to produce switching of a few watts. Another experiment was carried out by Richardson et al. in 1990 [67], in which an EDFA was used in a fiber loop 336 m long. The required switching pulse's peak power was only 200 μW.

Another way to remove the symmetry between the counter-propagating signals was proposed by Blow et al. in 1990 [68]. A control signal at 1.3 μm was used to switch a

desired probe signal at 1.53 μm in a 500 m long loop of polarization maintaining fiber. In this method, a dichroic coupler is used to couple a high-power pump signal and a low-power (~5 mW) probe signal into the loop. The coupling ratios are 100:0% and 50:50% for the pump and the probe signals, respectively. XPM effect is exploited to break up the symmetry in the fiber loop, where one direction in the loop has both the pump and probe signals, while the other direction has only the probe signal. The direction that has both signals acquires a nonlinear phase shift produced by both XPM and SPM nonlinear effects. The other direction has only an SPM nonlinear effect. This configuration is the basis for all-optical signal demultiplexing. A similar experiment based on the same principle was conducted by Jinno et al. [69]. In 1990, Blow et al. [70] used two-wavelength operation of the nonlinear loop mirror as an all-optical demultiplexer. Switching of a signal generated from a DFB laser diode at 1.53 μm is demonstrated using pump pulses of 100 ps duration generated from a mode-locked Nd:YAG laser at 1.3 μm, with a repetition rate of approximately 76 MHz in a fiber loop 100 m long.

Different modifications to demultiplex optical signals in the multigigahertz range with lower signal power and simpler designs for the demultiplexers were realized. Long fiber loops were proposed to reduce the required switching power, but stability is then questionable. Nelson et al. [71] demultiplexed a signal at a rate of 20 GHz to 2.5 GHz, where a signal with a 10 GHz repetition rate was generated using a mode-locked laser diode at a wavelength of 1.53 μm. It was then interleaved to 20 GHz using a Mach-Zehnder interferometer. The pump signal was generated using a gain-switched DFB laser at 1.56 μm with a rate of 2.5 GHz. The nonlinear loop length was 6.4 km DSF and the

switching power was ~160 mW. In another experiment, Andrekson et al. [72] used the NOLM to demultiplex a data stream at 16, 32, and 64 Gbps. Two actively mode-locked external-cavity semiconductor laser diodes at 1.53 μm were used with a 3 nm separation between the control and data signals. The data steam (4Gbit/s) was externally modulated and passively time-division multiplexed into the desired data rate using a series of fiber couplers. The pulse widths at the input of the loop were approximately 12 ps and 7 ps for the control and data signals, respectively. The data and control signals traveled the same distance in a DSF fiber loop 14 km long. Switching was controlled using a dummy coupler and a polarization controller installed in the loop.

The nonlinear loop is polarization dependent, i.e. the signals change their state of polarization as they travel in the loop due to random fluctuations in the core shape and stress-induced anisotropy. This affects the required switching signal power and the quality of the switched pulses, which are measured in terms of the amount of energy reflected back to the input terminal. It is therefore, difficult to implement a system if the signal polarization fluctuates with time.

Different alternatives were proposed by Morioka et al. [73,74] to overcome this problem. They suggested either using a cross-splicing technique with two identical polarization-maintaining fibers in which their optical axes are rotated by 90 degrees, or using polarization rotation mirrors that are placed at the end of the fiber. In these methods, the polarization of the pump and the data signals are flipped to their orthogonal states which, as a result, cancels the fiber birefringence. By adopting this technique, a 60 Gbps data stream was demultiplexed using 1 km of polarization maintaining and absorption reducing (PANDA) fiber. In addition to canceling the fiber birefringence, this

configuration has the advantage of doubling the nonlinear interaction length. On the other hand, the group delay difference between the data and the pump signal is large (20 ps) which limits the device speed as a switch.

Uchiyama et al. [75] suggested another way of overcoming this problem by using a polarization diversity scheme. The control signal enters the fiber loop (which is constructed from PANDA fiber) using a WDM coupler at 45^{o} polarization. This ensures that the two orthogonal components of the control signal have the same amplitude. Signal pulses enter the loop using a 50/50% fiber coupler. The signal in each direction is further split into two orthogonally polarized components. The control signal components thus induced equal phase shifts identical to the two orthogonal polarization of the data signal in each path. When returning to the 50/50% fiber coupler, the counterparts of the polarization components of the counter-propagating signals interfere independently. To compensate for the transit-time delay of the fast and the slow axes in the loop, the fiber is cross spliced at the middle of the loop. In this experiment, a 32 Gbps stream is demultiplexed into 8 Gbps. The disadvantages of this method are the need for a special type of fiber in the loop which is also long (approximately 6 km), and the high peak power for the control signal to achieve signal demultiplexing.

An alternative approach was proposed by Bülow and Veith [76]. In their scheme the control pulses were generated using two orthogonal-polarized DFB lasers instead of one. The two states of polarization oscillate with the beat frequency of the two lasers. If the signal and the control pulses travel at the same speed in the loop (which is 12.5 km long dispersion shifted fiber), every point of the signal sees a different SOP of the control pulse. Therefore, the induced phase shifts of the signal will oscillate with the beat signal

frequency, which causes rapid change of the switching state of the loop. When the walk-off between the signal and the control pulses is enough for every point to see all SOPs of the control pulse and suffer a constant average cross-phase modulation, a polarization-independent switching is achieved. Another approach which will comply with the polarization sensitivity is proposed in Subsection 4.2.3.

4.2.2 Theory Of All-Optical Demultiplexing In NOLM

All-optical demultiplexing using nonlinear optical loop mirrors is the most promising demultiplexing technique in the time domain. These devices require lower pumping powers because the optical signals propagate for several kilometers before exiting the fiber loop, and it is possible to use commercially-available semiconductor laser diodes as the optical sources. The main problem the fiber loop encounters is the polarization sensitivity of the device to the state of polarization of the incoming signals (data and control) due to polarization fluctuations, and random fluctuations in the core shape and stress-induced anisotropy.

Signal demultiplexing in the NOLM is based on the cross-phase modulation nonlinear effect that exists in the fiber loop. This effect is generated by the interaction between a high-intensity, lower-rate control signal and a high-repetition-rate, low-intensity data signal as shown in Fig. 4.1. A 50/50% directional coupler is used to split the input data signal into the two arms of the fiber loop. A WDM is used to launch the control signal propagating in one direction of the loop. The XPM nonlinear effect is present for propagation in only one direction in the loop. This produces a phase difference between the counter-propagating data signals. To perform pulse demultiplexing (switching), the phase difference between the data pulses (at the control pulse temporal

positions) in each arm of the fiber loop should be π; otherwise, incomplete switching will take place and part of the switched pulse energy will be reflected back at the coupler input terminal. The cross-phase modulation effect between the signal and control pulses can be achieved in one of the following three cases [11]:

(I) the two signals have the same state of polarization but propagate at different center frequencies; (II) the two signals have different states of polarization but propagate at the same center frequencies; or (III) the two signals have different states of polarization and propagate at different center frequencies. For each of the above cases, the strength of the cross-phase modulation effect differs; and thus, so does the nonlinear phase shift produced.

I. Signals at the same state of polarization but with propagation at different center frequencies:

Using the quasi-monochromatic approximation (i.e., when the two copropagating signals center frequencies are close to each other) the effective nonlinear refractive index is given by:

$$\Delta n \approx n_2\left[\left|E_j\right|^2 + 2\left|E_{3-j}\right|^2\right] \qquad j = 1, 2, \tag{4.2.2}$$

where $\left|E_j\right|^2$ is the intensity of the propagating signal; and $n_2 = \frac{3}{8n}\mathrm{Re}(\chi^{(3)}_{xxxx})$ is the nonlinear refractive index, where n is the linear refractive index, and $\chi^{(3)}_{xxxx}$ is the third order susceptibility that gives the nonlinear effect. The propagating waves inside the fiber acquire an intensity-dependent nonlinear phase given by:

$$\phi_j^{NL} = \frac{\omega_j z}{c}\Delta n_j = \frac{\omega_j z n_2}{c}\left[\left|E_j\right|^2 + 2\left|E_{3-j}\right|^2\right], \qquad j = 1, 2, \tag{4.2.3}$$

where the first term is the phase produced by self-phase modulation and the second term is the phase produced by cross-phase modulation. It is noticed that the effect of XPM is twice that of SPM. The propagation equations that govern the two copropagating signals in the fiber loop are given by:

$$\frac{\partial A_1}{\partial Z} + \frac{1}{v_{g1}}\frac{\partial A_1}{\partial T} + \frac{i}{2}\beta_{21}\frac{\partial^2 A_1}{\partial T^2} + \frac{1}{2}\alpha_1 A_1 = i\gamma_1\left[|A_1|^2 + 2|A_2|^2\right]A_1, \text{ and} \tag{4.2.4}$$

$$\frac{\partial A_2}{\partial Z} + \frac{1}{v_{g2}}\frac{\partial A_2}{\partial T} + \frac{i}{2}\beta_{22}\frac{\partial^2 A_2}{\partial T^2} + \frac{1}{2}\alpha_2 A_2 = i\gamma_2\left[|A_2|^2 + 2|A_1|^2\right]A_2, \tag{4.2.5}$$

where v_{gj} $(j=1,2)$ is the group velocity of the propagating signal, and A_1 and A_2 are the slowly varying amplitudes of the signal and control electrical fields, respectively. The normalized coupled equations are:

$$i\left[\frac{\partial u}{\partial z} + \delta_0\frac{\partial u}{\partial t}\right] + \frac{i}{2}\frac{\partial^2 u}{\partial t^2} + i\Gamma u + \left[|u|^2 + 2a|v|^2\right]u = 0, \text{ and} \tag{4.2.6}$$

$$i\left[\frac{\partial v}{\partial z} + \delta_1\frac{\partial v}{\partial t}\right] + \frac{i}{2}\frac{\partial^2 v}{\partial t^2} + i\Gamma v + \left[|v|^2 + \frac{2}{a}|u|^2\right]v = 0, \tag{4.2.7}$$

where $a = \frac{T_u^2\gamma_1\beta_{22}}{T_v^2\gamma_2\beta_{21}}$, $\delta_0 = \frac{(\beta_{11}-\beta_{12})}{2|\beta_{21}|}T_u$, $\delta_1 = \frac{(\beta_{12}-\beta_{11})}{2|\beta_{22}|}T_v$, T_u and T_v are the 1/e intensity-point widths of the signal and control pulses, respectively.

II. Signals at different states of polarization but with propagation at the same center frequencies:

Single mode fiber is not truly single mode because it can support two degenerate modes that are polarized in two orthogonal directions. The mode-propagation constant β is slightly different at each axis due to the variation of the effective refractive index. As a result, light propagates at different speeds in each axis. The axis with the lower effective

mode index is called the "fast axis" and the other is called the "slow axis". This phenomenon is known as modal birefringence. The degree of modal birefringence $\overline{B}$ is defined by:

$$\overline{B} = \frac{|\beta_x - \beta_y|\lambda}{2\pi} = |n_x - n_y|. \tag{4.2.8}$$

where n_x and n_y are the effective mode indices. Through propagation in the fiber, power is exchanged between the two modes of polarization in a periodic manner with a period given by the beat length L_B:

$$L_B = \frac{2\pi}{|\beta_x - \beta_y|} = \frac{\lambda}{\overline{B}}. \tag{4.2.9}$$

For strongly birefringent fibers ($\overline{B} \sim 10^{-4}$), the beat length is approximately 1 cm.

When two linearly-polarized signals propagate in a fiber at the same central frequency and they are orthogonally polarized to each other, the total field in the fiber is given by:

$$\tilde{E}(r,t) = \mathrm{Re}\{(\hat{x}E_x + \hat{y}E_y)e^{-i\omega_0 t}\}, \tag{4.2.10}$$

where E_X and E_Y are the complex amplitudes of the two normally-polarized fields in the directions x and y. For strongly birefringent fibers, where the fiber length is $L>>L_B$, the effective nonlinear refractive index in the two normal axes is given by:

$$\Delta n_x = n_2(|E_x|^2 + \frac{2}{3}|E_y|^2), \text{ and} \tag{4.2.11}$$

$$\Delta n_y = n_2(|E_y|^2 + \frac{2}{3}|E_x|^2). \tag{4.2.12}$$

It is noticed that the XPM in this case is weaker than when two different frequency signals are used, due to the factor 2/3 (instead of 2) that appears in (4.2.2). The propagation equations governing pulse evolution of the two copropagating signals in the fiber loop are given by:

$$\frac{\partial A_x}{\partial Z} + \beta_{1x}\frac{\partial A_x}{\partial T} + \frac{i}{2}\beta_{2x}\frac{\partial^2 A_x}{\partial T^2} + \frac{1}{2}\alpha A_x = i\gamma\left[|A_x|^2 + \frac{2}{3}|A_y|^2\right]A_x, \text{ and} \tag{4.2.13}$$

$$\frac{\partial A_y}{\partial Z} + \beta_{1y}\frac{\partial A_y}{\partial T} + \frac{i}{2}\beta_{2y}\frac{\partial^2 A_y}{\partial T^2} + \frac{1}{2}\alpha A_y = i\gamma\left[|A_y|^2 + \frac{2}{3}|A_x|^2\right]A_y. \tag{4.2.14}$$

These equations may be solved numerically, assuming that the GVD in the two polarization axes are equal. The normalized equations are:

$$i\left[\frac{\partial u}{\partial z} + \delta_u\frac{\partial u}{\partial t}\right] + \frac{1}{2}\frac{\partial^2 u}{\partial t^2} + \left[|u|^2 + \frac{2}{3}c_2|v|^2\right]u = 0, \text{ and} \tag{4.2.15}$$

$$i\left[\frac{\partial v}{\partial z} + \delta_v\frac{\partial v}{\partial t}\right] + \frac{1}{2}\frac{\partial^2 v}{\partial t^2} + \left[|v|^2 + \frac{2}{3}c_2|u|^2\right]v = 0, \tag{4.2.16}$$

where $\delta_u = \frac{\beta_{1x} - \beta_{1y}}{2|\beta_2|}T_u$, $\delta_v = \frac{\beta_{1y} - \beta_{1x}}{2|\beta_2|}T_v$, and $c_2 = \left(\frac{T_u}{T_v}\right)^2$.

III. Signals at different states of polarization with propagation at different center frequencies:

The NOLM can be realized in practice using either DSF [71,77] or polarization maintaining fiber [78,79]. In the latter type, the input signals preserve their polarization through propagation. In birefringent fibers, and when the data and control signals propagate at different center frequencies and have different SOPs, the input signals not

only interact with each other through XPM on each axis, but also interact with the components at the other polarization axis for a total of four nonlinear interacting terms.

The general SOP for the input signals is elliptical where the electrical field vector can be defined by:

$$\vec{E}(r,t) = \mathrm{Re}\{(\hat{x}E_{1} + \hat{y}E_{2})e^{-i(\omega_0 t-\theta)}\}, \tag{4.2.17}$$

where θ is the angle defined between the electric field vector and the slow axis of polarization. The total electrical field of the two elliptically-polarized signals is:

$$\vec{E}(r,t) = \mathrm{Re}\{[(\hat{x}E_{1x} + \hat{y}E_{1y})e^{-i(\omega_0 t-\theta_1)} + (\hat{x}E_{2x} + \hat{y}E_{2y})e^{-i(\omega_0 t-\theta_2)}]\} \tag{4.2.18}$$

The slowly varying amplitudes of the two electrical fields are coupled in a strongly birefringent fiber defined by the following set of equations [80]:

$$\begin{aligned}
&\frac{\partial U_s}{\partial Z}+\beta_{1U}\frac{\partial U_s}{\partial T}+i\frac{1}{2}\beta_{2U}\frac{\partial^2 U_s}{\partial T^2}-i\gamma_U(|U_s|^2+\frac{2}{3}|U_f|^2+2|V_s|^2+\frac{2}{3}|V_f|^2)U_s+\frac{1}{2}\alpha U_s=0\\
&\frac{\partial U_f}{\partial Z}+\beta_{1U}\frac{\partial U_f}{\partial T}+i\frac{1}{2}\beta_{2U}\frac{\partial^2 U_f}{\partial T^2}-i\gamma_U(\frac{2}{3}|U_s|^2+|U_f|^2+\frac{2}{3}|V_s|^2+2|V_f|^2)U_f+\frac{1}{2}\alpha U_f=0\\
&\frac{\partial V_s}{\partial Z}+\beta_{1V}\frac{\partial V_s}{\partial T}+i\frac{1}{2}\beta_{2V}\frac{\partial^2 V_s}{\partial T^2}-i\gamma_V(2|U_s|^2+\frac{2}{3}|U_f|^2+|V_s|^2+\frac{2}{3}|V_f|^2)V_s+\frac{1}{2}\alpha V_s=0\\
&\frac{\partial V_f}{\partial Z}+\beta_{1V}\frac{\partial V_f}{\partial T}+i\frac{1}{2}\beta_{2V}\frac{\partial^2 V_f}{\partial T^2}-i\gamma_V(\frac{2}{3}|U_s|^2+2|U_f|^2+\frac{2}{3}|V_s|^2+|V_f|^2)V_f+\frac{1}{2}\alpha V_f=0.
\end{aligned} \tag{4.2.19}$$

where U_s and U_f are the slowly varying field envelopes for the data signal on the slow and fast axes of polarization, respectively; while V_s and V_f are the slowly varying field envelopes for the control signal on the slow and fast axes of polarization, respectively.

When the control and data pulses propagate in the birefringent fiber, the interaction between the pulses stops as the pulses separate from each other due to the

difference in the group velocities. This effect is known as pulses "walk-off". In this case, the group velocity of each component of the signal and control pulses at the two polarization axes is different from the other. The fiber length after which the two overlapping pulses separate from each other is known as the "walk-off length" $L_w = T_0/|d_{12}|$, where d_{12} is the walk-off parameter defined by:

$$d_{12} = \beta_1(\lambda_1) - \beta_1(\lambda_2). \tag{4.2.20}$$

where β_1 is evaluated using:

$$\beta_1 = \frac{1}{c}\left[n + \omega\frac{\partial n}{\partial \omega}\right]. \tag{4.2.21}$$

where n is the refractive index approximated using the Sellmeier equation given by:

$$n^2(\omega) = 1 + \sum_{j=1}^{m} \frac{B_j \omega_j^2}{\omega_j^2 - \omega^2}. \tag{4.2.22}$$

where ω is the optical signal frequency, ω_j is the resonance frequency of the medium at which the medium absorbs the electromagnetic radiation through oscillations of bound electrons, and B_j is the strength of resonance [11]. For bulk-fused silica, these parameters are found to be B_1=0.6961663, B_2=0.4079426, B_3=0.8974794, λ_1=0.0684043 μm, λ_2=0.1162414 μm, and λ_3=9.896161 μm, where $\lambda_j = 2\pi c/\omega_j$ and c is the velocity of light in a vacuum.

4.2.3 Polarization-Insensitive All-Optical Signal Demultiplexing

Polarization-insensitive all-optical demultiplexing using the NOLM was first implemented using polarization-maintaining fiber. These systems are sensitive to any drift in the SOP of the input signals, since a change in the SOP affects the power distribution on each of the polarization axes, and hence affects the switching quality at the loop output ports. To overcome this problem, a modification to the NOLM is proposed, which introduces a variable-gain erbium-doped fiber amplifier into the control signal input as shown in Fig. 4.3. The purpose of the variable gain is to allow the level of the control signal to be adjusted to compensate for the SOP of the input and control signals. By controlling the gain using a feedback signal derived from the loop output, the requirement for a careful initial adjustment of the SOP of the signals is removed, making the system polarization independent.

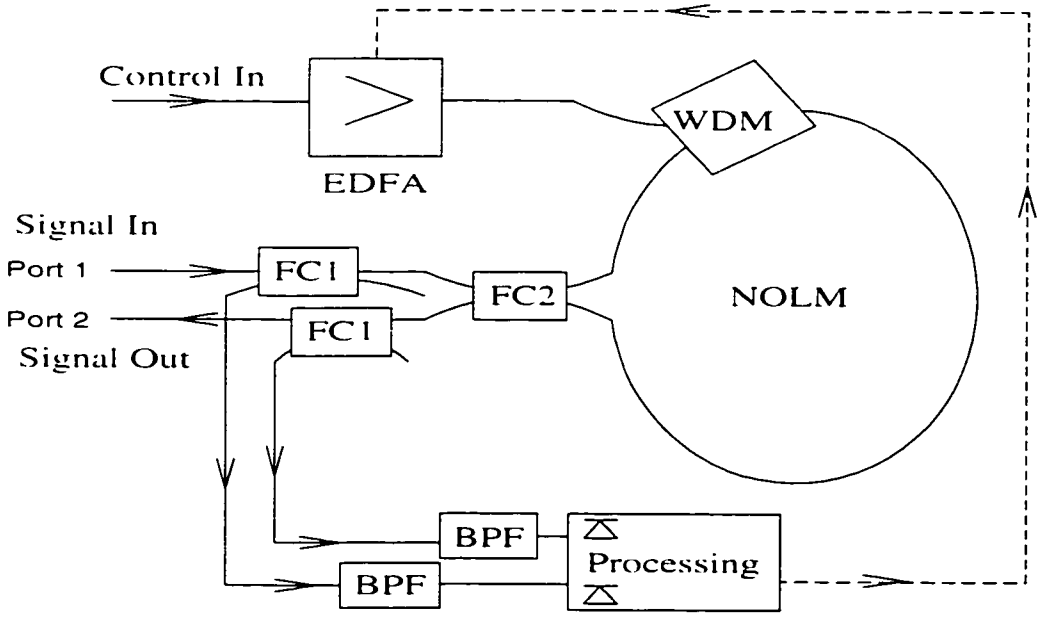

Fig. 4.3 Polarization-insensitive demultiplexer block diagram. FC1: 95/5% fiber coupler; FC2: 50/50% fiber coupler; EDFA: erbium-doped fiber amplifier; WDM: wavelength division multiplexer; BPF: bandpass filter.

A design of the system for a 50 GHz pulse train at a wavelength of 1553 nm was undertaken, wherein a 10 GHz control pulse train at 1545 nm is used, allowing every fifth pulse to be switched to port 2 of the loop. These pulse trains were assumed to be fundamental soliton pulse trains with a FWHM of 4 ps (data signal) and 10 ps (control signal). The control signal pulses were assumed to be wider than the data pulses, so that the interaction between control and data pulses would be greater in the face of pulse walk-off, and would also enable the data pulses to acquire a constant nonlinear phase shift across the pulse width. The parameters of the fiber were taken to match those of the available fiber which has a relative walk-off of 2 ps/km between the signal and control pulses, a fiber dispersion of 0.02 ps/(km nm) at 1553 nm and -0.5 ps/(km nm) at 1545 nm, and an effective core area of 55 μm^2.

The set of coupled equations given in (4.2.19) was solved numerically using the standard split-step Fourier method to determine the loop length required to produce the switching action [11]. To simplify the calculations, a normalised set of equations was used. The optimum loop length that produces complete switching under ideal conditions (neither pulse walk-off nor synchronisation offset between the signal and control pulses) was found to be 4.5 km.

The output of the loop was calculated over an entire range of possible polarization states for the signal and control pulses assuming no walk-off due to the fiber birefringence (by assuming that the fiber is cross spliced at the middle and the polarization axes are flipped). The losses due to cross-spliced the fiber are accounted for within the fiber attenuation which is assumed to equal 0.25 dB/km. It was found that

incomplete signal demultiplexing occurs whenever the power of the control pulses in each of the two principal polarization axes are unequal, the optimal state of polarization of the control pulses is 45^0, in agreement with [75], and any drift of the polarization of the signal and control pulses also results in incomplete switching. By changing the gain of the erbium-doped fiber amplifier which boosts the control pulse's power, it is possible to compensate for the effects of input-signal polarization drift. The gain of the optical amplifier is controlled using a feedback signal generated from the detected signal pulses at the output ports of the NOLM.

Fig. 4.4 shows the signal pulse train fed into the NOLM and the resulting switching at the output ports of the loop for 45^0 SOP for both the signal and control pulses. The signal and control pulses are synchronised at the loop input. The switched pulses of the signal train are monitored at port 2, and the unswitched part is reflected back to port 1. It was observed that a small part of the switched pulse around its center is reflected back. This is mainly due to an unequal XPM effect produced over the desired signal pulse. Fig. 4.5 shows the required gain of the EDFA for a full range of possible SOP of the signal and control pulses expressed in terms of the angles θ_s and θ_c, respectively. The angles θ_s and θ_c are defined between the slow-polarization principal axis of the fiber and the directions of the electrical field vectors of the signal and control pulses, respectively. The required EDFA gain ranges from approximately 16 dB to 21dB.

The effect of pulses walk-off can be alleviated by delaying the signal and control pulses with respect to each other at the loop input. This delay prolongs the pulses interaction in the loop. It was found that a 1.7 ps synchronisation offset between the signal and control pulses at the loop input minimises the effect of a walk-off. Fig. 4.6

shows the required EDFA gain when a 1.7 ps synchronisation offset is used for a full range of possible SOP of the signal and control pulses. It is clear that lower amplifier gain (14.5 dB - 19.5 dB) is required to perform signal switching. The effect of the control pulses SOPs drift at the loop input on the required amplifier gain is shown in Fig. 4.7 for a 45^{0} SOP with 5^{0} change. The amplifier gain should be adjusted within 1 dB to compensate for such a drift. It is therefore, important to account for any drift in the SOP of the incoming signals to improve the quality of signal demultiplexing.

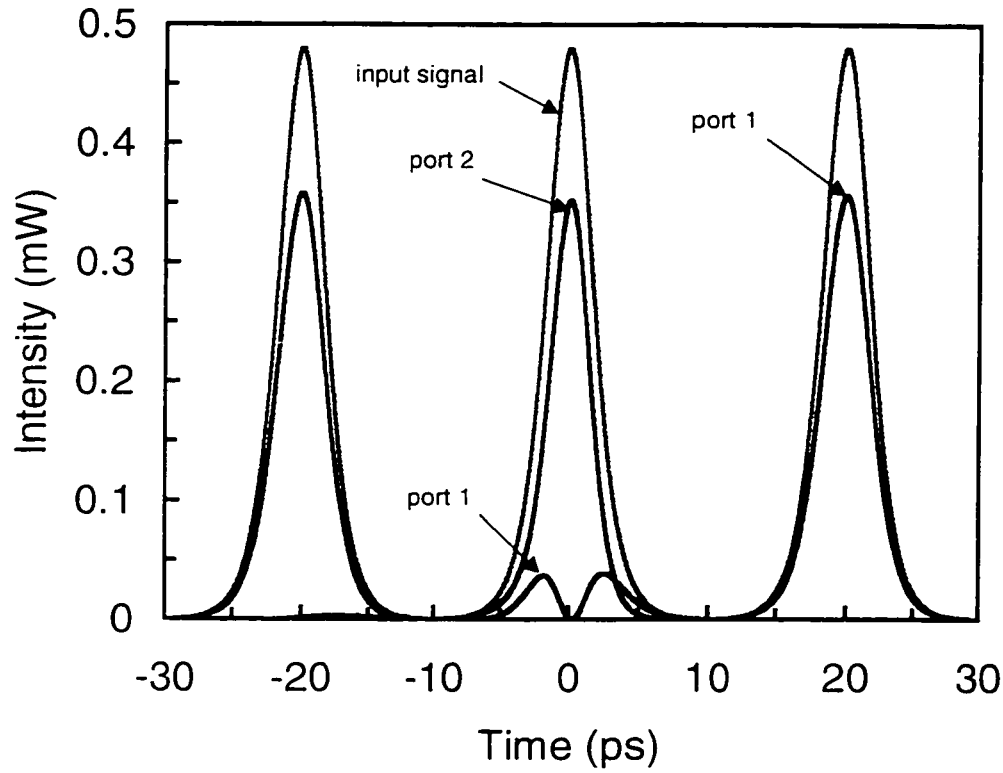

Fig. 4.4 The input signal and the resultant switched pulses at the loop output ports. Note the incomplete switching at the middle pulse.

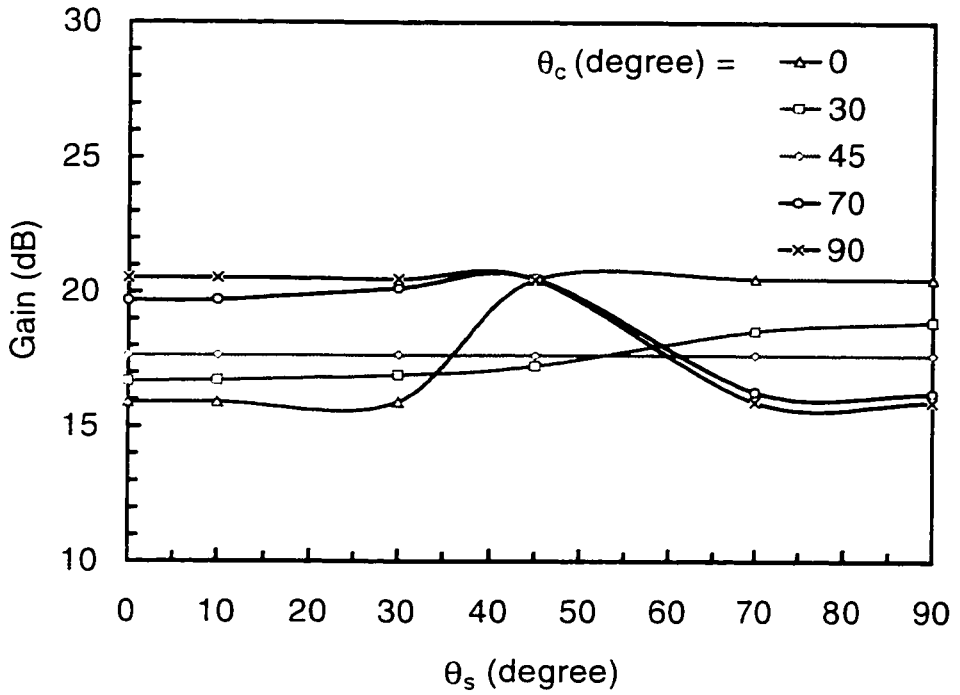

Fig. 4.5 Required erbium-doped fiber amplifier (EDFA) gain for different signal and control pulses state of polarisation (SOP).

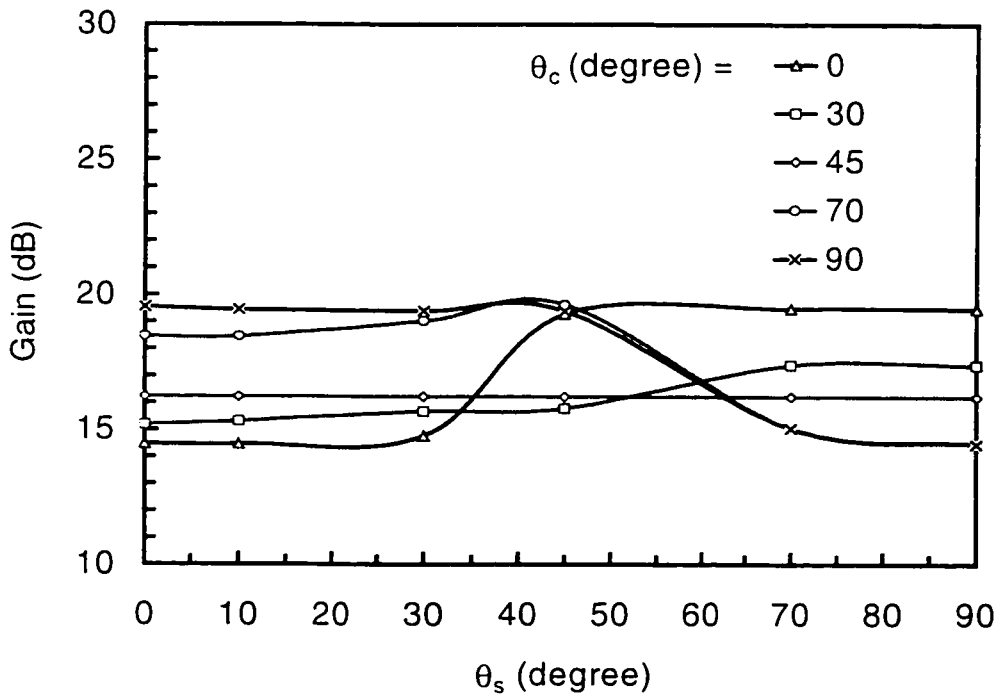

Fig. 4.6 Required EDFA gain for 1.7 ps synchronization offset between the signal and control pulses.

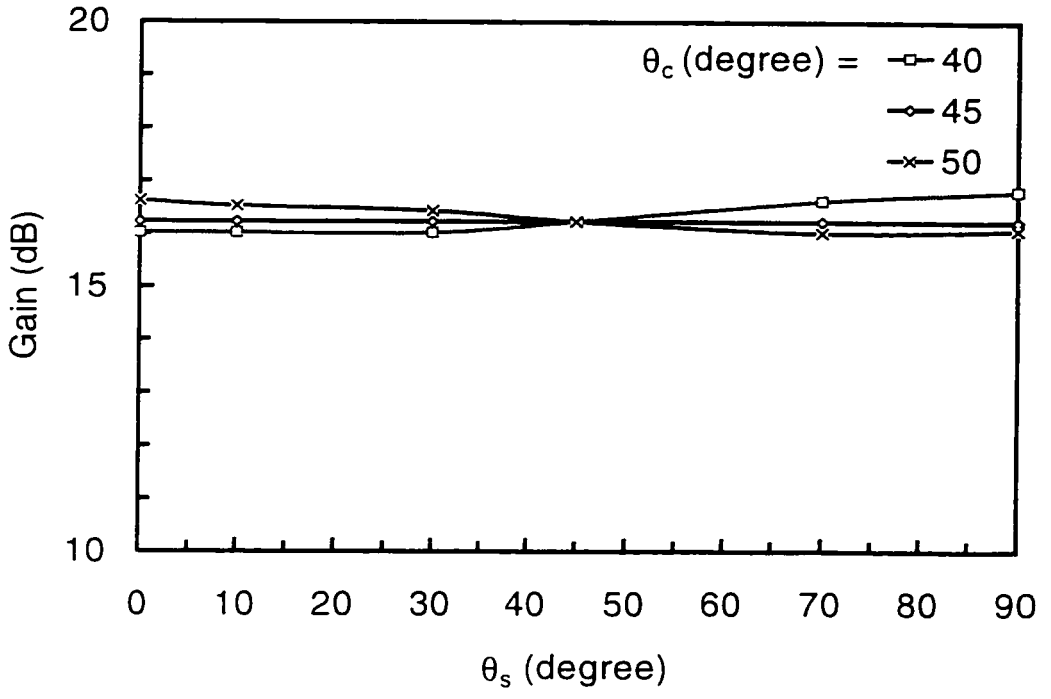

Fig. 4.7 Required EDFA gain for control pulses' state of polarization drift.

4.3 Signal Demultiplexing In The Frequency Domain

All-optical signal demultiplexing in the time domain was demonstrated using the nonlinear optical loop mirror. For all the experiments conducted in the literature, the data signal launched into the NOLM was generated by either time division multiplexing of lower-rate signals or by data interleaving. In both cases, a clock recovery circuit that employs all-optical phase-locked loops is needed to generate the signal required to synchronize between the data and control pulses at the NOLM ports. This is not easy to construct. To avoid this complexity, an all-optical multilevel soliton transmission system was proposed [63], which uses the Raman self-frequency shift nonlinear effect to perform

demultiplexing. A key technology to implement this system is soliton pulse compression. Pulse compression helps separating the data channels in the frequency domain to enable signal demultiplexing. In the following subsections, the theory of multilevel soliton communication systems is discussed, an experimental demonstration of the system feasibility is presented, and a device for pulse compression using a comblike dispersion profile fiber structure is developed.

4.3.1 Theory of Multilevel Soliton Communication Systems

A multilevel soliton communication system is based on two basic principles: soliton eigenvalues [81] and the Raman self-frequency shift [82]. Each soliton pulse can be described by a set of parameters called "eigenvalues" (in particular the imaginary part), which remain constant as they propagate in single mode fiber according to the NSE. For a lossless NSE and an initial pulse shape of $Q(T,0)=A\,sech(T)$; where Q is the electric field envelope, the eigenvalues are given by:

$$i[A-n+\frac{1}{2}]=i\frac{\eta_n}{2}. \tag{4.3.1}$$

with $A-\frac{1}{2}<N\leq A+\frac{1}{2}$, where η_n is the eigenvalue, and N is the number of eigenvalues. In the presence of fiber attenuation, the eigenvalues deviate from those determined from the initial pulse shape. The use of a guiding center-soliton concept overcomes this problem as shown in [81].

The Raman self-frequency shift effect was discovered by Mitschke and Mollenauer [83]. It was found that a soliton pulse experiences a continuous frequency downshift as it propagates through a fiber. The amount of frequency shift depends on

both the pulse peak power and soliton pulse width. The rate of Raman self-frequency shift for a fundamental soliton pulse is given by [84]:

$$\frac{dv_0}{dz} = \frac{2.2\times10^{-3} g(\tau)(ps)\beta_2(ps^2/km)}{\tau^4(ps^4)}, \tag{4.3.2}$$

where τ is the FWHM of the pulse, and $g(\tau)$ is related to the slope of the Raman gain spectrum of the fiber (typical value of ~ 1ps for few picosecond soliton pulses and ~2ps for subpicosecond soliton pulses).

A multilevel communication system is constructed, restricting each channel to transmit its data using a different soliton energy (i.e. amplitude and pulse width). The time multiplexed signal can be expressed as:

$$Q(T,0) = \sum_{i=1}^{n} A_i \operatorname{sech}(A_i t - T_i), \tag{4.3.3}$$

where A_i is the relative amplitude of fundamental solitons to the widest pulse with amplitude A_1=1, and T_i represents the pulse temporal position in the transmitted signal time frame. The transmitted signal represents a multilevel amplitude shift keying, time-division multiplexed (ASK/TDM) signal. At the receiver end, the ASK/TDM signal is converted to a WDM signal by exploiting the Raman self-frequency shift nonlinear effect. From (4.3.2), the Raman self-frequency shift is inversely proportional to the fourth order of the pulse width. Therefore, the received signal is compressed to the subpicosecond regime in order to obtain a large separation between the data channels in the frequency domain. A filter bank may then be used to select the desired channel. The implementation of this approach rests on the construction of a device that is capable of compressing the received pulses. This can be accomplished by using comblike dispersion

profile fiber structures similar to those employed to generate bright and dark soliton pulse trains. The design of such a device which allows pulse widths as low as 200 fs is considered in the next subsection [85].

4.3.2 Soliton Pulse Compressor

Pulse compression to picosecond or subpicosecond regimes has been demonstrated using different schemes such as fiber gratings [86], stimulated Raman effect with XPM in a single mode fiber [87], dispersion decreasing fiber [88], or step-like dispersion profiling in optical fiber [89]. In systems incorporating fiber gratings, there is usually a large insertion loss that ranges between 2 dB and 6 dB. In addition, these devices are relatively expensive. The other techniques require long fibers or a special type of fiber (in the case of DDF). The fabrication of the DDF has many manufacturing problems which make it noncommercial at present.

In this thesis, the CDPF structure is used to compress optical soliton pulses at 1547 nm to approximately 300 fs. The fiber structure is constructed from 12 alternating pieces of commercially-available DSF and STF. The fiber structure is 380 m long with only 1.1 dB total insertion loss. The CDPF structure was designed based on numerical calculations in an automated process to achieve the desired pulse compression. The design process is similar to that used in Section 2.4 for designing the CDPF structure for bright solitons. The required pulse compression determines the length and the number of fiber pieces in the structure. For example, 20 pieces with a total length of approximately 400 m are necessary to compress a 2.2 ps soliton pulse to 200 fs. The fiber parameters used in the calculation are either measured (as is the case for the fiber nonlinear ratio (n_2/A_{eff}) [42], splice loss between the fiber pieces, and the fiber piece length), or specified

by the fiber manufacturer such as the zero dispersion wavelength, zero dispersion slope, and the fiber attenuation. As a result, a very good agreement between the experiments conducted and the numerical calculations is achieved without any fitting parameter. Fig. 4.8 shows the experimental setup used to compress 2.2 ps soliton pulses generated by a Figure-8 fiber laser. The pulses generated are amplified to the required energy, using an EDFA, and launched into the CDPF structure. The output pulses are measured using a second harmonic optical autocorrelator.

Fig. 4.9 shows a block diagram of a Figure-8 fiber laser developed at the NRC. It is a mode-locked fiber laser that incorporates a nonlinear fiber loop. The laser cavity consists of two loops, a linear loop that contains an output fiber coupler, optical isolator, and a tuning filter, and a nonlinear loop that is known as the nonlinear amplifying loop mirror. This loop has an active fiber (erbium-doped fiber) where the amplification of the propagated pulses is achieved by using a 980 nm pump. The propagated pulses in both directions of the loop encounter SPM effect and they exit the loop if they acquire π phase difference. The generated pulses are solitons at low repetition rate (3.2 MHz). A piezo-electric transducer is used to initiate the mode-locked operation.

Fig. 4.10 shows the intensity autocorrelation of the input pulse launched into the fiber structure and the resultant compressed pulse. The measured autocorrelation pulse full width at half maximum τ_a=460 fs, which corresponds to a pulse with a width τ_p=300 fs. The compressed pulse is background-noise and pedestal free. The fiber structure is able to compress pulses within a 20 nm signal wavelength range. Various designs of the CDPF structure produce different amounts of pulse compression.

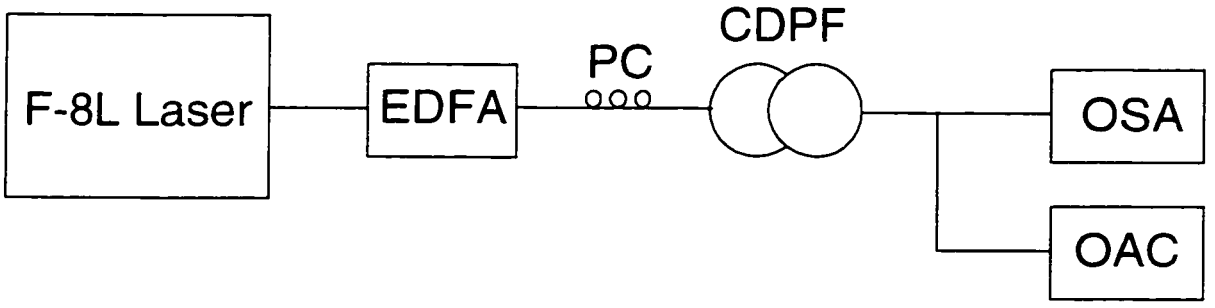

Fig. 4.8 Experimental setup used for pulse compression. EDFA: erbium-doped fiber amplifier: OSA: optical spectrum analyzer; OAC: optical autocorrelator; PC: polarization controller; CDPF: comblike dispersion profile fiber structure; F-8L: figure-8 fiber laser.

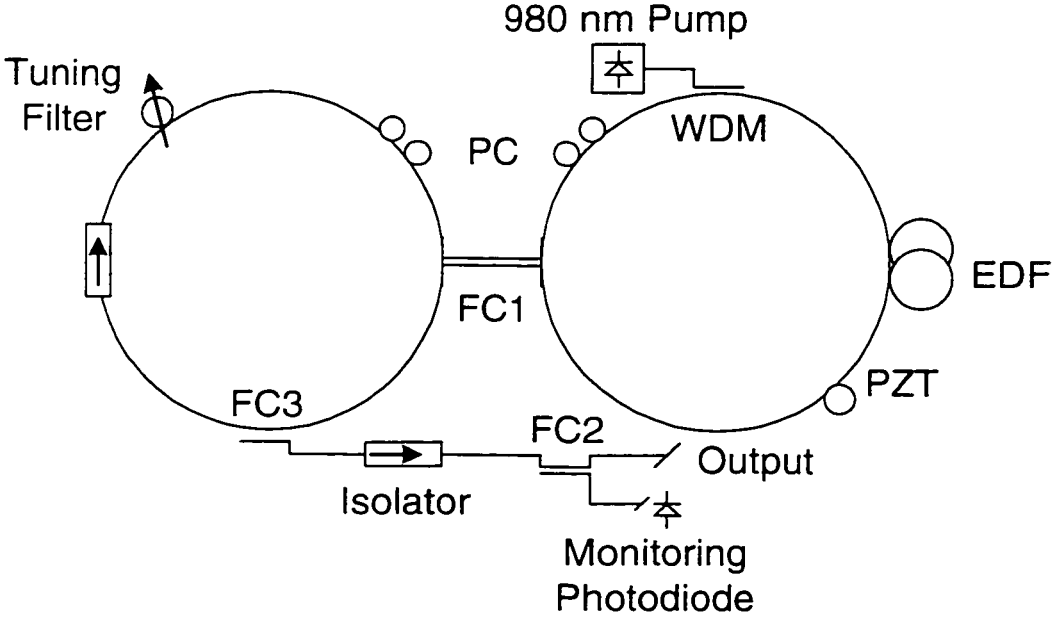

Fig. 4.9 Figure-8 fiber laser block diagram, WDM: wavelength division multiplexer; PC: polarization controller; FC1: 50/50 % fiber coupler; FC2: 10/90% fiber coupler; FC3: 20/80% fiber coupler; EDF: erbium-doped fiber; PZT: piezo-electric transducer.

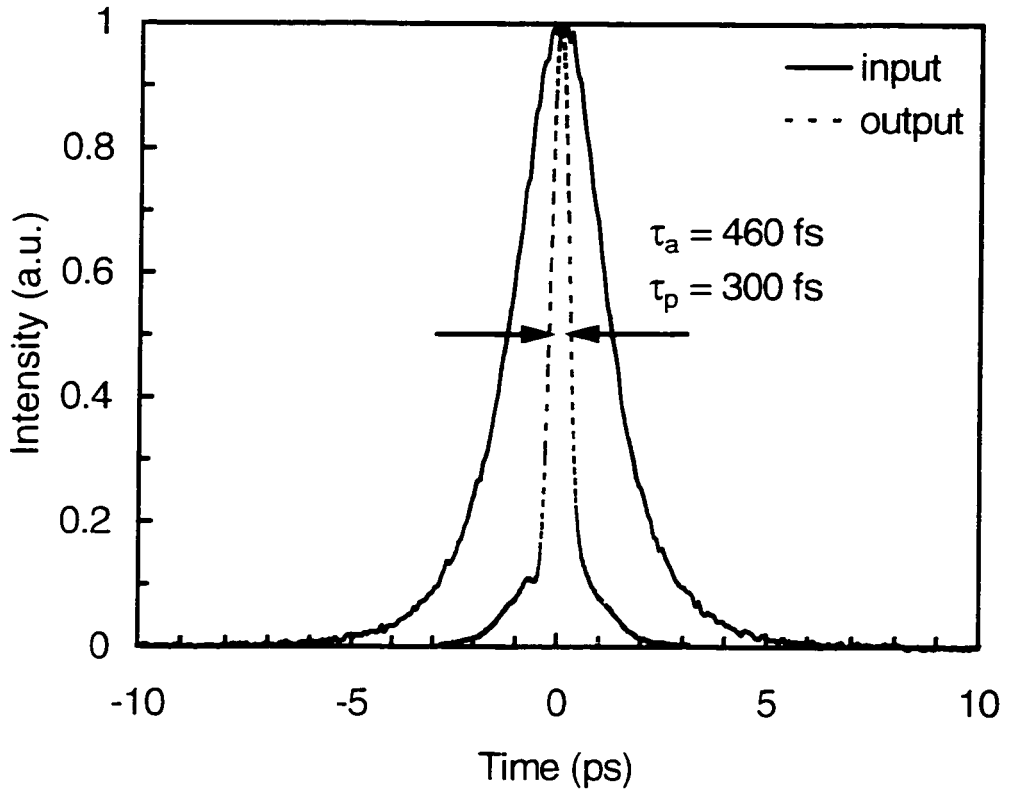

Fig. 4.10 Intensity autocorrelation of the input soliton pulse and of the resulting compressed pulse. τ_p and τ_a are the pulse and autocorrelation full width at half maximum, respectively.

4.3.3 Experimental Demonstration of ASK/TDM Signal Demultiplexing

Fig. 4.11 shows the experimental setup used to demonstrate the feasibility of all-optical demultiplexing of an ASK/TDM signal in the frequency domain. A figure-8 fiber laser is used as an optical source that produces soliton-like pulses. The ASK/TDM signal is constructed by splitting the laser output into four branches using three 50/50% fiber couplers. At each branch, an attenuator and a time-delay element are placed to control the power level and the temporal position of the soliton pulse in the signal time frame. These branches are then combined to form a burst of soliton pulses. Pulses with a FWHM of 2

ps at 1547.5 nm are interleaved to produce a burst of 40 Gbps data stream. The signal burst is amplified using an EDFA to produce high-order solitons. The peak powers of the individual pulses are estimated to be 18, 23, 30 and 38 Watts. The optical signal is then launched into 11.5 km, and 34.5 km, of STF.

The soliton pulses experience compression as they propagate in the fiber, due to the high-order soliton effect. These pulses then experience soliton fission due to the Raman self-frequency shift [90]. Due to soliton fission, each propagated soliton pulse produces a number of new soliton pulses equal to the number of eigenvalues N. Fig. 4.12 shows the spectrum of the multiplexed signal after propagating at 11.5 km and 34.5 km in the fiber. The intensity spectrum at 11.5 km shows a noticeable overlap between the four channels, which makes detection difficult. Therefore, a larger wavelength separation is necessary. This can be achieved either by increasing the ASK/TDM signal power launched into the fiber or by propagating the signal further. The resulting intensity spectrum after propagating at 34.5 km is also shown in Fig. 4.12. Each channel experienced spectral narrowing due to the pulses' temporal broadening as a result of fiber attenuation. Each channel was then selected, using a bandpass filter. Fig. 4.13.a and Fig. 4.13.b show the intensity spectrum and the intensity autocorrelation of channel 2, respectively. The crosstalk from the other channels is less than 28 dB. The autocorrelation shows a soliton-like pulse with a FWHM of 8 ps.

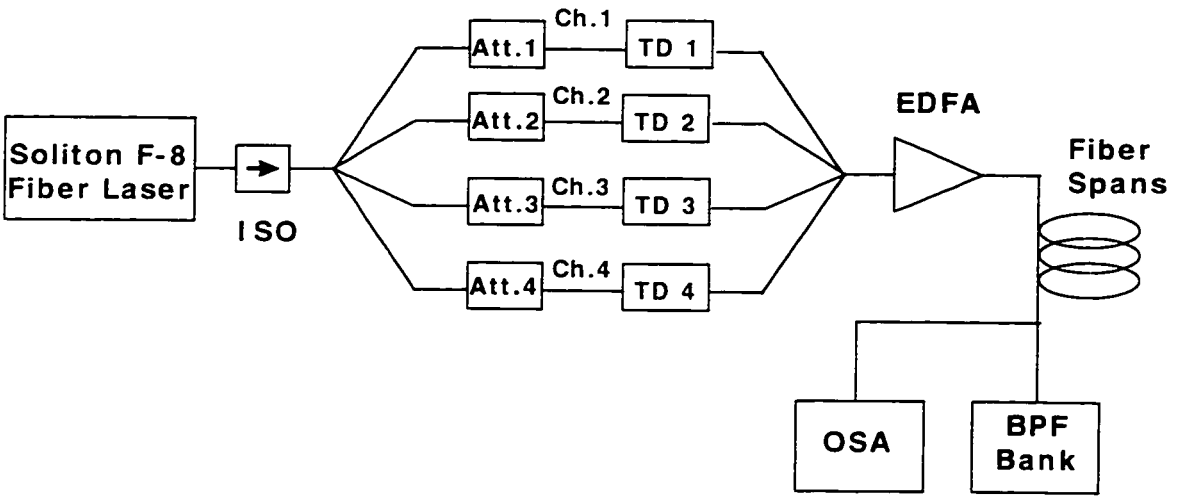

Fig. 4.11 Experiment setup used for signal demultiplexing in the frequency domain. ISO: optical isolator; Att.: attenuator; TD: time delay; EDFA: erbium-doped fiber amplifier; BPF: bandpass filter; OSA: optical spectrum analyzer.

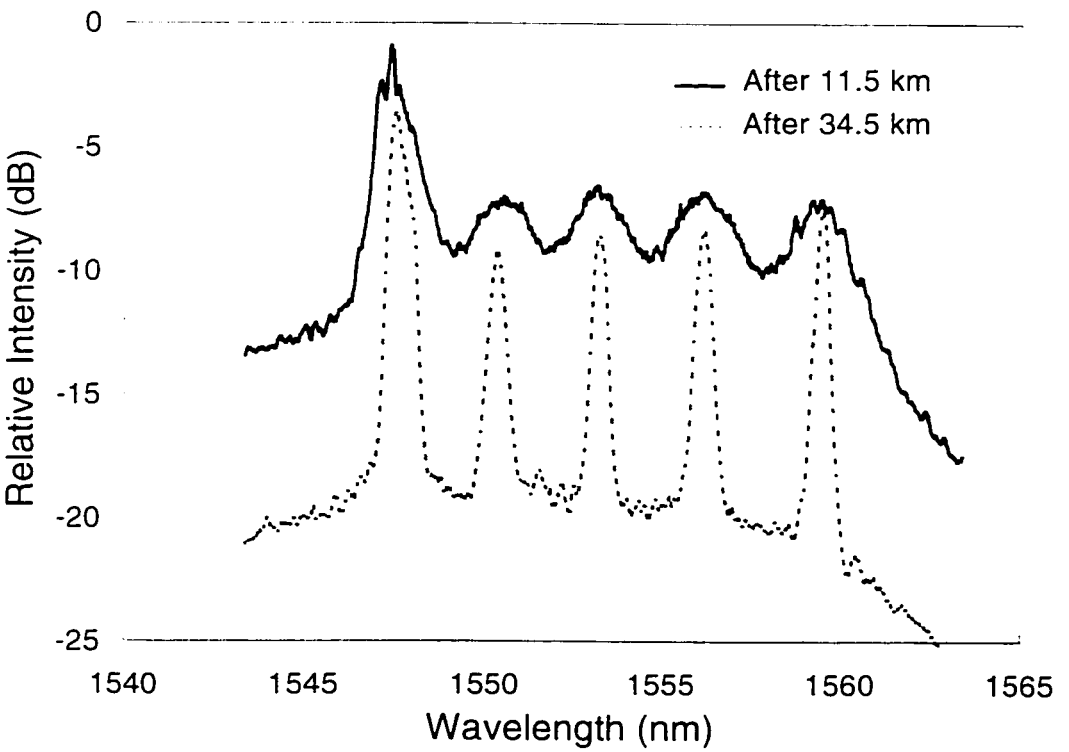

Fig 4.12 Intensity spectrum of the signal after 11.5 km and 34.5 km propagation through a standard telecommunication fiber (STF).

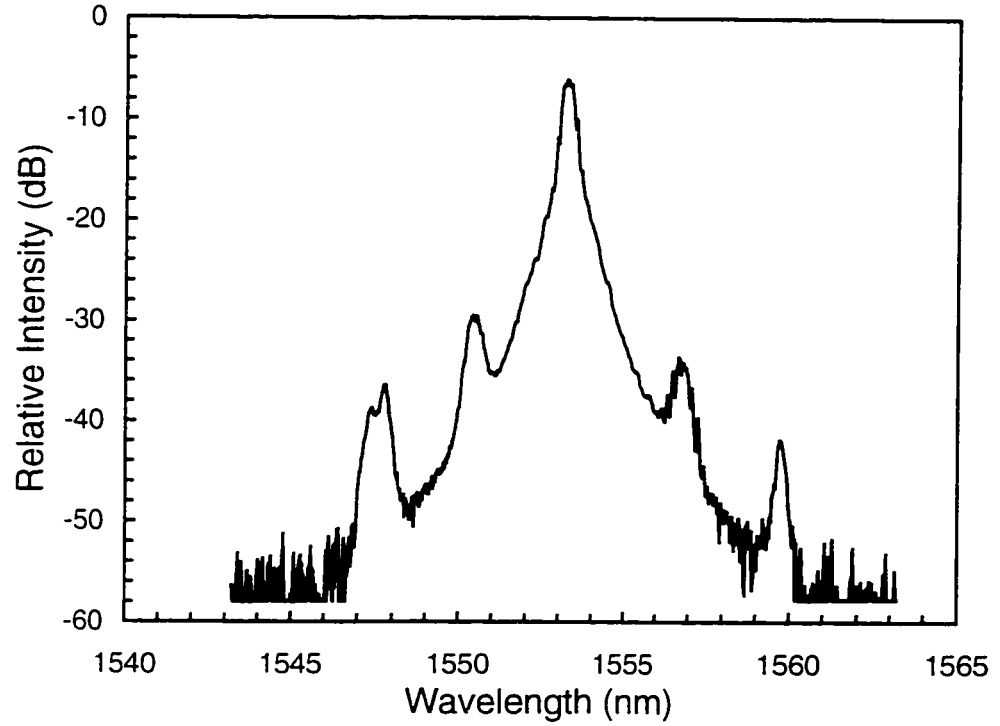

Fig. 4.13(a) Intensity spectrum of channel 2 after being demultiplexed using a bandpass filter (BPF).

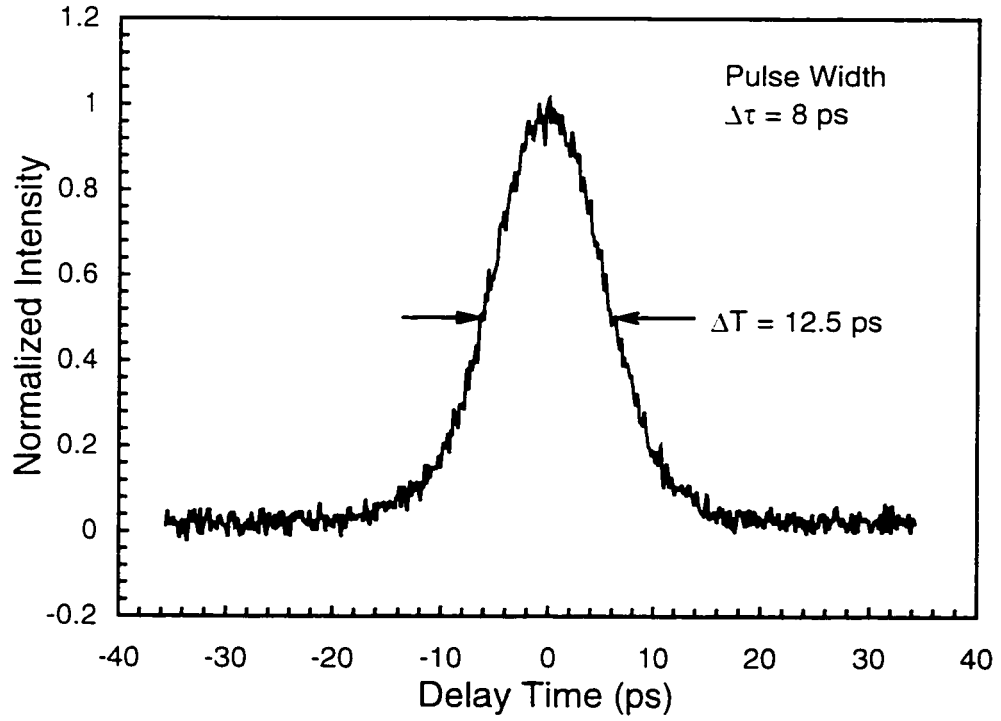

Fig. 4.13(b) Intensity autocorrelation of the demultiplexed channel 2.

Chapter 5

Fiber Link Characterization

5.1 Introduction

As mentioned earlier, it is important for the optical fiber communication link designer to have all the parameters that define the physical phenomena in the fiber. The significant phenomena necessary to describe the propagation of light pulses of widths as short as 50 fs in SMF are well described by the generalized nonlinear Schrödinger equation given by Kodama and Hasegawa [91]:

$$\frac{\partial A}{\partial Z}+\beta_1\frac{\partial A}{\partial T}+i\frac{1}{2}\beta_2\frac{\partial^2 A}{\partial T^2}+\frac{1}{2}\alpha A-i\gamma|A|^2A=\frac{1}{6}\beta_3\frac{\partial^3 A}{\partial T^3}-\frac{\gamma}{\omega_0}\frac{\partial}{\partial T}(|A|^2A)-i\gamma T_R A\frac{\partial|A|^2}{\partial T}, \tag{5.1.1}$$

where the left-hand side represents the simplified NSE presented in Chapter 2 and given by equation (2.2.5), which is suitable for propagation of light pulses in the picosecond regime; β_3 is the third order dispersion; and T_R is the Raman time constant (which is related to the slope of the Raman gain). Fiber dispersion and attenuation are well known and are usually specified by the manufacturer. The other parameters, such as the fiber nonlinear ratio (n_2/A_{eff}) that describes the strength of the fiber nonlinearity and T_R are under investigation. Different values have been assumed for T_R in the literature, ranging from 3 fs to 6 fs [92-95]. These values produce significantly different results when solving (5.1.1); therefore, it is important to determine its value with reasonable accuracy.

In this chapter, two experiments which were conducted to measure the fiber nonlinear ratio and the Raman time constant are presented. In Section 5.2, a simple and

reliable technique for measuring the fiber nonlinear ratio is presented. The nonlinear ratio was measured in STF, DSF and DCF. In Section 5.3, the Raman time constant is measured in SMF around 1550 nm.

5.2 Fiber Nonlinear Ratio (n_2/A_{eff}) Measurement

5.2.1 Introduction

Future optical communication systems will have to provide ultra-high-speed transmission rates over long distances. An important limitation for such systems is imposed by the fiber's nonlinearity typically described by the coefficient

$$\gamma = \frac{2\pi}{\lambda}\frac{n_2}{A_{eff}}. \qquad (5.2.1)$$

where n_2 is the nonlinear refractive index of the fiber, A_{eff} is the fiber effective core area, and λ is the wavelength of the propagating signal. To design systems for such applications, it is necessary to determine the ratio n_2/A_{eff} with high precision. In this thesis, the ratio n_2/A_{eff} is measured not the separate parameters n_2 and A_{eff} as only the ratio is necessary to evaluate the strength of the fiber nonlinearity required in modelling pulse propagation (see equation (5.2.1)).

The nonlinear properties of the fibers have been determined recently by measuring the SPM effect using propagation of a short pulse at 1.3 μm through the tested fibers [96]. A different technique was employed by Kato et al. [97], where the XPM effect between a low-power probe signal at 1550 nm and a high-power pump signal at 1540 nm was used to find the nonlinear characteristics of the fiber. The ratio n_2/A_{eff} was also measured based on the generation of beating frequency components through FWM of two DFB laser diodes operating around 1555 nm [98]. In this scheme, two CW laser

beams, with frequencies ν_1 and ν_2, are launched into the fiber under test. The two beams with different power levels generate new beat frequencies $(2\nu_1-\nu_2)$ and $(2\nu_2-\nu_1)$ through the FWM process. All these schemes measure the nonlinear ratio of the fiber and an independent measurement of the effective core area then enables the estimation of the nonlinear refractive index.

In subsection 5.2.2, a simple and accurate method for determining the fiber nonlinear ratio is presented. The technique is used to measure the nonlinear ratio in three types of fiber: (i) standard telecommunication fiber; (ii) dispersion shifted fiber; and (iii) dispersion compensating fiber. This scheme is attractive because it evaluates the fiber nonlinear ratio under the same circumstances as are used in experiments designed for generating trains of ultra-high-repetition rate (50 GHz) bright and dark soliton pulses using fiber structures with comblike dispersion profile [40].

5.2.2 Principle and Results

Fig. 5.1 shows the block diagram of the proposed scheme. The beat signal generated by two CW DFB laser diodes operating around 1553 nm is launched into the fiber under test. The frequency of the signal is adjusted by tuning the temperature of the DFB diodes, which controls their wavelength spacing. The two polarization controllers, PC1 and PC2, adjust the polarization of the two laser diodes to maximize the SPM effect presented in the fiber. This is achieved when the outputs of the DFB laser diodes have the same polarization. The input signal to the tested fiber was amplified to the desired levels using an EDFA and erbium/ytterbium-doped fiber amplifier. The two DFB laser diodes are externally modulated by a 10 KHz sine wave signal in order to SBS that otherwise

appears at high intensities present in the fiber. The modulation of the laser diodes increases their line widths to 420 MHz, which is sufficient to avoid any SBS power loss during light propagation in the fibers under test.

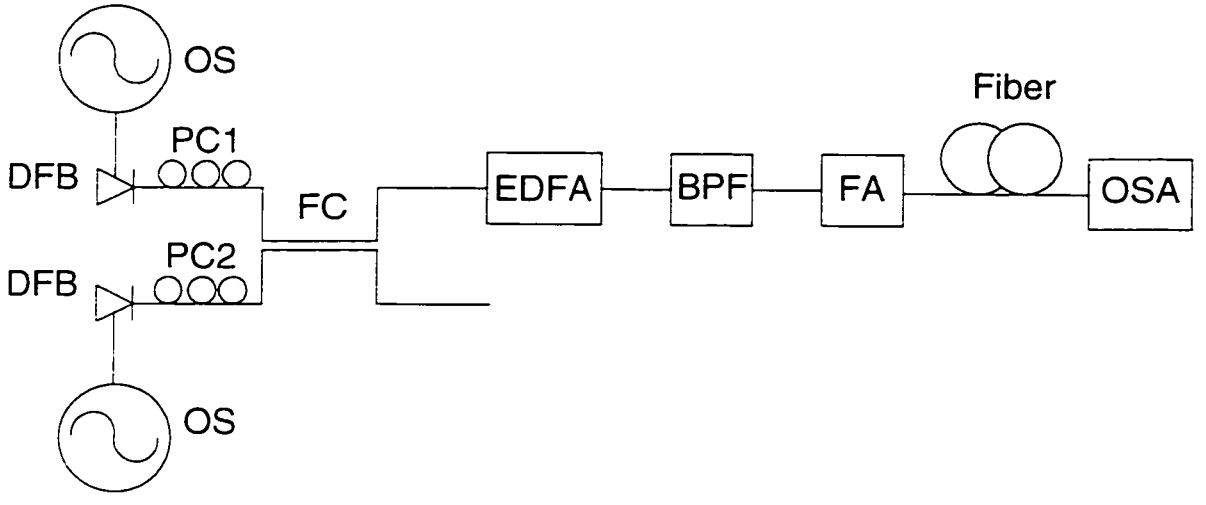

Fig. 5.1 Experimental setup for measuring n_2/A_{eff} in optical fiber. OS: oscillator; DFB: distributed feedback laser; PC: polarization controller; EDFA: erbium-doped fiber amplifier; BPF: bandpass filter; FA: high power amplifier; OSA: optical spectrum analyzer; FC: 50/50% fused silica fiber coupler.

The proposed scheme is based on the SPM nonlinear effect, where the beat signal that is launched into the fiber under test experiences spectral broadening. The measured intensity spectrum produced by the SPM effect at the fiber output depends on the ratio n_2/A_{eff}. The measured intensity spectrum is fitted to a calculated spectrum, which was obtained by solving numerically the simplified NSE given in (2.2.5). The spectral fitting determines the nonlinear ratio of the test fiber with good accuracy.

Different values of the input beat signal frequency and power were used in the experiments to obtain a wide range of measurements. The repetition rates are varied to 36, 50, and 70 GHz for an average power level between 20 dBm and 22 dBm. The sample

average and standard deviation of the measured ratio n_2/A_{eff} are shown in Table 5.1. The measured values of n_2/A_{eff} are reproducible with an accuracy (standard deviation/average) of better than 3%. The main sources of error in the measurements are the accuracy of the spectrum analyzer, the fluctuations of the state of polarization in the tested fiber, and the uncertainty in the fiber parameters specified by the manufacturer, such as the fiber length, dispersion, and attenuation. Fig. 5.2.a shows the measured intensity spectrum produced by the SPM effect in DSF1 for a 50 GHz beat signal launched into the fiber with an average power of 21.7 dBm. The corresponding simulated intensity spectrum is shown in Fig. 5.2.b. The remarkable agreement between the model and the experimental results, clearly indicates the accuracy of the measurements.

Fiber Type	Length[1] (km)	Dispersion[1] @ 1553 nm (ps/km/nm)	n_2/A_{eff} (1×10^{-10} W^{-1})	Standard Deviation
DSF1	2.511	-0.63	5.82	0.18
DSF2	0.425	0.83	5.63	0.07
DCF	0.195	-87.0	15.01	0.44
STF	11.795	17.0	3.27	0.10

[1] From the manufacturer.

Table 5.1 The fiber nonlinear ratio n_2/A_{eff} measured for different types of optical fiber.

(a)

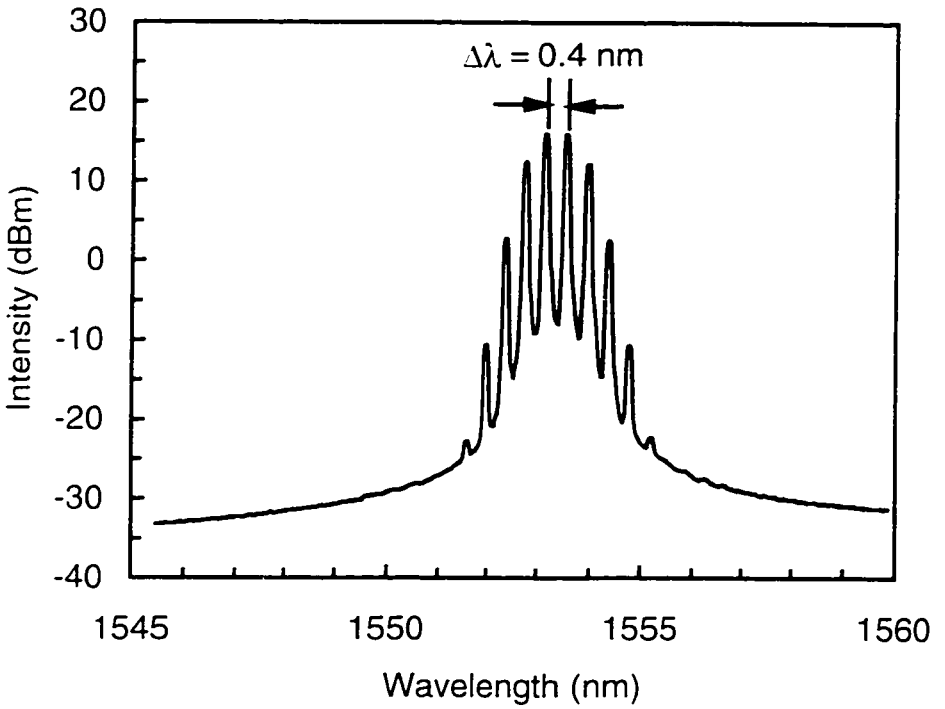

(b)

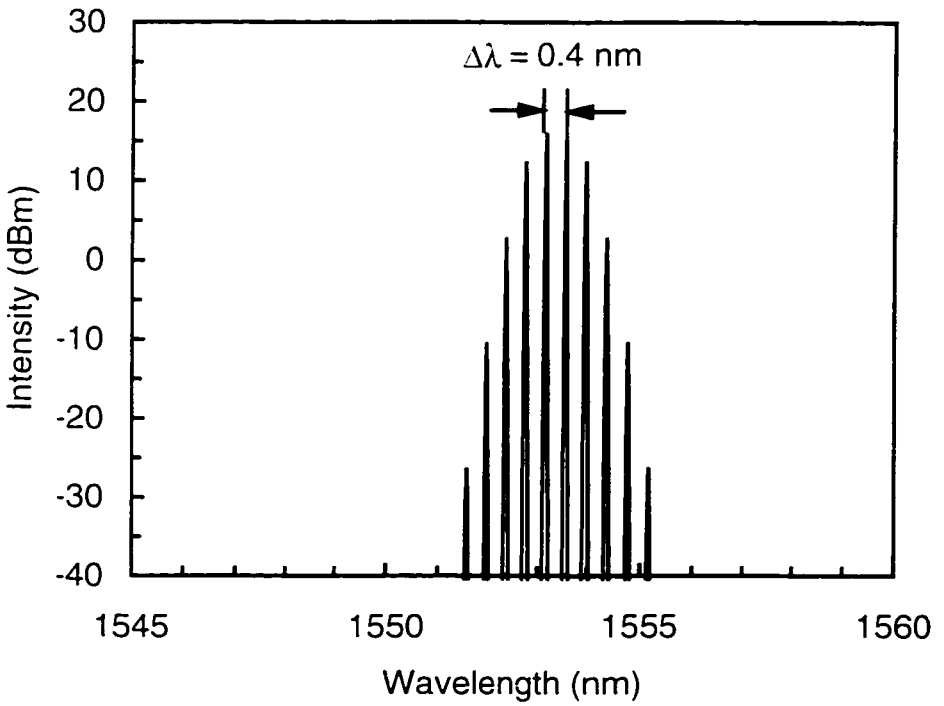

Fig. 5.2 Intensity spectrum for DSF1. (a) Measured. (b) Numerically calculated.

5.3 Raman Time Constant Measurement

5.3.1 Introduction

When a narrow fundamental soliton pulse propagates in an optical fiber, the center wavelength of its spectrum shifts toward the red frequencies. This is due to the Raman self-frequency shift phenomenon [83], where the pulse spectrum is wide enough that the Raman gain of the fiber can amplify the low-frequency components by transferring energy from the higher-frequency components of the same pulse. The theory of the soliton self-frequency shift was discussed by Gordon [82], in which he modified the nonlinear Schrödinger equation to have a nonlinear response function given by:

$$-i\frac{\partial u}{\partial z} = \frac{1}{2}\frac{\partial^2 u}{\partial t^2} + u(t)\int_0^{\infty} f(t')\left|u(z,t-t')\right|^2 dt', \tag{5.3.1}$$

where the nonlinear response function $f(t)$ is the inverse Fourier transform of the nonlinear susceptibility of the fiber, and $u(z,t)$ is the normalized electrical field amplitude at position z and time t.

The nonlinear third-order susceptibility of silica-based optical fiber consists of an electronic part and a Raman part expressed by Golovchenko et al. [99] as:

$$\chi^{(3)}(\omega) = \chi^{(3)}_{NR} + \chi^{(3)}_{R}(\omega), \tag{5.3.2}$$

where $\chi^{(3)}_{NR}$ is the electronic non-resonant part, which is real-valued, and $\chi^{(3)}_{R}(\omega)$ is the Raman resonant part, which is complex valued. The real part of the susceptibility is responsible for SPM and parametric nonlinear effects, while the imaginary part is responsible for Raman effects. The imaginary part of the resonant susceptibility is

antisymmetric in $\Delta\omega$ ($\Delta\omega=\omega-\omega_0$, where ω_0 is the center angular frequency of the propagated light in the fiber), and it determines the Raman gain coefficient:

$$g_R(\Delta\omega) = \frac{4\pi\omega_0}{cn_0}\,\mathrm{Im}(\chi_R^{(3)}(\Delta\omega)), \tag{5.3.3}$$

where c is the speed of light, n_0 is the linear refractive index of the fiber, and Im(.) represents the imaginary part of the argument.

For soliton pulses of duration greater than 100 fs, the integral form in (5.3.1) can be approximated by using two first-order partial-derivative terms. After adding high-order dispersion and loss terms to this approximation, light propagation is governed by (5.1.1) in which the Raman time constant is defined by Mamyshev and Chernikov [92] as:

$$T_R = \frac{2\pi}{n_0 n_2}\left[\frac{d(\mathrm{Im}(\chi_R^{(3)}))}{d(\Delta\omega)}\right]_{\Delta\omega=0}. \tag{5.3.4}$$

The generalized NSE was derived for linear approximation of the actual Raman gain curve. The linear approximation is valid for pulses of widths greater than 100 fs (spectral widths less than approximately 3 THz). Different values for T_R have appeared in the literature, such as 3.0 fs [92], 5.0 fs [93], and 6.0 fs [94,95]. These values are estimated from the Raman gain spectrum shown in Fig. 5.3. The significant differences between these values affect the modeling of pulse propagation in optical fibers when they experience Raman self-frequency shift. Raman self-frequency shift has many applications in the generation of femtosecond pulses [92] based on the optical soliton fission principle [90], the generation of spectral super continuum, and signal demultiplexing in multilevel soliton communication systems [62]. Therefore, it is important to use the proper value of T_R when modeling these applications.

In subsection 5.3.2, T_R was measured experimentally in STF fibers at 1550 nm. The measurement of T_R is based on the Raman self-frequency shift nonlinear effect. Transform-limited (TL) soliton pulses, amplified by an EDFA, were launched into the fiber under test. The spectrum produced by solving the generalized NSE numerically was fitted to the measured spectrum at the fiber output. All parameters used in the calculation were either independently measured (pulse peak power, pulse width, fiber length, fiber nonlinear ratio (n_2/A_{eff}) [42], fiber losses) or specified by the manufacturer (fiber dispersion). The only unknown parameter in the calculation is T_R, which is determined by this process. In Subsection 5.3.2, error analysis was performed to assess the accuracy of the measurement.

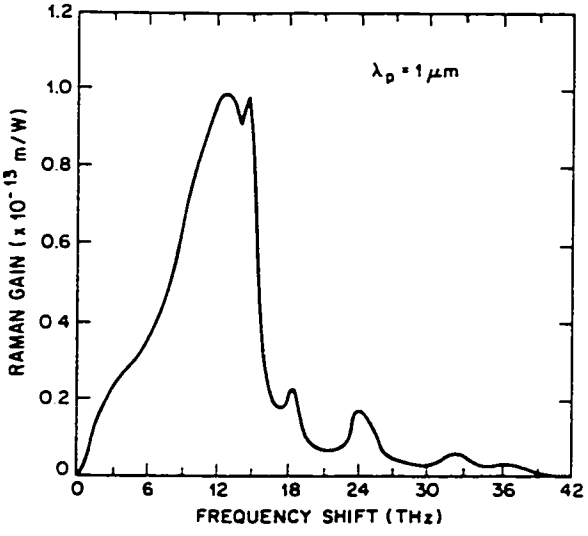

Fig. 5.3 Measured Raman gain spectrum for fused silica at 1 μm (after Ref. 11).

5.3.2 Experimental results

Fig. 5.4 shows the setup used for the experiment to measure T_R in standard telecommunication fibers. Transform-limited soliton pulses (generated by a figure-8 soliton fiber laser and amplified by an EDFA) are launched into a 1 km of STF piece. This length of fiber was chosen to reduce the sensitivity of the measured intensity spectrum at the output of the fiber to the pulse polarization. A polarization controller placed before the fiber controls the polarization of the pulses launched into the fiber. The figure-8 laser (F-8L) produces tunable soliton pulses around 1550 nm at a repetition rate of 3.2 MHz. Great care was taken in measuring the power and duration of the pulses produced. The average power of pulses launched into the test fiber was measured with a Newport power meter calibrated using two different methods: first, a thermal power meter was used; second, the energy of a transform-limited pulse (measured with a calibrated pin photodiode) was compared to the energy calculated from the pulse power (measured using the Newport power meter), and pulse width (measured using an optical autocorrelator). The discrepancies in all measurements were found to be less than 3%.

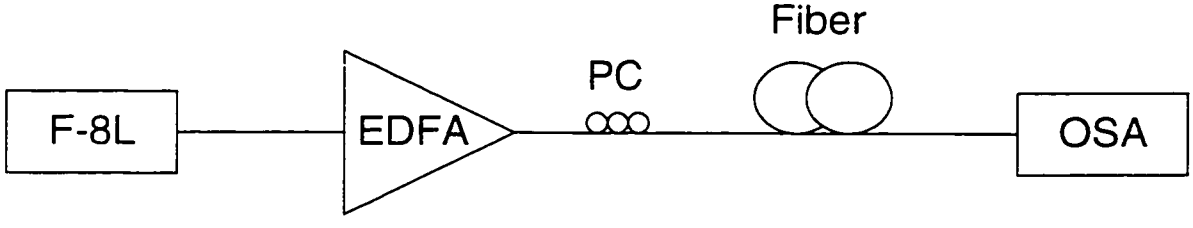

Fig. 5.4 Experiment setup block diagram used to measure the Raman time constant (T_R). F-8L: figure-8 soliton fiber laser; EDFA: erbium-doped fiber amplifier; PC: polarization controller; OSA: optical spectrum analyzer.

After amplification by the EDFA, the amplified spontaneous emission noise produced approximately 15% of the total measured pulse's average power. The actual average power launched into the fiber was calculated by subtracting the measured ASE noise power (generated by both the F-8L laser and the EDFA) from the measured total average power which includes ASE. The ASE noise power can be measured by adjusting the F-8L laser diode pumping current to obtain, at the EDFA output only, ASE noise equal in intensity to that of the operating lasers. An optical autocorrelator was used to measure the pulse widths at the output of both the F-8L laser and the erbium-doped fiber amplifier. The pulse widths at the output of the F-8L laser and EDFA were different because the erbium-doped fiber of the amplifier acts as a nonlinear medium which compresses and distorts the TL pulses generated by the F-8L laser source at high EDFA pumping currents. In addition, when high-power pulses are launched into the fiber, the soliton pulses split into many solitons. Based on the soliton fission principle, emerging pulses have different widths and travel at different speeds. In this experiment, the 980 nm laser diode of the erbium-doped fiber amplifier was driven at low-current levels to keep the soliton pulses in the test fiber close to transform-limited. Different pulse widths were used in the measurements at different center wavelengths, ranging from 1546 nm to 1551 nm. The launched soliton pulses had a soliton order (N) of less than1.6.

The nonlinear Schrödinger equation given by (5.1.1) was solved numerically. In the calculation, the number of elements that the fiber length is divided into, the time window used, and the number of samples taken in the time window were chosen after extensive analysis to make the calculation fully insensitive to the choice of these

parameters. It was found that dividing the fiber length into 1000 elements and using 4096 samples in 1 200 ps time window were adequate to produce accurate numerical results.

The STF piece was Corning SMF-28, with a length of 1km, dispersion of 17 ps/(km nm), third-order dispersion (β_3) at 1551 nm of 0.13 ps^3/km, 0.7 dB total fiber loss (which included splicing, attenuation, and connector loss) measured in the experiment, and an independently-measured, nonlinear ratio (n_2/A_{eff}) of $3.27\times^{-10}$ W^{-1} [42]. The accuracy in measuring (n_2/A_{eff}) is better than 3.0%, calculated as the ratio of standard deviation to the average. The pulses launched into the test fiber had spectral widths of 1.25 nm and 1.5 nm. The third-order dispersion and self-steepening nonlinear effects have minor impact on these relatively wide (~1.7 ps) pulses.

The amount of Raman self-frequency shift that fundamental solitons experience in optical fibers is given by Gordon and Wood [82,84] as:

$$\Delta f(THz) = 2.2\times 10^{-3}\,\frac{g(\tau)(ps)\,\beta_2(ps^2/km)\,l(km)}{\tau_{FWHM}^4(ps^4)}, \qquad (5.3.5)$$

where τ_{FWHM} is the pulse's FWHM, g(τ) is a constant equal to approximately 1 ps for τ_{FWHM} greater than 1 ps and to 2 ps for τ_{FWHM} around 100 fs, and l is the fiber length. To check the accuracy of the numerical calculations in predicting the amount of Raman self-frequency shift experienced by the propagated pulses in the fiber, the solution of equation (5.3.5) is compared to the shift results from solving equation (5.1.1) numerically. Very good agreement is achieved.

The measured intensity spectrum at the STF piece output and the fitted spectrum from the numerical calculation for a soliton pulse at 1551 nm are shown in Fig. 5.5 and Fig. 5.6.a in linear and logarithmic scales, respectively. The measured spectrum is

indicated as a solid line. A HP-70004A optical spectrum analyzer was used for measuring the intensity spectra. The soliton order of the pulse is 1.4 and T_R used in the modeling is 3.0 fs. The intensity spectra in all figures were corrected for the effects of back-reflection from the fiber cable connectors. The spectral fits for T_R = 5.0 fs and T_R = 6.0 fs are shown in Fig. 5.6.b and Fig. 5.6.c, respectively. It is clear that T_R cannot be as high as 5.0 fs or 6.0 fs as previously estimated in the literature [93-95]. The same analyses were done for different spectral pulse widths of 1.25 nm and 1.5 nm at center wavelengths of 1546 nm and 1548 nm, where the spectral fittings of these measurements with T_R = 3.0 fs are shown in Fig. 5.7.a and Fig. 5.7.b, respectively.

Fig. 8 illustrates the difference in the solutions of the generalized NSE given by (5.1.1) and the simplified NSE, which includes only the group velocity dispersion, the self-phase modulation nonlinear effect, and the fiber attenuation (i.e. the right hand side of equation (5.1.1) is equal to 0). This figure clearly shows the Raman self-frequency shift that is produced due to soliton pulse propagation in the fiber.

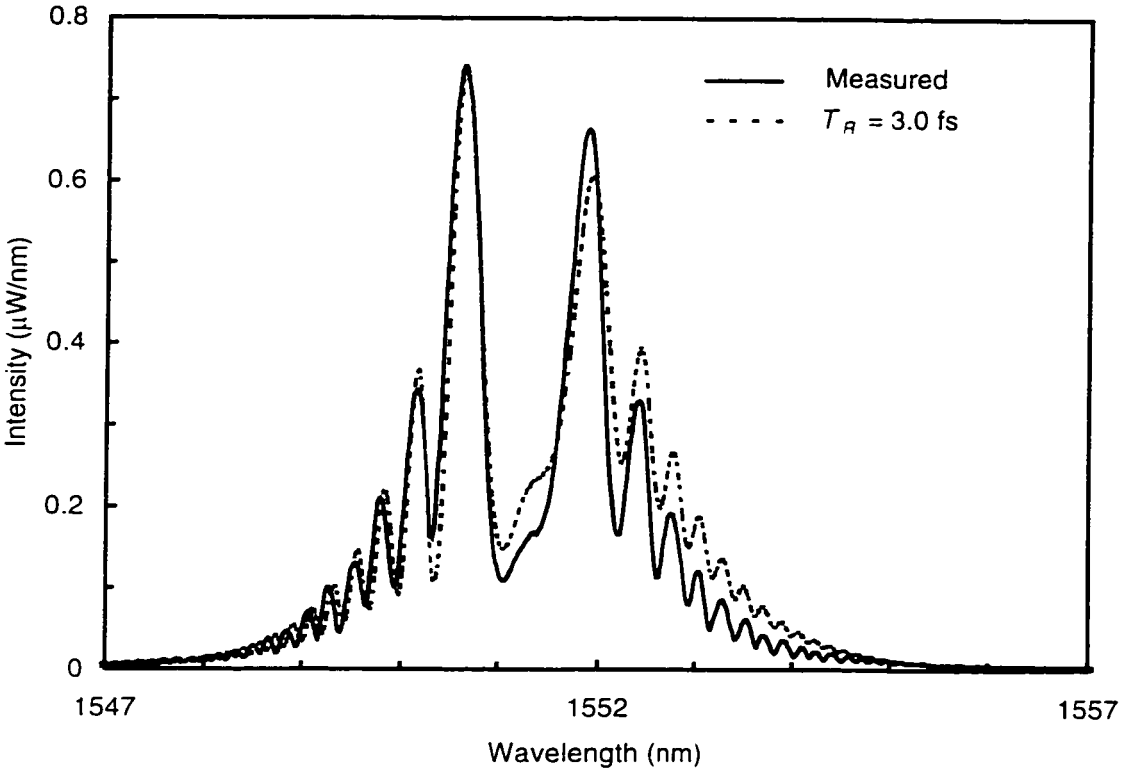

Fig. 5.5 Intensity spectra at the output of 1 km of STF for T_R = 3.0 fs. Solid line, measured; dashed line, numerical calculation using linear scale.

(a)

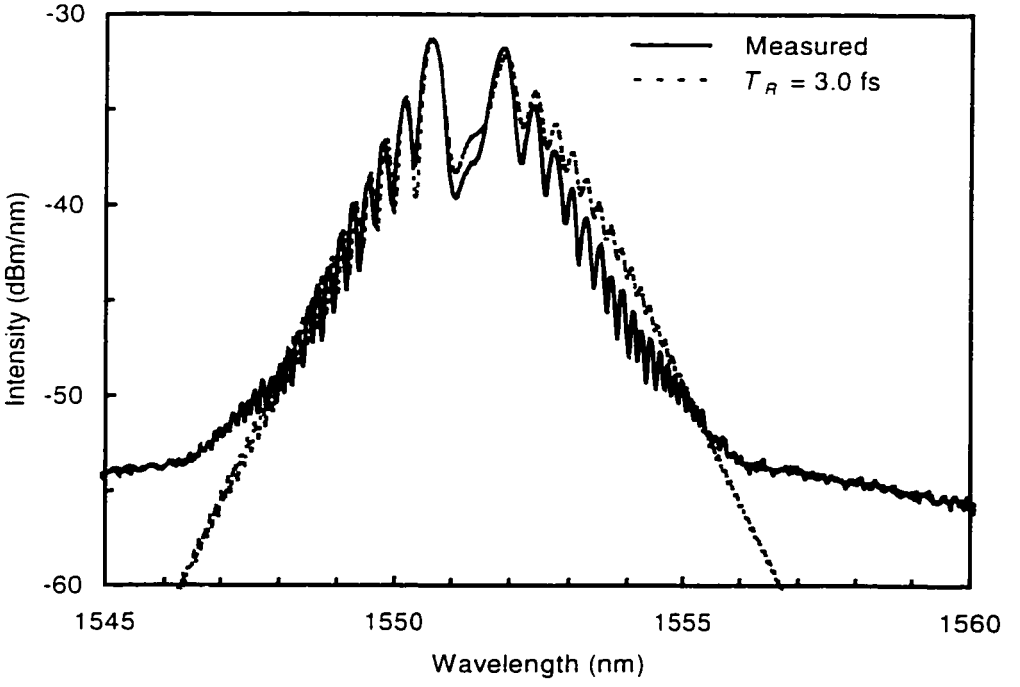

(b)

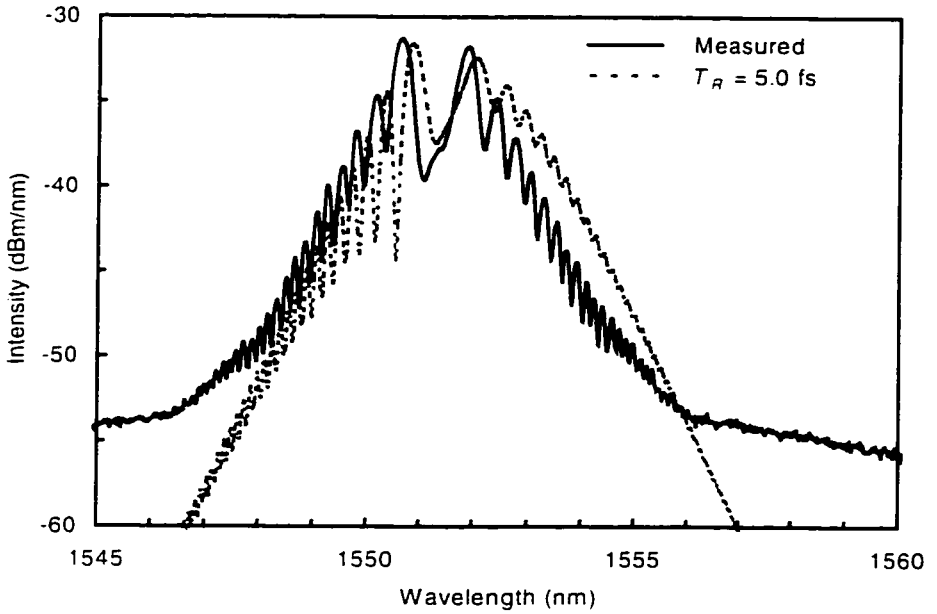

(c)

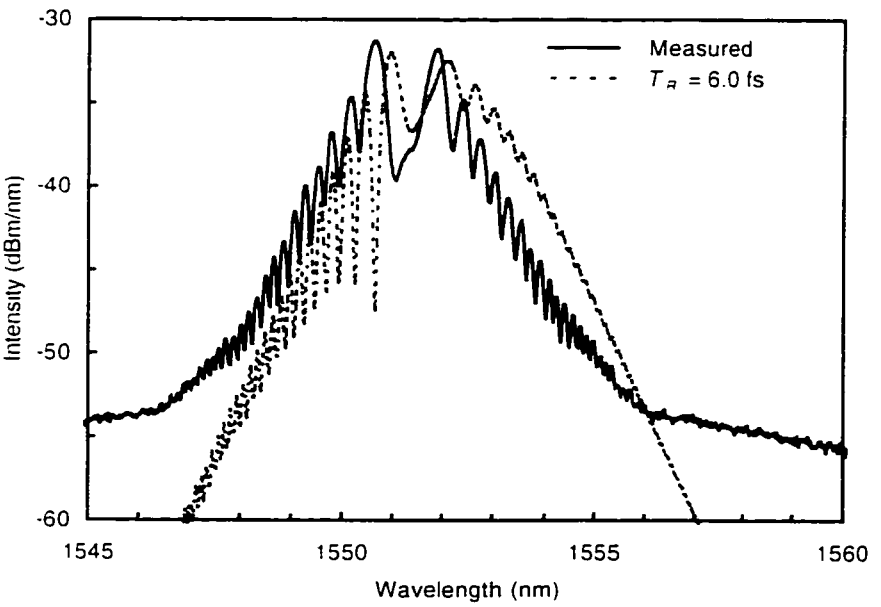

Fig. 5.6 Intensity spectra at the output of 1 km of STF for (a) T_R = 3.0 fs; (b) T_R = 5.0 fs; (c) T_R = 6.0 fs. Solid line, measured; dashed line, numerical calculation using logarithmic scale.

(a)

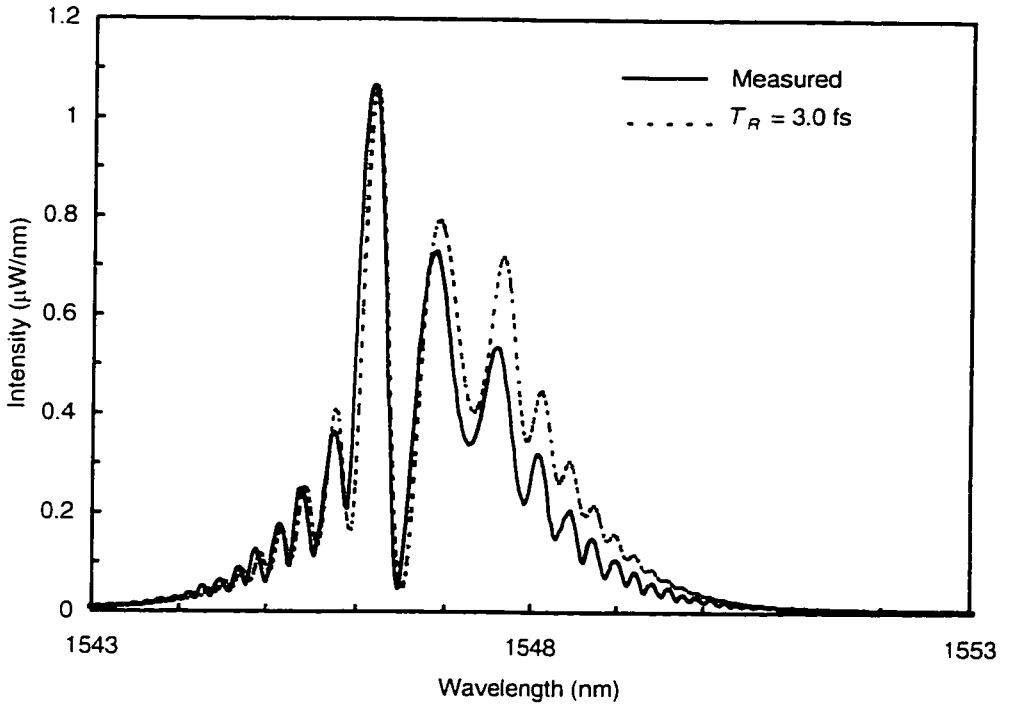

(b)

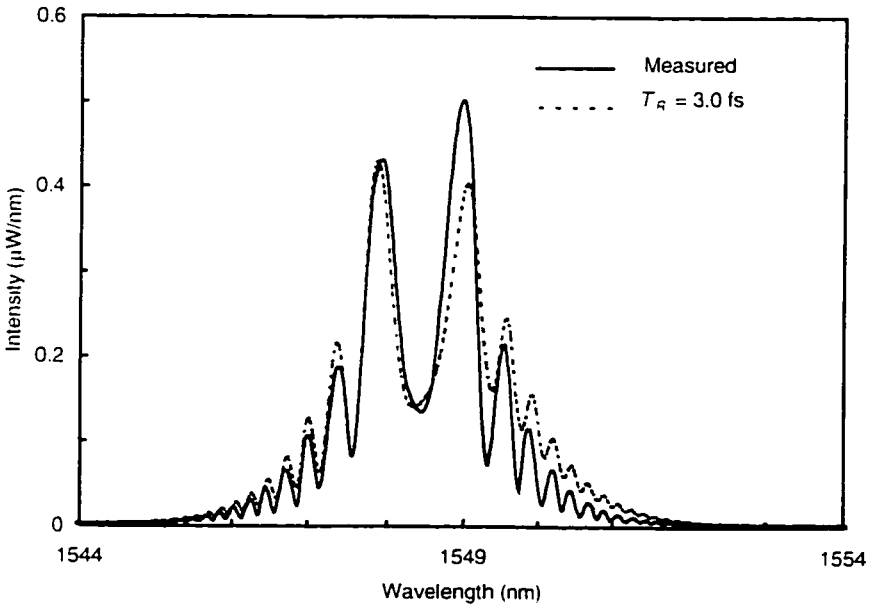

Fig. 5.7 Intensity spectra at the output of 1 km of STF for T_R = 3.0 fs. Solid line, measured; dashed line, numerical calculation using linear scale. (a) λ = 1546 nm. (b) λ = 1548 nm.

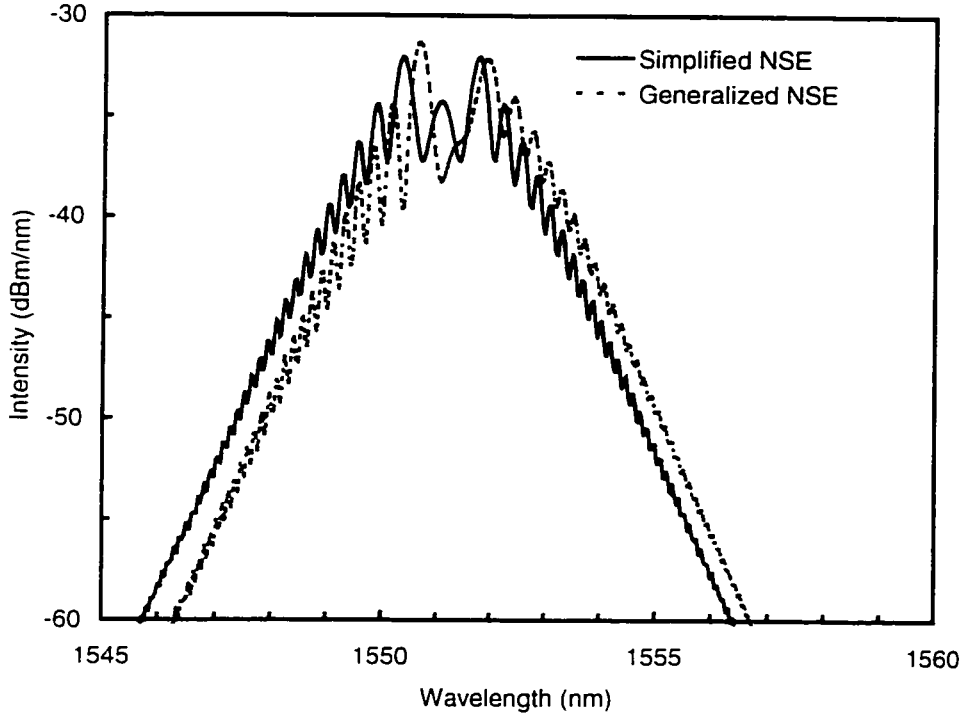

Fig. 5.8 Numerically-calculated intensity spectra at the output of 1 km fiber for the Raman time constant (T_R) = 3.0 fs. Solid line, solution of simplified NSE; dashed line, solution of generalized NSE.

5.3.3 Error Analysis

When fundamental soliton pulses experience Raman self-frequency shift while propagating in optical fibers, they preserve their shape. The amount of frequency shift is inversely proportional to the fourth power of the pulse width as given by (5.3.5). On the other hand, the behavior of higher-order solitons is completely different. The propagating pulses do not preserve their shapes and new soliton pulses usually emerge due to the soliton fission effect [90]. Each emerging pulse has different amplitude and travels in the fiber at a different group velocity. The number of emerging pulses depends on the order of the soliton input pulse [81].

In the experiment presented in this work for determining the value of T_R, higher-order soliton pulses are used with order (N) equal to 1.4 at 1551 nm, 1.3 at 1548 nm, and 1.6 at 1546 nm, launched into 1 km of single mode (SMF-28) fiber. There is a possibility that only one additional soliton pulse will emerge, but the length of the fiber is insufficient to show it. The shape of the intensity spectrum of the soliton pulses at the output of the fiber will vary depending on the launched soliton order. The value of T_R affects the amount of frequency shift that the soliton pulse will experience at the output of the fiber. In the measurement of T_R, a numerically calculated intensity spectrum was fitted to one measured at the output of the fiber. The measured value of T_R was found to be 3.0 fs.

To test the accuracy of the measurement of T_R, all parameters (pulse peak power, pulse width, fiber loss, dispersion, and fiber nonlinear ratio) were varied by ±3% in the numerical calculations. These parameters define the soliton order (N) given by:

$$N^2 = 0.32 \frac{\tau_{FHWM}^2}{|\beta_2|} \frac{2\pi}{\lambda} \left(\frac{n_2}{A_{eff}}\right) P, \qquad (5.3.6)$$

where P is the soliton peak power. A 3.0% variation was chosen because it is slightly larger than the accuracy of measuring all of the above parameters. In the worst case, the total error accumulation in N^2 was less than ±15.0%. The numerical calculations were repeated for different combinations of varied parameters. The value of T_R was varied in the calculations to compensate for the effect of increasing or decreasing the soliton order which produces different spectral shapes with different frequency shifts. These spectra were compared with the one fitted to the measured spectrum using T_R = 3.0 fs. It was found that increasing the soliton order by 15.0% requires lower values of T_R (less than 3.0

fs), and decreasing the soliton order by 15.0% requires higher values of T_R (greater than 3.0 fs) to get intensity spectra close to the fitted one.

Fig. 5.9 shows the numerically calculated intensity spectrum at the output of the fiber for T_R = 3.0 fs (indicated as a solid line) and the spectra that result from changing all parameters in (5.3.6) by (a), +3.0%, and by (b), -3.0%, at 1551 nm. The intensity shown in Fig. 5.9 is normalized by the average power of the input pulse used in the numerical calculation. The calculated spectrum with T_R = 3.0 fs was used in the spectral fitting shown in Fig. 5.5. The value of T_R used to compensate for varying the parameters in Fig. 5.9.a was 2.0 fs, and 4.0 fs in Fig. 5.9.b. These values give the best shape and frequency shift fit, although they did not predict the experimental shape and the frequency shift as accurately as the result by using the 3.0 fs value. Due to the excellent fit between the measured and numerically-calculated intensity spectra, it is concluded that T_R equals 3.0 fs. The numerical calculations and the spectral fitting show that T_R need be varied no more than ±1.0 fs. This error margin is less than the values of T_R often reported in the literature. The above calculations were repeated at 1546 nm and 1548 nm, and similar results were obtained.

The measured value of T_R was compared with different values calculated according to equation (5.3.4) for linear approximation of the Raman gain spectrum as shown in Fig. 5.10. These approximations represent the appropriate Raman gain characteristic that is suitable for certain soliton pulse widths. The figure shows that T_R is 2.5-3.5 fs for pulses longer than 1 ps (spectral width less than 1 THz measured as three times the FWHM), and for pulses of duration around 200 fs (spectral width of approximately 5 THz measured as three times the FWHM). The analysis is performed for

a spectral width equal to three times the full width at half maximum to ensure that over than 95 % of the pulse energy exists within this width of the pulse which encounters the Raman gain. On the other hand, pulses with intermediate spectral widths experience T_R between 4.0-5.0 fs. For modeling higher-order soliton propagation in single-mode fibers, it is recommended to use an average value of T_R = 3.0 fs. An average value is used because these pulses are usually compressed to shorter widths and broaden during propagation which covers all possible values of T_R estimated in Fig. 5.10.

A T_R of 3.0 fs was used in designing comblike dispersion profile fiber structures for compressing soliton pulses down to 200 fs, as presented in Chapter 4. The excellent agreement that was achieved between the numerical calculations and the experimental measurements shows without a doubt that T_R is 3.0 fs ±1.0 fs.

(a)

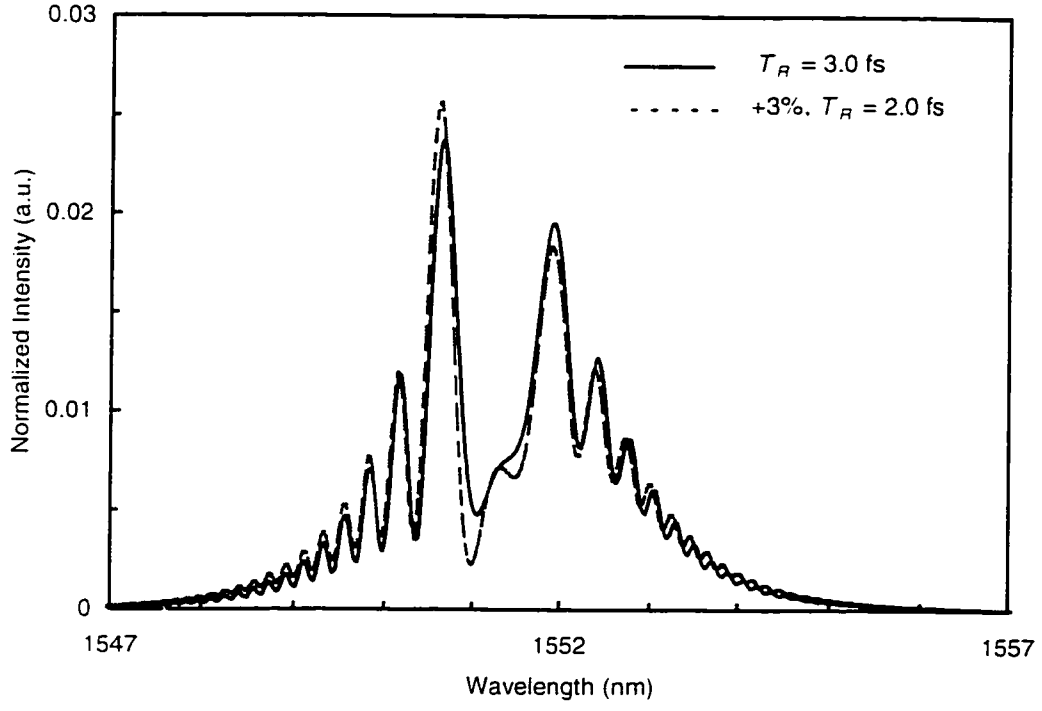

(b)

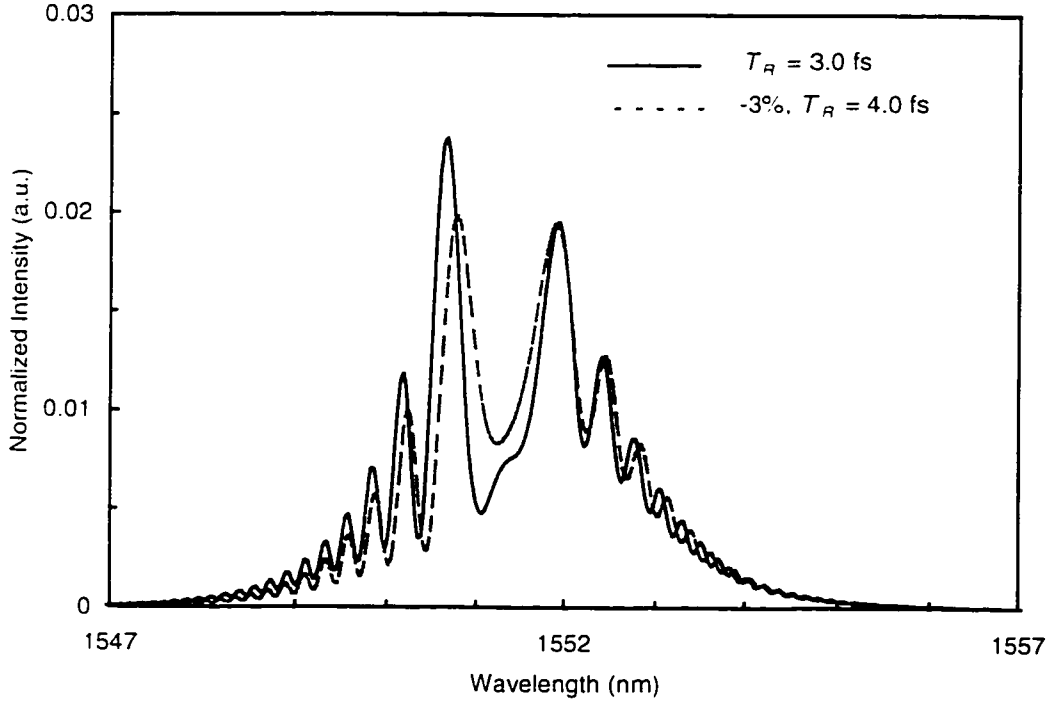

Fig. 5.9 Numerically-calculated intensity spectra at the output of 1 km STF at 1551 nm for T_R = 3.0 fs (indicated as solid line) and varied parameters of the soliton order. (a) +3%, T_R = 2.0 fs. (b) -3% T_R = 4.0 fs.

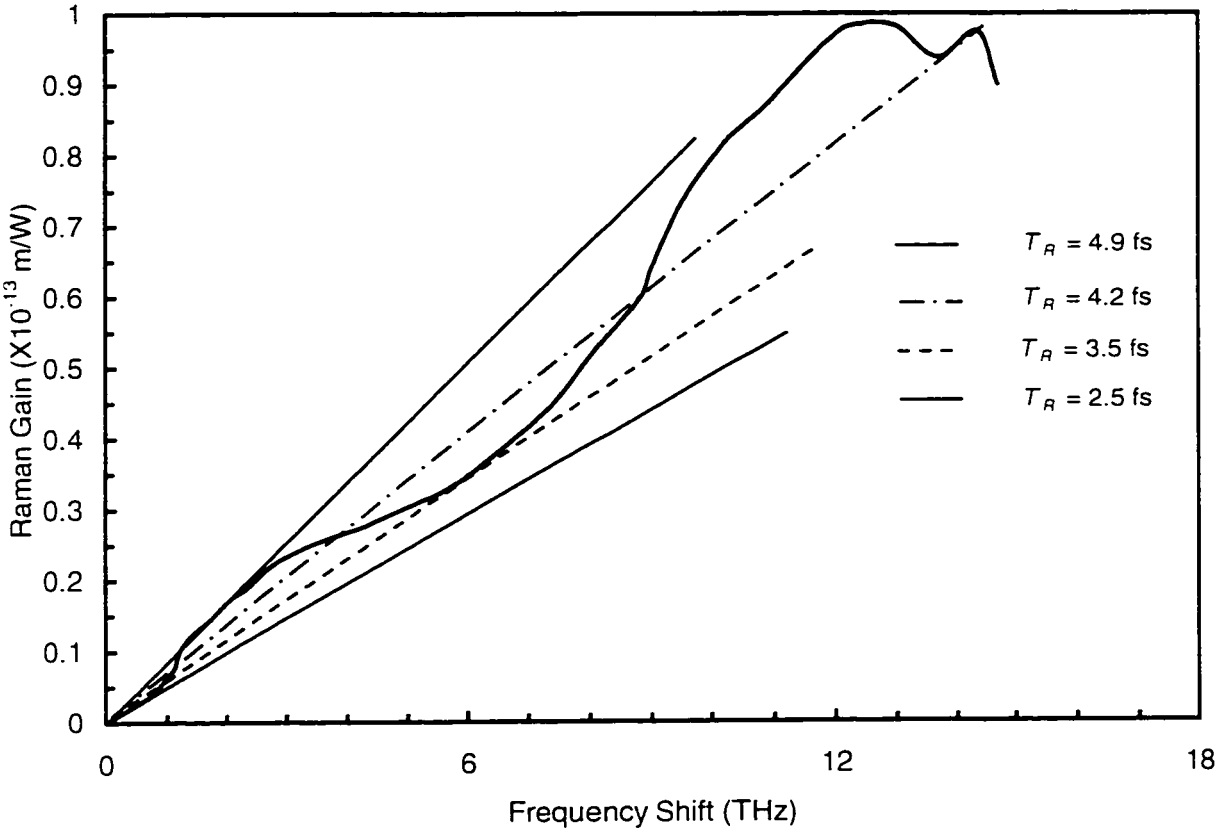

Fig. 5.10 Estimated Raman time constant (T_R) for linear approximation of the Raman gain spectrum.

Chapter 6

Conclusions and Future Work

6.1 Summary

Fig. 6.1 shows the block diagram of a general optical communication system that is investigated in this thesis. Both modeling based on numerical calculations and experiments are presented. At the transmitter end, ultra-high rate (50 GHz) bright and dark soliton pulse trains are demonstrated [40]. The sources are developed based on transforming a sinusoidal beat signal (generated by two CW DFB laser diodes) using alternating pieces of dispersion shifted fiber and standard telecommunication fiber. The resulting fiber structure is known as CDPF structure because the dispersion profile of the fiber pieces looks like a comb. The fiber structure used to generate the bright soliton pulse train uses the lowest average power of the beat signal reported in the literature. Additionally, the comblike fiber structure is used for the first time to generate dark soliton pulses with a constant background.

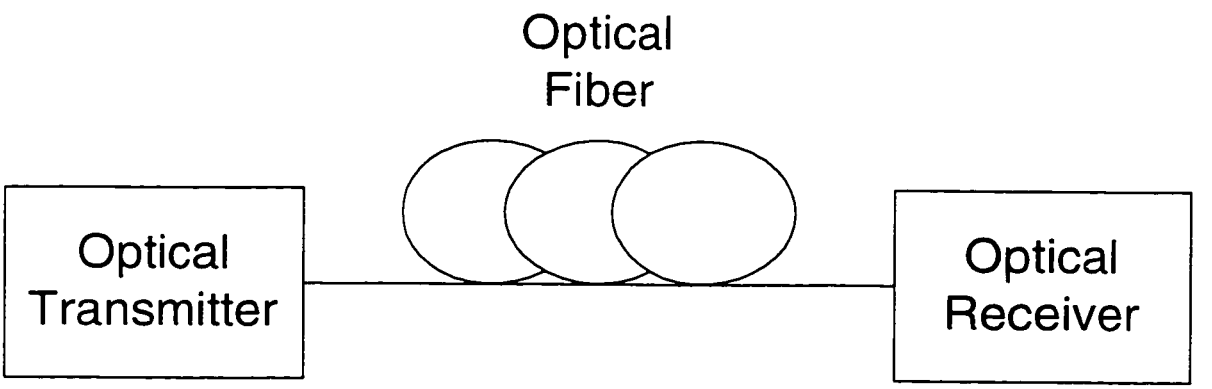

Fig. 6.1 General optical communication system block diagram.

At the receiver end, all-optical signal demultiplexing (from ultra-high data rates to lower rates that are suitable for detection with available technologies) is investigated in both time and frequency domains. In the time domain, a NOLM is the device of choice used for signal demultiplexing. The NOLM principle is based on XPM nonlinear effect that is produced between the high-rate, low-intensity signal and a high-intensity, low-rate control signal in optical fibers. The polarization fluctuation of both signals affects signal demultiplexing. An all-optical polarization-insensitive NOLM was investigated [61]. A feedback signal from the demultiplexer output was used to adjust an EDFA used to boost the control signal power. Numerical calculations were conducted to study the performance of this scheme. The NOLM uses only 4.5 km of DSF. There was no experimental realization of such a demultiplexer because of budget restrictions for the Photonic Systems group at the NRC.

In the frequency domain, signal demultiplexing is achieved based on the Raman self-frequency shift nonlinear effect. This technique is applicable for multilevel soliton communication systems [63], where each channel's pulse stream has different energy (defined by pulse peak power and FWHM). To make this scheme efficient, pulse compression (to the subpicosecond regime) at the receiver end is required [85]. The advantage of pulse compression is to achieve more Raman self-frequency shift for each channel at the output of shorter fiber pieces. CDPF structures are used to massage soliton pulses to widths down to 200 fs. A demonstration of signal demultiplexing using the Raman self-frequency shift is presented herein. A burst of 4 pulses generated by a F-8L source are multiplexed to a 40 GHz rate. Each of these pulses has a different energy and

experiences different Raman self-frequency shift while propagating in the fiber. A bandpass filter is used to select each channel pulse at the fiber output.

The conducted numerical calculations fit the experimental results well. This is due to the use of parameters in the computations that were either measured independently (fiber nonlinear ratio (n_2/A_{eff}) [42], T_R [100], and pulse power) or were specified by the manufacturer (fiber attenuation, and dispersion). The fiber nonlinear ratio is measured for all fibers (DSF, STF, and DCF) used in the experiments. The principle of measuring the nonlinear ratio (n_2/A_{eff}) was based on SPM nonlinear effect. The accuracy of the measurements was better than 3%. The Raman time constant was measured in a careful experiment by fitting the intensity spectrum resulting from solving the generalized NSE numerically and the measured spectrum. In the calculations, T_R was the only unknown parameter. The measured T_R has a value of 3.0 fs (not 5.0 fs or 6.0 fs, as estimated in the literature) based on the slope of Raman gain of fused silica at 1 μm.

6.2 Future work

In the next century, the market for data communications is expected to require ultra-high bit rates. In addition, the expected data rates will have to be transmitted over all sizes of networks (local, metropolitan, and wide area). Optical soliton transmissions have been investigated for ultra-long distances (transoceanic). These experiments used repetition rates around 10 GHz, i.e. soliton pulse widths of 10 ps or longer [3,4]. The transmission schemes were based on controlling the in-line optical amplifier spacing and using sliding frequency filters that minimize timing jitter produced by the ASE. Problems that appear when using ultra-high data rates higher than 50 GHz result due to the use of short pulses with widths less than 2 ps. These pulses are more susceptible to interaction

while propagating and are more sensitive to the fiber dispersion slope (which requires the inclusion of higher-order dispersion effects when modeling pulse propagation). Moreover, other nonlinear effects such as self-steepening and the Raman self-frequency shift are more apparent. In addition, the amplifier spacing is shorter for such rates because of the lower soliton periods ($z_0 = (\pi/2)(T_0^2/|\beta_2|)$) which make soliton transmission in the average regime impossible. One solution is to use dispersion management. Numerical studies conducted by Essiambre et al. [94] showed that the maximum possible amplifier spacing for 2 ps pulse streams is around 20 km. Preliminary calculation showed that with dispersion management of four pieces of fiber, each 10 km long and with a dispersion decreasing profile, it is possible to transmit 50 GHz pulses up to 200 km. For future work, it may be possible to increase the transmission distance to 1000 km when sliding frequency filters are used with dispersion management.

Optical networks may be implemented in the frequency domain using WDM technologies or in the time domain using TDM. The technology using WDM to implement optical networks is more mature. In the time domain, research is evolving and expected to compete with WDM by using optical solitons as a basis for implementing these networks. One of the promising networks in the time domain is the one presented by the ARPA group [101], where a 100 Gbps local/metropolitan area shared media networks based on slotted TDM is proposed. In this network, all nodes that are capable of bursting data at rates up to 100 Gbps share one fast channel. This kind of network can serve a heterogeneous population of users. The slotted TDM network architecture is implemented, based on a helical unidirectional bus to achieve both guaranteed bandwidth and bandwidth-on-demand services. The NRC is investigating a similar network by

exploiting the technologies that were developed by the Photonics group. Issues like fiber type, amplifier spacing, timing jitter, protocols and topologies are the main questions to be answered.

Dark solitons have shown more stable behavior than bright solitons. One of the problems that dark solitons encounter is modulation and detection. Fig. 6.2 shows a scheme suggested by Ngo et al. [102] to detect 10 GHz dark soliton pulses. This method converts the dark soliton pulses into either a return- to- zero, or non-return-to-zero, pulse at the output of a Mach-Zehnder interferometer constructed from two 50/50% fiber couplers. It is possible to implement this device using either fiber interferometers or planar lightwave circuit technology with a single-mode waveguide. The disadvantage of the fiber interferometer is its sensitivity to vibration.

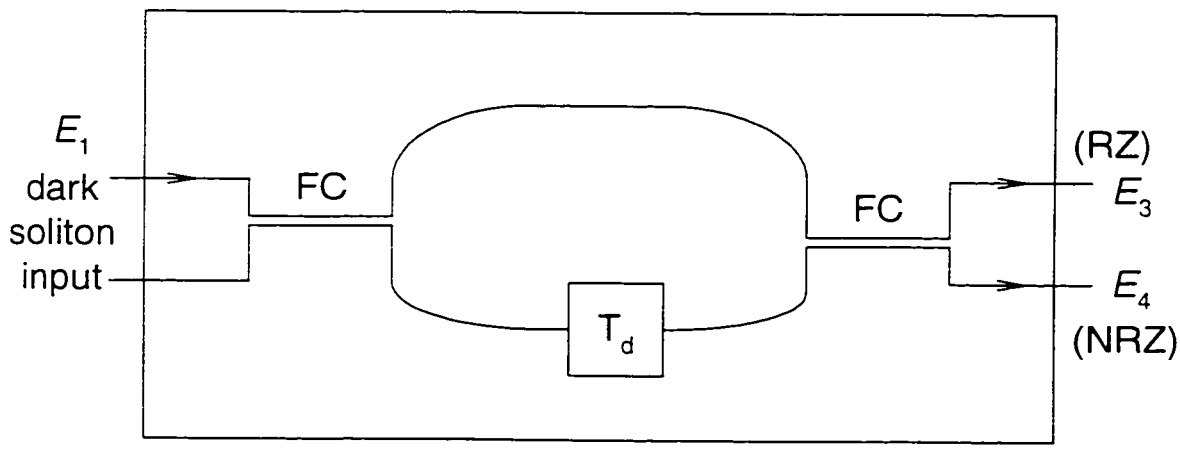

Fig 6.2 Dark soliton detector block diagram. FC: 50/50% fiber coupler; Td: time delay element; RZ: return to zero; NRZ: non return to zero.

Appendix A

Stimulated Brillouin Scattering

A.1 Introduction

Stimulated Brillouin scattering is a nonlinear process that occurs in optical fibers at particular input-power levels. The vibration of the fiber glass lattices generates sound waves in the fiber medium. This causes a localised variation in the refractive index, which produces an effect similar to a diffraction grating. As a result, part of the light propagating down the fiber will scatter in the form of a backward-travelling wave (usually) called a "Stokes wave". The Stokes wave is down shifted from the input's optical frequency by an amount determined by the properties of the medium. This phenomenon can be useful in some applications (such as fiber Brillouin lasers and amplifiers), or detrimental in optical communication systems (because the backward scattered light depletes the pump light and may cause serious problems at the receiver). In addition, the backward-travelling Stokes wave provides feedback to the transmitting laser, which may destabilise the laser operation. In this section, the harmful effects of SBS on the generation of trains of soliton pulses, and methods to suppress it, will be discussed.

A.2 Theory

The process of SBS can be described as a parametric interaction between the pump wave that is launched into the fiber, the Stokes wave, and an acoustic wave. The pump wave generates acoustic waves through the process of electrostriction which also produces localised variations in the refractive index. The propagated pump wave

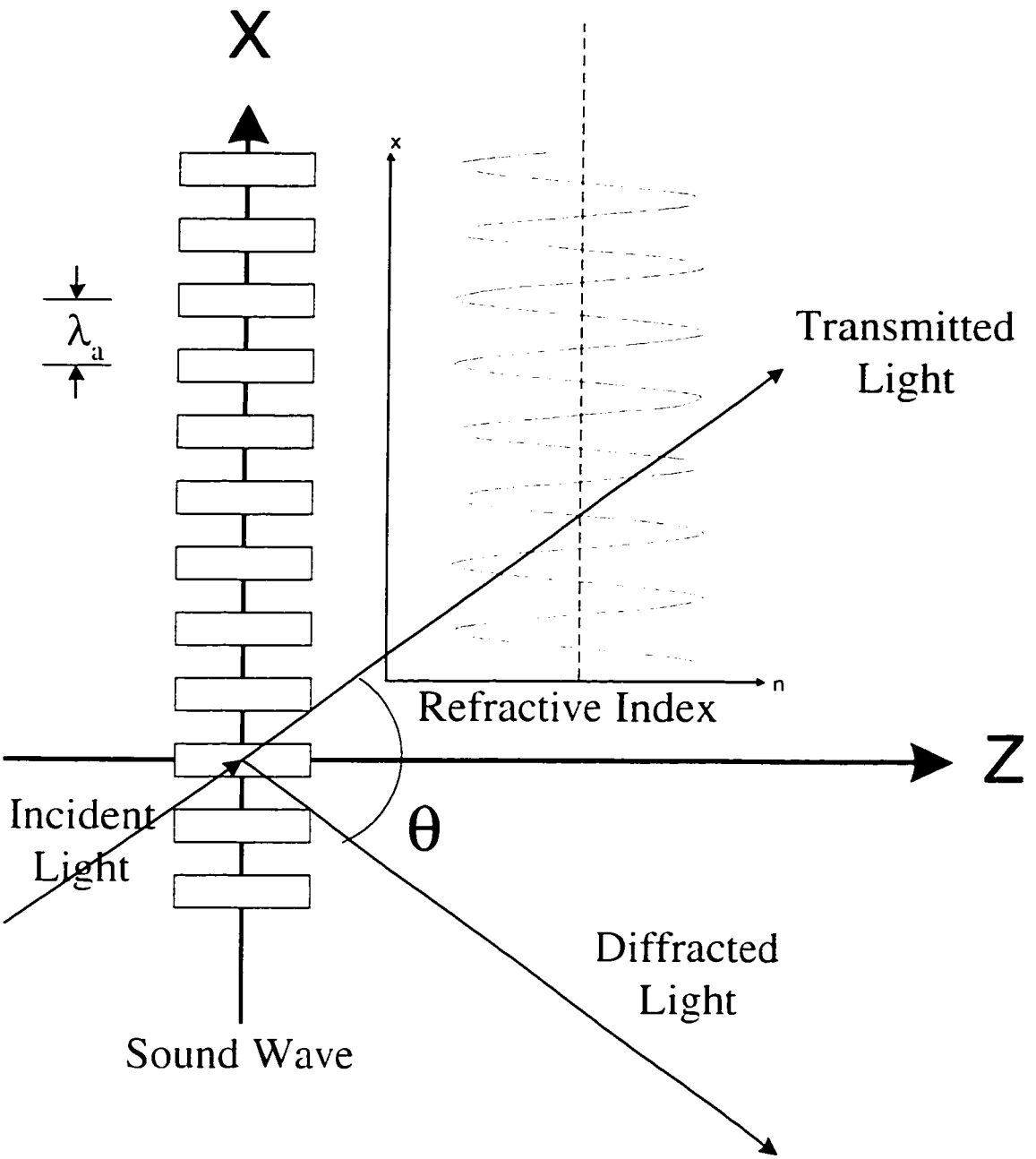

Fig. A.1 Bragg diffraction: an acoustic plane wave with wavelength λ_a acts as a beam splitter when the angle θ satisfies the Bragg condition. Note the periodic localised variation of the refractive index.

experiences Bragg diffraction, which produces the backward scattered Stokes wave as shown in Fig. A.1. The light diffracted by the periodically-modulated refractive index satisfies the Bragg condition:

$$\sin\left\{\frac{\theta}{2}\right\} = \frac{\lambda_p}{2\lambda_a}, \tag{A.2.1}$$

where θ is the angle between the pump and the Stokes waves; λ_a is the wavelength of the acoustic wave; and λ_p is the optical wavelength of the pump. The scattered light is accompanied by a frequency shift equal to the acoustic wave frequency, which is known as the "Doppler shift". This process may also be viewed quantum-mechanically, where the pump's wavelength with frequency ω_p and wave vector $\vec{K}_p$ is viewed as a stream of photons, each with energy $h\omega_p$ and momentum $h\vec{K}_p$, where h is Plank's constant. The acoustic wave of frequency ω_a and wave vector $\vec{K}_a$ is regarded as a stream of phonons each with energy $h\omega_a$ and momentum $h\vec{K}_a$. The pump photon simultaneously creates a Stokes photon with frequency ω_s and wave vector $\vec{K}_s$, and an acoustic phonon. Since the energy and momentum are conserved, the frequencies and the wave vectors are related by:

$$\omega_a = \omega_p - \omega_s, \text{ and} \tag{A.2.2}$$

$$\vec{K}_a = \vec{K}_p - \vec{K}_s. \tag{A.2.3}$$

Given that $|\vec{K}_p| \approx |\vec{K}_s|$, the angular frequency shift ω_a is given by:

$$\omega_a = 2\pi\nu_a = 2v_a|\vec{K}_p|\sin(\theta/2), \tag{A.2.4}$$

where v_a is the acoustic speed and $|\vec{K}_p| = 2\pi n/\lambda_p$, in which n is the average refractive

index of the medium. The frequency shift is at its maximum in the backward direction ($\theta=\pi$) and vanishes in the forward direction ($\theta=0$). The backward frequency shift ν_B is given by

$$\nu_B = \frac{2n\nu_a}{\lambda_p}. \tag{A.2.5}$$

In silica fibers with n=1.45, ν_B≈11.1 GHz at λ_p=1.55 μm.

The growth of SBS is characterised by the Brillouin-gain coefficient $g_B(\nu)$ which peaks at $\nu=\nu_B$. The spectral width $\Delta\nu_B$ of the Brillouin gain spectrum depends on the phonon life time T_B through the relationship $\Delta\nu_B=(\pi T_B)^{-1}$; it is approximately 10 MHz. The Brillouin gain that has a Lorentzian spectral profile and is evaluated under steady-state conditions (i.e., valid for CW or quasi-CW light [where the pulse width $T_0>>T_B$]), is given as:

$$g_B(\nu) = \frac{(\Delta\nu_B/2)^2}{(\nu-\nu_B)^2+(\Delta\nu_B/2)^2}\, g_B(\nu_B). \tag{A.2.6}$$

The peak value of the Brillouin-gain coefficient at $\nu=\nu_B$ is given by:

$$g_B(\nu_B) = \frac{2\pi n^7 P_{12}^2}{c\lambda_p^2 \rho_0 \nu_a \Delta\nu_B}, \tag{A.2.7}$$

where P_{12} is the longitudinal elasto-optic coefficient, and ρ_0 is the material density. g_B is approximately 5×10^{-11} m/W for fused silica.

When the input pump power launched into the fiber exceeds the threshold value, the backward reflected Stokes wave results in severe power attenuation to the forward-travelling light. Therefore, the SBS threshold sets an upper limit on the power inputted

into the fiber in optical communication systems. It was found that the SBS threshold strongly depends on the pump light linewidth $\Delta\nu_p$. The SBS threshold for narrow linewidth light ($\Delta\nu_p << \Delta\nu_B$) is given by:

$$P_{th} = 21\frac{A_{eff}\ K}{g_B\ L_{eff}}. \qquad \text{(A.2.8)}$$

where A_{eff} is the effective core area of the fiber, K is the polarization factor ($1 \le K \le 2$) [103], α is the fiber attenuation (m^{-1}), and g_B is the peak value of the Brillouin gain given in equation (A.2.7). For optical fibers used around 1.55 μm, $g_B \approx 5\times10^{-11}$ m/W, K=1.5 for complete polarization scrambling between the input pump light and the backward-scattered signal, and $L_{eff} = 1 - e^{-\alpha L}/\alpha$ is the effective interaction length of the fiber that accounts for the exponential decay of the input power of the pump with fiber length L due to fiber attenuation. For CW light where $\Delta\nu_p > \Delta\nu_B$, the SBS threshold may be written as:

$$P_{th}^{CW} = 21\frac{A_{eff}\ K}{g_B\ L_{eff}}\ \frac{\Delta\nu_p \otimes \Delta\nu_B}{\Delta\nu_B}, \qquad \text{(A.2.9)}$$

where $\otimes$ denotes the convolution operation. For Gaussian Brillouin gain spectral profile, $\Delta\nu_p \otimes \Delta\nu_B = (\Delta\nu_p^2 + \Delta\nu_B^2)^{1/2}$ and $\Delta\nu_p \otimes \Delta\nu_B = \Delta\nu_p + \Delta\nu_B$ for Lorentzian profiles.

A.3 SBS Suppression

Optical communication systems with high-input power levels that exceed the SBS threshold suffer from the SBS nonlinear effect. Methods were investigated to suppress this nonlinear effect by increasing the SBS threshold. These schemes include modulating the input signal using commonly-known modulation techniques such as (i) amplitude shift keying (ASK); (ii) frequency shift keying (FSK); (iii) phase shift keying (PSK)

[101], or by using frequency sweeping-spread spectrum (FS-SS) modulation [104]. The modulation of the input signal broadens the pump light spectral width, which increases the SBS threshold. The amount by which $\Delta\nu_p$ increases depends on the bit rate B and the modulation scheme. It was found that only in the PSK modulation [103], does the Brillouin gain decrease with the bit rate as:

$$g_B^{PSK} \cong \frac{\Delta\nu_B}{B + \Delta\nu_B} g_B^{CW}, \tag{A.3.1}$$

while in both ASK and FSK, the increase in the SBS threshold is limited by a factor between 2 and 4. In different approaches, SBS was suppressed by placing optical isolators at various points in uniform fiber spans [105], or by applying intentional strain in the fiber [106], or by controlling the fiber core germanium concentration in the production process.

An alternative method was used by Fishman and Nagel [107], which will be used here to suppress the SBS that appears in the comblike dispersion profile fiber structures used to generate the bright and dark soliton pulse trains. This scheme is based on directly modulating the laser diodes at much lower frequencies than the low-frequency cutoff of the receiver detector. This frequency modulation of the laser diode gives broader laser linewidth [108]. It is recommended that the dither frequency should not be greater than $(c/2n)L_{eff}$ to achieve maximum SBS suppression through the entire effective length of the fiber. The resulting laser spectral linewidth is given by:

$$(\Delta\nu)_{chirp} \approx \frac{\Gamma_a A\bar{\alpha}}{4\pi eV} \frac{\omega_m}{\omega_R^2} i_f, \tag{A.3.2}$$

where $\bar{\alpha}$ is the material parameter which depends on temperature and the carrier density

$(3<|\hat{\alpha}|<6)$; Γ_a is the filling factor; e is the electron charge; V is the active-region volume; i_I is the modulating current amplitude; ω_m is the modulating frequency; and ω_R is the relaxation oscillation frequency of the laser diode which is given by:

$$\omega_R \approx \sqrt{\frac{A\ p_0}{\tau_p}}. \qquad \text{(A.3.3)}$$

where p_0 is the photon concentration in the laser cavity; τ_p is the photon lifetime; and A is a constant ($A=Bc/n_0$, where B is the spatial gain parameter, c is the speed of light, and n_0 is the refractive index of the active layer medium). The advantage of this method is understood upon examination of the slow variation of the laser spectrum, which implies that for a high-data-rate communication system, not every pulse in a large stream of pulses will encounter broadening. This is contrary to what happens when modulating the input signal using conventional modulation schemes, where each pulse encounters broadening due to the increase of the laser linewidth and the fiber dispersion.

A.4 Experimental Results

Stimulated Brillouin scattering that exists in the comblike dispersion profile fiber structures was measured experimentally. Fig. A.2 illustrates the block diagram of the experiment setup that was used to measure the SBS light. A CW light from a DFB laser diode at 1553 nm was amplified using an erbium-doped fiber amplifier and launched into the fiber structures through a 90/10% fiber coupler. Three power meters were used to measure the transmitted light, the backward-reflected light, and a portion of the input pump light. Fig. A.3 shows both the measured backward-scattered light (due to the SBS nonlinear effect), and the transmitted power through the fiber versus the input pump's

power launched into the fiber structure. The measured SBS threshold is approximately 10 dBm. These measurements were performed using a single DFB laser diode with 43.4 mA of bias current. When the bias current decreases, the SBS threshold increases, due to broadening of the laser linewidth at lower bias currents.

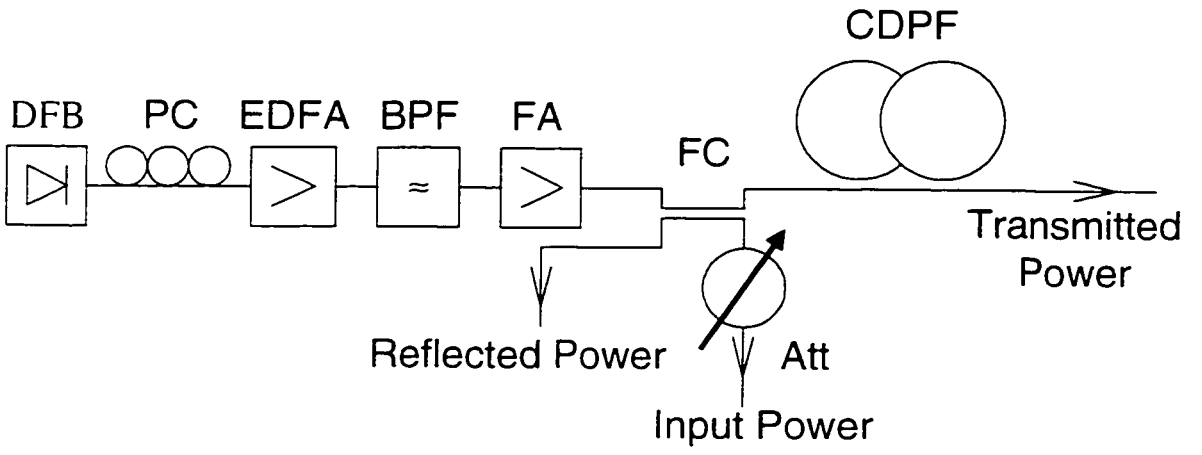

Fig. A.2 Experimental setup used for measuring SBS reflected power. DFB: distributed feedback laser diode; PC: polarisation controller; EDFA: erbium-doped fiber amplifier; BPF: bandpass filter; FA: high power fiber amplifier; FC: 90/10% fiber coupler; CDPF: comblike dispersion profile fiber structure; Att: attenuator.

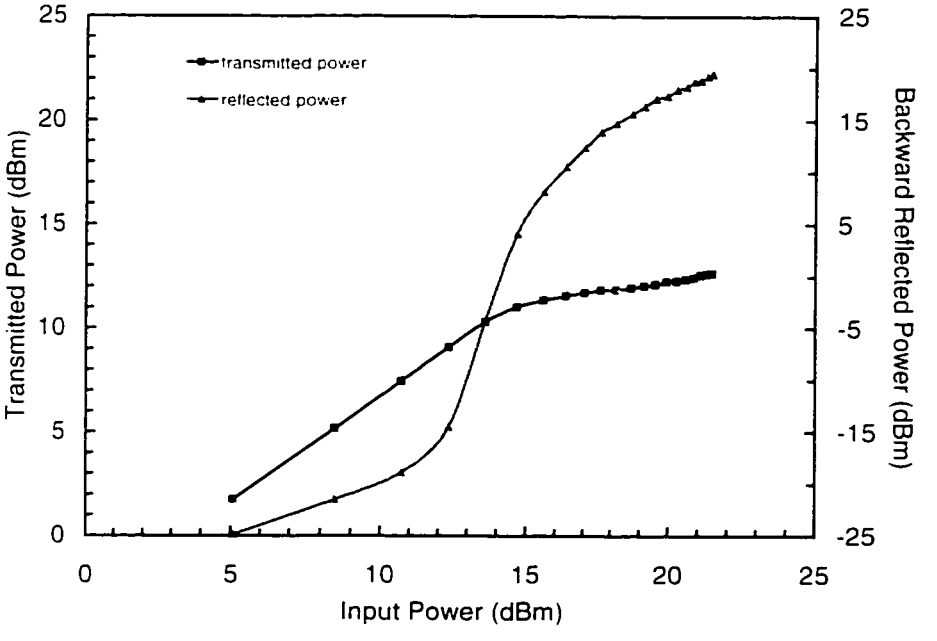

Fig. A.3 Measured backward-reflected and transmitted power versus input power launched into the comblike dispersion profile fiber (CDPF) structure.

Fig. A.4 shows the experimental setup used to measure the backward-travelling Stokes wave spectrum. The Stokes wave was extracted from the backward-scattered light by beating the input signal (at frequency ω_0) and the backward-scattered signal (at frequency ω_0-ω_B). To adjust the amplitudes of each signal, an optical attenuator was placed at each signal path to the 50/50% fiber coupler. An RF spectral analyzer was used to measure the Stokes wave's spectral characteristics. Fig. A.5 shows the Stokes signal, which is down-shifted to approximately 10.5 GHz to form the input signal frequency. The FWHM of the measured spectrum $\Delta\nu_B$ is approximately 23 MHz. It should be noted that the spectral width of the Brillouin gain differs from one fiber to another due to the dopant concentration of each fiber and to the inhomogenieties in the fiber cross section.

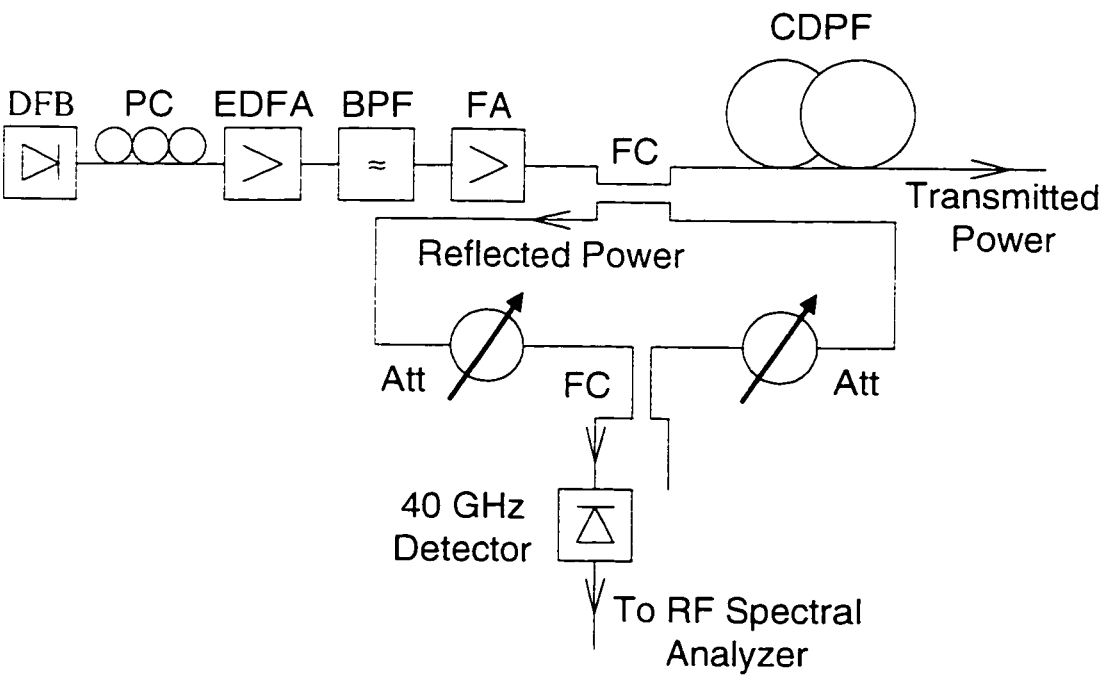

Fig. A.4 Experimental setup used for measuring SBS spectral characteristics. DFB: distributed feedback laser diode; PC: polarisation controller; EDFA: erbium-doped fiber amplifier; BPF: bandpass filter; FA: high power fiber amplifier; FC: 50/50% fiber coupler; CDPF: comblike dispersion profile fiber structure; Att: attenuator; RF: radio frequency.

Here, the stimulated Brillouin scattering nonlinear effect presented in CDPF structures was suppressed using direct modulation of the two DFB laser diodes, employing a sinusoidal signal. The dither frequency of the modulating signal was experimentally measured. Fig. A.6 shows the backward-scattered light versus modulating frequency at maximum input-power launched into the CDPF structure. The optimal frequency is approximately 40 kHz measured, for a 1 mA signal amplitude, which corresponds to a 0.5% dither amplitude modulation. The effect of DFB laser diode direct-modulating on the SBS suppression is shown in Fig A.7, where a 40 kHz sinusoidal signal with a 1 mA amplitude is used. It is clear that the SBS threshold is above 19.5 dBm.

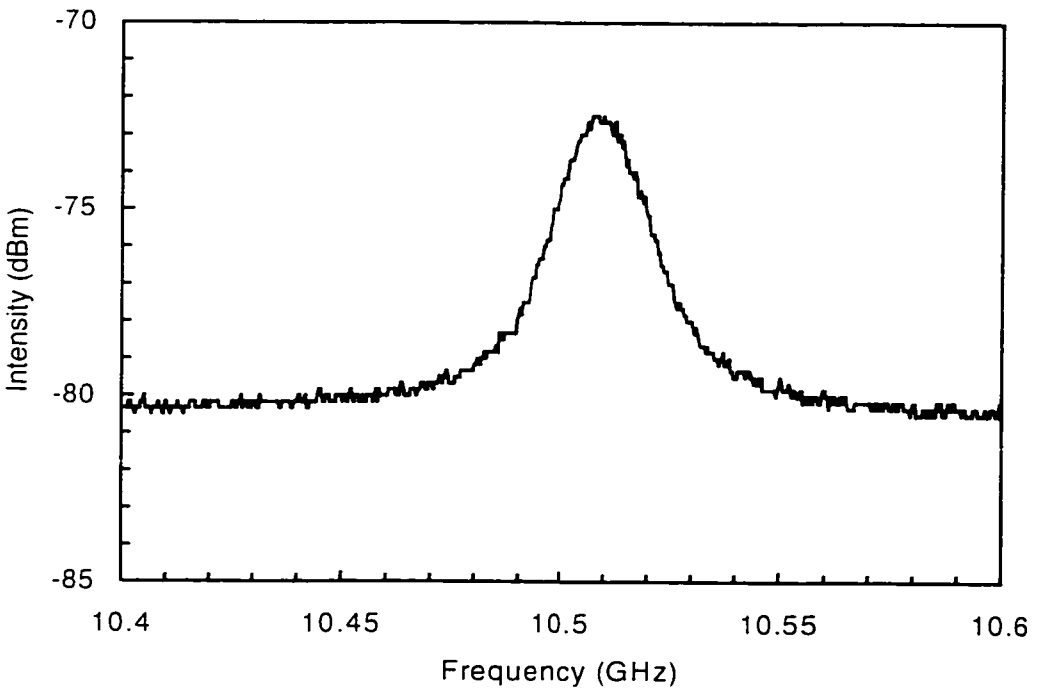

Fig. A.5 Stimulated Brillouin scattering (SBS) spectrum for a comblike dispersion profile fiber (CDPF) structure.

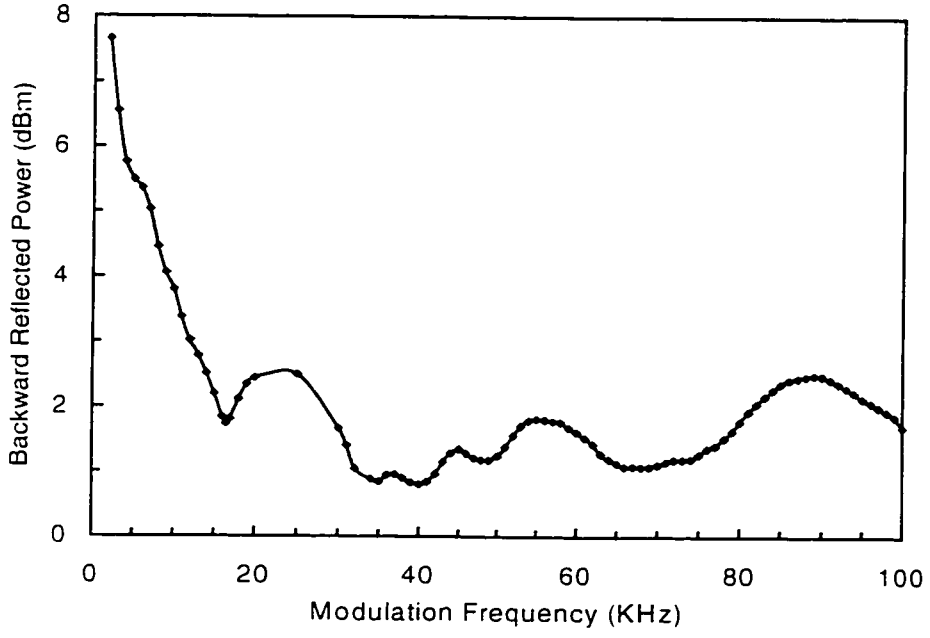

Fig. A.6 Backward-reflected power versus modulation frequency for the comblike dispersion profile fiber (CDPF) structure measured at 21.5 dBm input power launched into the fiber structure.

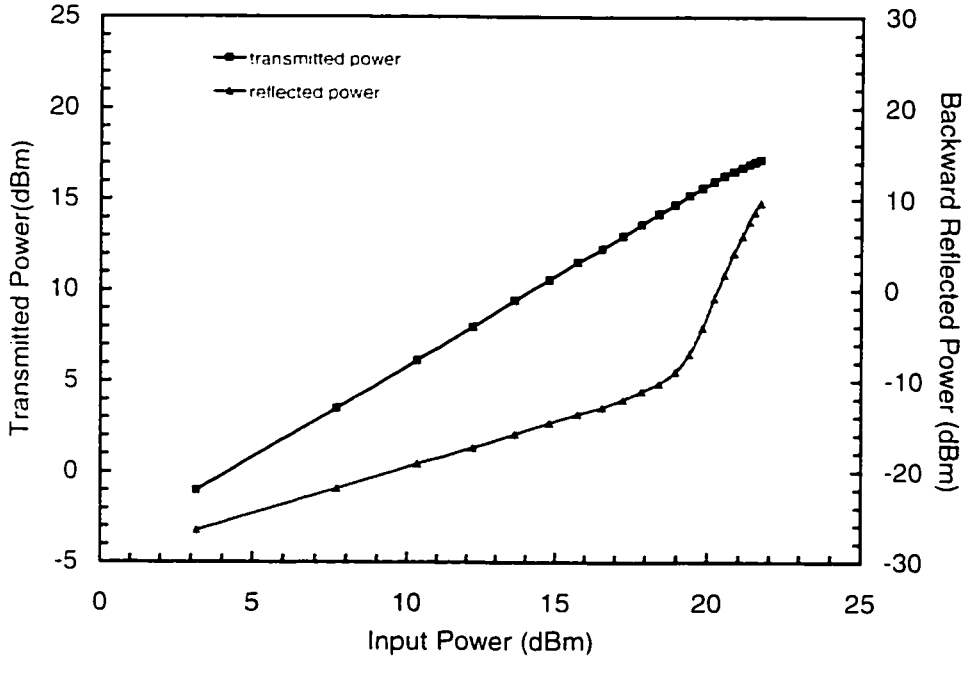

Fig A.7 Backward-reflected power for a comblike dispersion profile fiber structure (CDPF) using directly modulating DFB laser diodes with a 40 kHz sinusoidal signal

References

[1] D. Cotter, J. K. Lucek, and D. D. Marcenac, "Ultra-high-bit-rate networking: from the transcontinental backbone to the desktop", *IEEE Comm. Mag.*, 90-95, April 1997.

[2] J. Chesnoy, B. Clesca, R. Heidemann, and B. Wedding, "Ultrahigh bit rate transmission for the years 2000", *Electrical Comm. Mag.*, 3rd Quarter, 241-250, 1994.

[3] L. F. Mollenauer, E. Lichtman, M. J. Neubelt, and G. T. Harvey, "Demonstration, using sliding-frequency guiding filters, of error-free soliton transmission over more than 20 Mm at 10 Gbit/s, single channel, and over more than 13 Mm at 20 Gbit/s in a two - channel WDM", *Electron. Lett.*, Vol. 29, No. 10, 910-911, 1993.

[4] A. Naka, T. Matsuda, S. Saito, and K. Sato, "5200 km straight-line soliton transmission experiment at 10 Gbit/s", *Electron. Lett.*, Vol. 31, No. 19, 1679-1681, 1995.

[5] S. V. Chernikov, J. R. Taylor, and R. Kashyap "Comblike dispersion-profiled fiber for soliton pulse train generation", *Opt. Lett.*, Vol. 19, No. 8, 539-541, 1994.

[6] E. A. Swanson, and S. R. Chinn, "40-GHz pulse train generation using soliton compression of a Mach-Zehnder modulator output", *IEEE Photon. Technol. Lett.*, Vol. 7, No. 1, 114-116, 1995.

[7] A. Hasegawa, and F. Tappert, "Transmission of stationary nonlinear optical pulses in dispersive dielectric fibers. II. Normal dispersion", *Appl. Phys. Lett.*, Vol. 23, No. 4, 171-172, 1973.

[8] L. F. Mollenauer, S. G. Evangelides, Jr., and H. A. Haus, "Long-distance soliton propagation using lumped amplifiers and dispersion shifted fiber", *IEEE J. Lightwave Technol.*, Vol. 9, No. 2, 194-197, 1991.

[9] R. Ohhira, A. Hasegawa, and Y. Kodama, "Methods of constructing a long-haul soliton transmission system with fibers having a distribution in dispersion", *Opt. Lett.*, Vol. 20, No. 7, 701-703, 1995.

[10] S. Kawanishi, H. Takara, O. Kamatani, T. Morioka, and M. Saruwatari "100 Gbit/s, 560 km optical transmission experiment with 80 km amplifier spacing employing dispersion management", *Electron. Lett.*, Vol. 32, No. 5, 470-471, 1996.

[11] G. Agrawal, Nonlinear fiber optics, 2nd ed., Academic Press, 1995.

[12] J. Scott-Russell, "Report on waves", *Proc. Roy. Soc. Edinburgh*, 319-320, 1844.

[13] D. J. Korteweg, and G. deVries, "On the change of form of long waves advancing in a rectangular canal, and on a new type of long stationary waves", *Phil. Mag.*, Vol. 39, 422-443, 1895.

[14] N. J. Zabusky, and M. D. Kruskal, "Interaction of 'solitons' in a collisionless plasma and the recurrence of initial state", *Phys. Rev. Lett.*, Vol. 15, No. 6, 240-243, 1965.

[15] V. E. Zakharov, and A. B. Shabat, "Exact theory of two-dimensional self-focusing and one-dimensional self-modulation of waves in nonlinear media", *Sov. Phys.-JETP*, Vol. 34, 62-69, 1972.

[16] A. Hasegawa, and F. Tappert, "Transmission of stationary nonlinear optical pulses in dispersive dielectric fibers. I. Anomalous dispersion", *Appl. Phys. Lett.*, Vol. 23, No. 3, 142-144, 1973.

[17] L. F. Mollenauer, R. H. Stolen, and J. P. Gordon, "Experimental observation of picosecond pulse narrowing and solitons in optical fibers", *Phys. Rev. Lett.*, Vol. 45, No. 13, 1095-1098, 1980.

[18] L. F. Mollenauer, and R. H. Stolen, "The soliton laser", *Opt. Lett.*, Vol. 9, No. 1, 13-15, 1984.

[19] H. A. Haus, and M. N. Islam, "Theory of the soliton laser", *IEEE J. Quantum Electron.*, Vol. QE-21, No. 8, 1172-1188, 1985.

[20] M. Islam, and L. F. Mollenauer, in *Digest of International Quantum Electronics Conference* (Optical Society of America, Washington, D.C., 1986), paper TuHH1:in *Ultrafast Phenomena* V, G.R. Fleming and A. E. Siegman, eds. (Springer-Verlag, Berlin, 1986.

[21] J. D. Kafka, and T. Baer, "Fiber Raman soliton laser pumped by a Nd:YAG laser", *Opt. Lett.*, Vol. 12, No. 3, 181-183, 1987.

[22] A. S. Gouveia-Neto, A. S. L. Gomes, and J. R. Taylor, "Femtosecond Soliton Raman generation", *IEEE J. Quantum Electron.*, Vol. 24, No. 2, 332-340, 1988.

[23] B. Zysset, P. Beaud, and W. Hodel, "Generation of optical solitons in the wavelength region 1.37-1.49 μm", *Appl. Phys. Lett.*, Vol. 50, No. 16, 1027-1029, 1987.

[24] A. Hasegawa, "Numerical study of optical soliton transmission amplified periodically by the stimulated Raman process", *Appl. Opt.*, Vol. 23, No. 19, 3302-3309, 1984.

[25] K. Tai, A. Tomita, J. L. Jewell, and A. Hasegawa, "Generation of subpicosecond solitonlike optical pulses at 0.3 THz repetition rate by induced modulation instability", *Appl. Phys. Lett.*, Vol. 49, No. 5, 236-238, 1986.

[26] E. M. Dianov, P. V. Mamyshev, A. M. Prokhorov, and S. V. Chernikov, "Generation of a train of fundamental solitons at a high repetition rate in optical fibers", *Opt. Lett.*, Vol. 14, No. 18, 1008-1010, 1989.

[27] P. V. Mamyshev, S. V. Chernikov, and E. M. Dianov, "Generation of fundamental soliton trains for high-bit-rate optical fiber communication lines", *IEEE J. Quantum Electron.*, Vol. 27, No. 10, 2347-2355, 1991.

[28] S. V. Chernikov, J. R. Taylor, P. V. Mamyshev, and E. M. Dianov, "Generation of soliton pulse train in optical fibre using two CW singlemode diode lasers", *Electron. Lett.*, Vol. 28, No. 10, 931-932, 1992.

[29] S. V. Chernikov, P. V. Mamyshev, E. M. Dianov, D. J. Richardson, R. I. Laming, and D. N. Payne, "CW soliton train generation in the repetition rate range 60-90 GHz using a dispersion decreasing fibre", *Sov. Lightwave Commun.*, Vol. 2, 161-169, 1992.

[30] S. V. Chernikov, D. J. Richardson, R. I. Laming, E. M. Dianov, and D. N. Payne, "70 Gbit/s fibre based source of fundamental solitons at 1550 nm", *Electron. Lett.*, Vol. 28, NO. 13, 1210-1212, 1992.

[31] A. V. Shipulin, D. G. Fursa, E. A. Golovchenko, and E. M. Dianov, "High repetition rate CW fundamental soliton generation using multisoliton pulse compression in a varying dispersion fibre", *Electron. Lett.*, Vol. 29, No. 16, 1401-1403,1993.

[32] S. V. Chernikov, J. R. Taylor, and R. Kashyap, "Integrated all optical fibre source of multigigahertz soliton pulse train", *Electron. Lett.*, vol. 29, No. 20, 1788-1789, 1993.

[33] J. E. Bowers, P. A. Morton, A. Mar, and S. W. Corzine, "Actively mode-locked semiconductor lasers", *IEEE J. Quantum Electron.*, Vol. 25, No. 6, 1426-1439, 1989.

[34] R. S. Tucker, U. Koren, G. Raybon, C. A. Burrus, B. I. Miller, T. L. Koch, and G. Eisenstein, "40 GHz active mode-locking in a 1.5 μm monolithic extended-cavity laser", *Electron. Lett.*, Vol. 25, No. 10, 621-622, 1989.

[35] M. Nakazawa, K. Suzuki, and Y. Kimura, "Transform-limited pulse generation in the gigahertz region from a gain-switched distributed-feedback laser diode using spectral windowing", *Opt. Lett.*, Vol. 15, No. 12, 715-717, 1990.

[36] K. Suzuki, K. Iwatsuki, S. Nishi, M. Saruwatari, and T. Kitoh, "160 Gb/s Sub-picosecond transform-limited pulse signal generation utilizing adiabatic soliton

compression and optical time-division multiplexing", *IEEE Photon. Technol. Lett.*, Vol. 6, No. 3, 352-354, 1994.

[37] T. Geisler, K. A. Shore, M. P. Soerensen, P. L. Christiansen, J. Mørk, and J. Mark, "Nonlinear fiber external cavity mode locking of erbium-doped fiber lasers", *J. Opt. Soc. Am. B.*, Vol. 10, No. 7, 1166-1174, 1993.

[38] M. Suzuki, H. Tanaka, H. Taga, N. Edagawa, Y. Matsushima, and H. Wakabayashi, "Ultra-short pulse generation for soliton transmission using electroabsorption modulators", *Fiber and Integ. Opt.*, Vol. 12, 355-368, 1993.

[39] M. Suzuki, H. Tanaka, N. Edagawa, K. Utaka, and Y. Matsushima, "Transform-limited optical pulse generation up to 20-GHz repetition rate by a sinusoidally driven InGaAsP electroabsorption modulator", *IEEE J. Lightwave Technol.*, Vol. 11, No. 3, 468-473, 1993.

[40] A. K. Atieh, P. Myslinski, J. Chrostowski, and P. Galko, "Generation of multigigahertz bright and dark soliton pulse trains", *Optics Comm.*, Vol. 133, No. 1-6, 541-548, 1997.

[41] A. K. Atieh, M. Florjanczyk, P. Myslinski, J. Chrostowski, and P. Galko, "Generation of multigigahertz soliton pulse train", Proceedings of the 1994 Canadian Conference On Electrical And Computer Engineering, Halifax, B11, 356-358, 1994.

[42] A. K. Atieh, P. Myslinski, J. Chrostowski and P. Galko, "Measurement of the nonlinear ratio (n_2/A_{eff}) in optical fibers using self-phase modulation effect", Proceedings of International Conference on Applications of Photonics Technology ICAPT'96, Montreal, 1996, Plenum Publishing, in press.

[43] K. L. Sala, G. A. Kenney-Wallace, and G. E. Hall, "CW autocorrelation measurements of picosecond laser pulses", *IEEE J. Quantum Electron.*, Vol. QE-16, No. 9, 990-996, 1980.

[44] P. Myslinski, "Rapid scanning autocorrelator for measurements of ultrafast laser pulses", *Rev. Sci. Instrum.*, Vol. 58, No. 4, 711-713, 1987.

[45] W. Zhao, and E. Bourkoff, "Generation, propagation, and amplification of dark solitons", *J. Opt. Soc. Am. B*, Vol. 9, No. 7, 1134-1144, 1992.

[46] W. Zhao, and E. Bourkoff, "Propagation properties of dark solitons", *Opt. Lett.*, Vol. 14, No. 13, 703-705, 1989.

[47] Y. S. Kivshar, M. Haelterman, Ph. Emplit, and J.-P. Hamaide, "Gordon-Haus effect on dark solitons", *Opt. Lett.*, Vol. 19, No. 1, 19-21, 1994.

[48] P. Emplit, J. P. Hamaide, F. Reynaud, C. Froehly, and A. Barthelemy, "Picosecond steps and dark pulses through nonlinear single mode fibers", *Optics Comm.*, Vol. 62, No. 6, 374-379, 1987.

[49] D. Krökel, N. J. Halas, G. Giuliani, and D. Grischkowsky, "Dark-pulse propagation in optical fibers", *Phys. Rev. Lett.*, Vol. 60, No. 1, 29-32, 1988.

[50] A. M. Weiner, J. P. Heritage, R. J. Hawkins, R. N. Thurston, E. M. Kirschner, D. E. Leaird, and W. J. Tomlinson, "Experimental observation of the fundamental dark soliton in optical fibers", *Phys. Rev. Lett.*, Vol. 61, No. 21, 2445-2448, 1988.

[51] J. E. Rothenberg, "Colliding visible picosecond pulses in optical fibers", *Opt. Lett.*, Vol. 15, No. 8, 443-445, 1990.

[52] W. Zhao, and E. Bourkoff, "Generation of dark solitons under a cw background using waveguide electro-optic modulators", *Opt. Lett.*, Vol. 15, No. 8, 405-407, 1990.

[53] M. Haelterman, and Ph. Emplit, "Optical dark soliton trains generated by passive spectral filtering technique", *Electron. Lett.*, Vol. 29, No. 4, 356-357,1993.

[54] J. A. R. Williams, K. M. Allen, N. J. Doran, and Ph. Emplit, "The generation of quasi-continuous trains of dark soliton-like pulses", *Optics Comm.*, Vol. 112, No. , 333-338, 1994.

[55] Ph. Emplit, M. Haelterman, and J.-P. Hamaide, "Picosecond dark soliton over a 1-km fiber at 850 nm", *Opt. Lett.*, Vol. 18, No. 13, 1047-1049, 1993.

[56] D. J. Richardson, R. P. Chamberlin, L. Dong, and D. N. Payne, "Experimental demonstration of 100 GHz dark soliton generation and propagation using a dispersion decreasing fibre", *Electron. Lett.*, Vol. 30, No. 16, 1326-1327, 1994.

[57] M. Nakazawa, and K. Suzuki, "Generation of a pseudorandom dark soliton data train and its coherent detection by one-bit-shifting with a Mach-Zehnder interferometer", *Electron. Lett.*, Vol. 31, No. 13, 1084-1085, 1995.

[58] J. E. Rothenberg, "Dark soliton trains formed by visible pulse collisions in optical fibers", *Optics Comm.*, Vol. 82, No. 1,2, 107-111, 1991.

[59] J. E. Rothenberg, and H. k. Heinrich, "Observation of the formation of dark-soliton trains in optical fibers", *Opt. Lett.*, Vol. 17, No. 4, 261-263, 1992.

[60] J. P. Gordon, and H. A. Haus, "Random walk of coherently amplified solitons in optical fiber transmission", *Opt. Lett.*, Vol. 11, No. 10, 665-667,1986.

[61] A. K. Atieh, P. Myslinski, J. Chrostowski, and P. Galko, "Polarization-insensitive all-optical demultiplexing system," Proceedings of the 1996 Canadian Conference On Electrical And Computer Engineering, Calgary, 222-224, 1996.

[62] H. Hatami-Hanza, J. Hong, A. K. Atieh, P. Myslinski, and J. Chrostowski, "Demonstration of all-optical demultiplexing of a multilevel soliton signal employing soliton decomposition and self-frequency shift," *IEEE Photon. Technol. Lett.*, in press.

[63] H. Hatami-Hanza, A. Mostofi, and P. L. Chu, "A multilevel soliton communication system", *IEEE J. Lightwave Technol.*, Vol. 15, No. 1, 6-19,1997.

[64] N. J. Doran, and D. Wood, "Nonlinear-optical loop mirror," *Opt. Lett.*, Vol. 13, No. 1, 56-58, 1988.

[65] N. J. Doran, D. S. Forrester, and B. K. Nayar, "Experimental investigation of all-optical switching in fibre loop mirror device," *Electron. Lett.*, Vol. 25, No. 4, 267-269, 1989.

[66] M. E. Fermann, F. Haberl, M. Hofer, and H. Hochreiter, "Nonlinear amplifying loop mirror," *Opt. Lett.*, Vol. 15, No. 13, 752-754, 1990.

[67] D. J. Richardson, R. I. Laming, and D. N. Payne, "Very low threshold Sagnac switch incorporating an erbium doped fibre amplifier," *Electron. Lett.*, Vol. 26, No. 21, 1779-1781, 1990.

[68] K. J. Blow, N. J. Doran, B. K. Nayar, and B. P. Nelson, "Two-wavelength operation of the nonlinear fiber loop mirror," *Opt. Lett.*, Vol. 15, No. 4, 248-250, 1990.

[69] M. Jinno, and T. Matsumoto, "Ultrafast, low power, and highly stable all-optical switching in an all polarization maintaining fiber Sagnac interferometer," *IEEE Photon. Technol. Lett.*, Vol. 2, No. 5, 349-351, 1990.

[70] K. J. Blow, N. J. Doran, and B. P. Nelson, "Demonstration of the nonlinear fibre loop mirror as an ultrafast all-optical demultiplexer," *Electron. Lett.*, Vol. 26, No. 14, 962-964, 1990.

[71] B. P. Nelson, K. J. Blow, P. D. Constantine, N. J. Doran, J. K. Lucek, I. W. Marshall, and K. Smith, "All-optical Gbit/s switching using nonlinear optical loop mirror," *Electron. Lett.*, Vol. 27, No. 9, 704-705, 1991.

[72] P. A. Andrekson, N. A. Olsson, J. R. Simpson, D. J. Digiovanni, P. A. Morton, T. Tanbun-Ek, R. A. Logan, and K. W. Wecht, "64 Gb/s all-optical demultiplexing with the nonlinear optical-loop mirror," *IEEE Photon. Technol. Lett.*, Vol. 4, No. 6, 644-647, 1992.

[73] T. Morioka, H. Takara, K. Mori, and M. Saruwatari, "Ultrafast reflective optical Kerr demultiplexer using polarization rotation mirror," *Electron. Lett.*, Vol. 28, No. 6, 521-522, 1992.

[74] T. Morioka, and M. Saruwatari, "Ultrafast all-optical switching utilizing the optical Kerr effect in polarization-maintaining single-mode fibers," *IEEE J. Sel. Areas Commun.*, Vol. 6, No. 7, 1186-1198, 1988.

[75] K. Uchiyama, H. Takara, S. Kawanishi, T. Morioka, and M. Saruwatari, "Ultrafast polarization-independent all-optical switching using a polarization diversity scheme in the nonlinear optical loop mirror," *Electron. Lett.*, Vol. 28, No. 20, 1864-1866, 1992.

[76] H. Bülow, and G. Veith, "Polarization-independent switching in a nonlinear optical loop mirror by a dual-wavelength switching pulse," *Electron. Lett.*, Vol. 29, No. 7, 588-589, 1993.

[77] D. M. Patrick, A. D. Ellis, and D. M. Spirit, "Bit-rate flexible all-optical demultiplexing using a nonlinear optical loop mirror," *Electron. Lett.*, Vol. 29, No. 8, 702-703, 1993.

[78] K. Uchiyama, S. Kawanishi, H. Takara, T. Morioka, and M. Saruwatari, "100 Gbit/s to 6.3 Gbit/s demultiplexing experiment using polarisation-independent nonlinear optical loop mirror," *Electron. Lett.*, Vol. 30, No. 11, 873-875, 1994.

[79] H. Bülow, Th. Pfeiffer, and G. Veith, "Polarisation-insensitive all-optical demultiplexing over a wide wavelength range in a short-fibre nonlinear optical loop mirror," *Electron. Lett.*, Vol. 30, No. 1, 68-69, 1994.

[80] S. Kumar, A. Selvarajan, and G. V. Anand, "Nonlinear copropagation of two optical pulses of different frequencies in birefringent fibers," *J. Opt. Soc. Am. B.*, Vol. 11, No. 5, 810-817, 1994.

[81] A. Hasegawa, and T. Nyu, "Eigenvalue communication," *IEEE J. Lightwave Technol.*, Vol. 11, No. 3, 395-399, 1993.

[82] J. P. Gordon, "Theory of the soliton self-frequency shift," *Opt. Lett.*, Vol. 11, No. 10, 662-664, 1986.

[83] F. M. Mitschke, and L. F. Mollenauer, "Discovery of the soliton self-frequency shift," *Opt. Lett.*, Vol. 11, No. 10, 659-661, 1986.

[84] D. Wood, "Constraints on the bit rates in direct detection optical communication systems using linear or soliton pulses," *IEEE J. Lightwave Technol.*, Vol. 8, No. 7, 1097-1106, 1990

[85] A. K. Atieh, J. Hong, P. Myslinski, H. Hatami-Hanza, J. Chrostowski, and P. Galko, "Soliton pulse compression in comblike dispersion profile fiber structures", accepted in Tech. Dig. CLEO'97, Optical Society of America, Washington DC, 1997.

[86] A. Galvanauskas, P. A. Krug, and D. Harter, "Nanosecond-to-picosecond pulse compression with fiber gratings in a compact fiber-based chirped-pulse-amplification system" *Opt. Lett.*, Vol. 21, No. 14, 1049-1051, 1996.

[87] R. F. de Souza, E. J. S. Fonseca, J. M. Hickmann, and A. S. Gouveia-Neto, "Weak signal pulse compression and amplification through stimulated Raman scattering and cross-phase modulation in optical fibers", *Optics Comm.*, Vol. 124, No. ,79-82, 1996.

[88] M. J. Guy, S. V. Chernikov, J. R. Taylor, D. G. Moodie, and R. Kashyap, "200 fs soliton pulse generation at 10 GHz through nonlinear compression of transform-limited pulses from an electroabsorption modulator", *Electron. Lett.*, Vol. 31, No. 9, 740-741, 1995.

[89] S. V. Chernikov, J. R. Taylor, and R. Kashyap, "Experimental demonstration of step-like dispersion profiling in optical fibre for soliton pulse generation and compression", *Electron. Lett.*, Vol. 30, No. 5, 433-435, 1994.

[90] K. Tai, A. Hasegawa, and N. Bekki, "Fission of optical solitons induced by stimulated Raman effect", *Opt. Lett.*, Vol. 13, No. 5, 392-394, 1988.

[91] Y. Kodama, and A. Hasegawa, "Nonlinear pulse propagation in monomode dielectric guide", *IEEE J. Quantum Electron.*, Vol. QE-23, No. 5, 510-524, 1987.

[92] P. V. Mamyshev, and S. V. Chernikov, "Recent developments in the ultrashort pulse Raman effect in optical fibers", *Sov. Lightwave Commun.*, Vol. 2, 97-111, 1992.

[93] G. P. Agrawal, *Nonlinear Fiber Optics*, 2nd ed., Academic Press, see page 45-49, 1995.

[94] R.-J. Essiambre, and G. P. Agrawal, "Soliton communication beyond the average-soliton regime", *J. Opt. Soc. Am. B*, Vol. 12, No. 12, 2420-2425, 1995.

[95] R.-J. Essiambre, and G. P. Agrawal, "Ultrahigh-bit-rate soliton communication systems using dispersion-decreasing fibers and parametric amplifiers", *Opt. Lett.*, Vol. 21, No. 2, 116-118, 1996.

[96] K. S. Kim, R. H. Stolen, W. A. Reed, and K. W. Quoi, "Measurement of the nonlinear index of silica-core and dispersion-shifted fibers", *Opt. Lett.*, Vol.19, No. 4, 257-259, 1994.

[97] T. Kato, Y. Suetsugu, M. Takagi, E. Sasaoka, and M. Nishimura, "Measurement of the nonlinear refractive index in optical fiber by the cross-phase-modulation method with depolarized pump light", *Opt. Lett.*, Vol. 20, No. 9, 988-990, 1995.

[98] L. Prigent, and J.-P. Hamaide, "Measurement of fiber nonlinear Kerr coefficient by four-wave mixing", *IEEE Photon. Technol. Lett.*, Vol. 5, No. 9, 1092-1095, 1993.

[99] E. A. Golovchenko, P. V. Mamyshev, A. N. Pilipetskii, and E. M. Dianov, "Numerical analysis of the Raman spectrum evolution and soliton pulse generation in single-mode fibers", *J. Opt. Soc. Am. B*, Vol. 8, No. 8, 1626-1632, 1991.

[100] A. K. Atieh, P. Myslinski, J. Chrostowski, and P. Galko, "Measurement Of The Raman Time Constant (T_R) In Standard Single Mode Fiber", submitted to *Optics Comm.*

[101] R. A. Barry, V. W. S. Chan, K. L. Hall, E. S. Kintzer, J. D. Moores, K. A. Rauschenbach, E. A. Swanson, L. E. Adams, C. R. Doerr, S. G. Finn, H. A. Haus, E. P. Ippen, W. S. Wong, and M. Haner, "All-optical network consortium-ultrafast TDM networks", *IEEE J. Select. Areas Commun.*, Vol. 14, No. 5, 999-1012, 1996.

[102] N. Q. Ngo, L. N. Binh, and X. Dai, "Optical dark-soliton generators and detectors", *Optics Comm.*, Vol. 132, No. , 389-402, 1996.

[103] Y. Aoki, K. Tajima, and I. Mito, "Input power limits of single-mode optical fibers due to stimulated Brillouin scattering in optical communication systems", *J. Lightwave Technol.*, Vol. 6, No. 5, 710-719,1988.

[104] A. Hirose, Y. Takushima, and T. Okoshi, "Suppression of stimulated Brillouin scattering and Brillouin crosstalk by frequency-sweeping spread-spectrum scheme", *J. Opt. Commun.*, Vol. 12, No. 3, 82-85, 1991.

[105] X. P. Mao, R. W. Tkach, A. R. Chraplyvy, R. M. Jopson, and R.M. Derosier, "Stimulated Brillouin threshold dependence on fiber type and uniformity", *IEEE Photon. Technol. Lett.*, Vol. 4, No. 1, 66-69, 1992.

[106] N. Yoshizawa, and T. Imai, "Stimulated Brillouin scattering suppression by means of applying strain distribution to fiber with cabling", *IEEE J. Lightwave Technol.*, Vol. 11, No. 10, 1518-1522, 1993.

[107] D. A. Fishman, and J. A. Nagel, "Degradations due to stimulated Brillouin scattering in multigigabit intensity-modulated fiber-optic systems", *IEEE J. Lightwave Technol.*, Vol. 11, No. 11, 1721-1728, 1993.

[108] A. Yariv, Optical Electronics, 4th ed., Ch. 15, Saunders College Publishing, a division of Host, Rinehart and Winston Inc.

IMAGE EVALUATION TEST TARGET (QA-3)

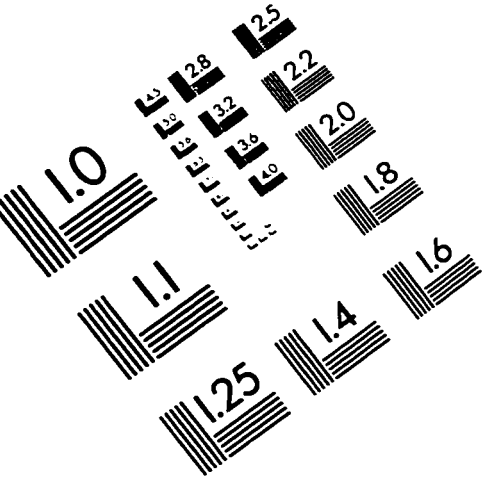

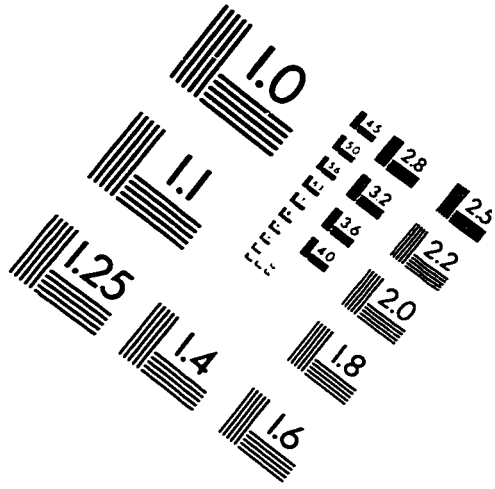

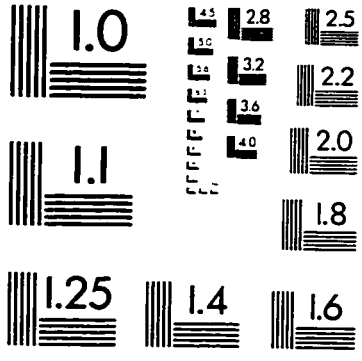

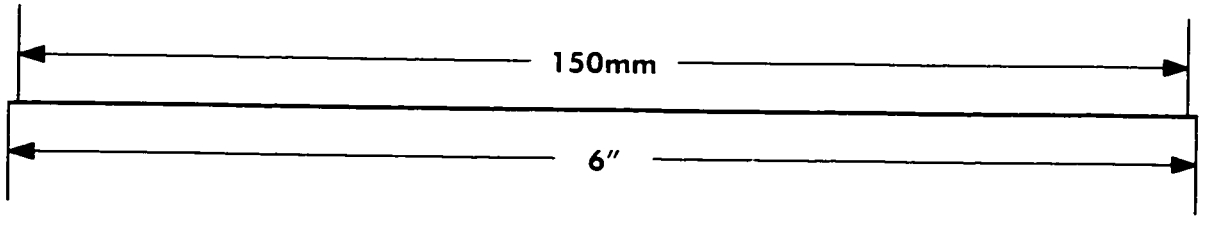

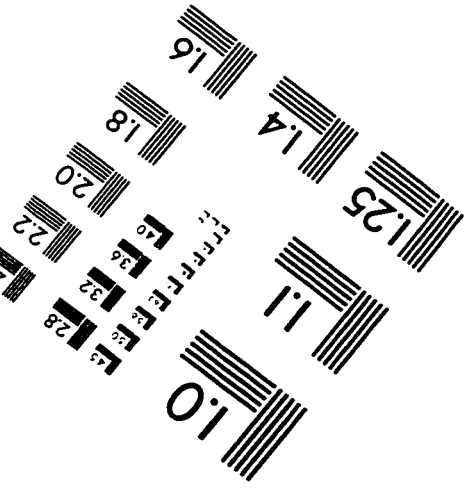

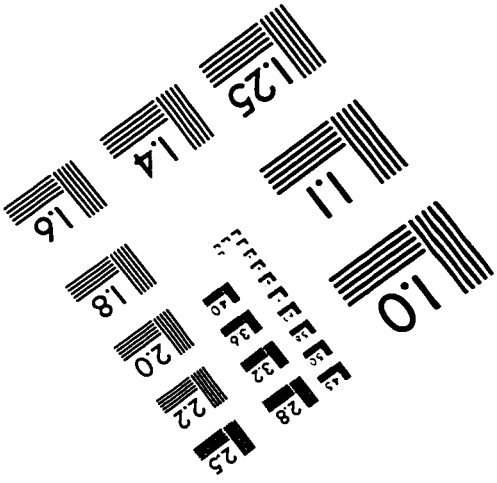

APPLIED IMAGE, Inc
1653 East Main Street
Rochester, NY 14609 USA
Phone: 716/482-0300
Fax: 716/288-5989